catalysts

MDPI

Review

Time Resolved Operando X-ray Techniques in Catalysis, a Case Study: CO Oxidation by O_2 over Pt Surfaces and Alumina Supported Pt Catalysts

Mark A. Newton

Department of Physics, University of Warwick, Gibbet Hill Road, Coventry CV4 7AL, UK; M.Newton.2@warwick.ac.uk or manewton68@gmail.com

Academic Editor: Juan J. Bravo-Suarez
Received: 26 September 2016; Accepted: 26 January 2017; Published: 14 February 2017

Abstract: The catalytic oxidation of CO by O_2 to form CO_2 over Pt surfaces and supported catalysts is one of the most studied catalytic reactions from both fundamental and applied points of view. This review aims to show how the application of a range of time resolved, X-ray based techniques, such as X-ray diffraction (XRD), Surface X-ray diffraction (SXRD), total X-ray scattering/pair distribution function (PDF), X-ray absorption (XAFS), X-ray emission (XES), and X-ray photoelectron spectroscopies (XPS), applied under operando conditions and often coupled to adjunct techniques (for instance mass spectrometry (MS) and infrared spectroscopy (IR)) have shed new light on the structures and mechanisms at work in this most studied of systems. The aim of this review is therefore to demonstrate how a fusion of the operando philosophy with the ever augmenting capacities of modern synchrotron sources can lead to new insight and catalytic possibilities, even in the case of a process that has been intensely studied for almost 100 years.

Keywords: operando; platinum; carbon monoxide; oxidation; aluminium oxide; surface chemistry; synchrotron X-ray techniques; combined techniques; catalysis

1. Introduction

CO oxidation by O_2 to yield CO_2 is one of the most important and most studied catalytic processes. It is a notionally simple reaction and therefore of fundamental interest within that canon of research devoted to the detailed understanding or heterogeneous gas-solid reactions. At the same time, it is a chemical conversion of considerable applied utility as a means to remove CO from places and systems where it is unwanted.

CO is highly toxic and a by-product of many processes, most notably the combustion of hydrocarbon based fuels that, in the modern era, is dominated by the automotive sector. Early research into CO removal via oxidation was also stimulated by problems of air quality, though in other areas: the military, where air purification technologies were required for gas-masks and maintaining clean atmospheres in such enclosed environments as submarines; and civil situations, such as mining, general energy production, and as a result of the use of coal, often in poorly ventilated surroundings, as a fuel in everyday life, were issues that needed to be addressed [1–3].

CO oxidation catalysis has been and continues to be a central theme (as many of these issues are still with us in one form or another) and today catalytic converters for exhaust gas clean-up are responsible for 37% to 50% of the world's usage of Pt [4,5]. Ever more stringent air quality regulations mean that the demand for effective CO removal technologies, especially those that may function at ambient temperatures, ensures that research into this most basic of conversions shows no signs of abating.

This application yields a fine example of the very wide ranging situations that CO oxidation over Pt must be achieved within which lie significant drivers for research and both fundamental and applied problems to overcome. In this application, the primary responsibility of Pt is the effective conversion of unspent fuel and CO arising from its incomplete combustion to CO_2. Ideally, this conversion should be efficiently accomplished from temperatures below ambient to over 1000 K and the catalyst to remain active under conditions of generally high space velocities (short contact times) within an environment that by design fluctuates rapidly between net oxidizing and net reducing conditions (so called Lambda cycling). For fundamental reasons that are delineated below, simple Pt/Al_2O_3 catalysts are mechanistically unable to achieve low temperature CO oxidation and, over time, suffer from agglomeration processes (sintering) that massively reduce the active surface of the Pt component and have long been understood to be a major source of catalyst deactivation [6].

CO is also a potent poison to many catalytic processes, most notably electrochemical methanol and hydrogen oxidations [7–10]—that also often have Pt at the core of their composition—used to generate energy. CO must therefore be removed from the feedstocks used in such application or the processes adapted to ameliorate the detrimental effects of any CO produced as a by-product of the chemistry.

The first attempts to understand the fundamentals of the reaction of CO with O_2 over Pt are due to Langmuir [11,12]. In these studies he established the basic kinetic character of CO oxidation over Pt wires. In doing so he also helped to define one of the fundamental mechanisms of heterogeneous catalytic processes—the Langmuir–Hinshelwood (LH) mechanism.

The central element of this mechanism is that both molecular CO and O (in a dissociated form as a result of its adsorption by the Pt) have to be present together on the surface of the (metallic) Pt for catalysis to yield CO_2 to occur. This is to contrast with two alternative mechanisms: the Eley–Rideal (ER) [13], wherein catalysis is achieved through the reaction of a surface adsorbed component and a gas phase molecule; and the Mars–van Krevelen (MvK) [14], where the products of the catalytic reaction contain species that are derived from the catalyst itself; in the 1954 paper, lattice oxygen drawn from a Vanadium oxide catalyst.

These are very basic and general designations and it is not the purpose of this review to go into great detail as to their invocations for catalysis or their kinetic discrimination; in these cases the reader is referred elsewhere [15,16]. It suffices here to note that the "pure" ER and LH mechanism may be kinetically discriminated and for a very long time, basic LH mechanism held sway in our description of CO oxidation by O_2 over Pt surface and catalysts.

This basic LH mechanism essentially states that the catalytic conversion involves only molecular adsorbed CO and dissociated O adsorbed in close proximity on the Pt surface as being the requirements for catalytic conversion. It successfully accounts for the fact that CO oxidation over Pt over simple oxide catalysts still requires a certain amount of thermal energy to "light off". Typically, for Pt surfaces and simple Pt catalysts this requires temperatures in excess of 373 K. The reason for this is that at low temperatures the competition for surface adsorption sites that exists between the CO and the O_2 results in the Pt surfaces becoming covered in CO to such degree that the dissociation of O_2 cannot occur. It also, therefore, supplies the classic example of the poisoning of catalysis by CO alluded to above.

As such, for Pt supported upon simple oxides the LH mechanism fundamentally limits their application to CO oxidation at, for example, ambient temperature; a fact that might be regarded as a major driver for the intense research that has been undertaken in recent years to achieve this goal using other metals (most notably Au [17–21]) and more complex, and reducible support systems [17–29]. These approaches aim to favorably modify the fundamental molecular interactions required for this conversion by weakening the M–CO interaction whilst still providing a kinetically appropriate supply of dissociated oxygen through an LH scenario and/or, in the case of employment of reducible oxides, introducing of another possible source of oxygen, and moving the whole reaction paradigm toward the MvK.

For the classic case of CO oxidation using Pt surfaces or Pt supported upon simple supports, such as Al_2O_3 or SiO_2, the basic LH mechanism, became generally accepted from a relatively early point. However, as of early 1970s a range of self-sustaining oscillatory phenomena in CO oxidation over Pt single crystal surfaces, wires, and supported catalysts started to be noted, studied, and theoretically modelled [30–39].

Such complex behavior in a notionally simple conversion, whilst not placing the basic LH mechanism directly into question was, however, suggestive of the presence of unknown elements at work, the precise chemical nature of which were beyond the capacity of the available techniques of the time—all purely kinetic in nature with no access to the dynamic structural behavior of the catalysts—to elucidate. Kinetics of itself cannot uniquely establish the underlying mechanisms responsible for such behaviors [15] that, in the case of oscillations, are potentially many fold and structurally diverse.

As a result, by the 1980s, these phenomena had become the object of intense theoretical and experimental research that resulted in numerous mechanistic possibilities for their explanation [39–68], e.g., spatial separation and self-organization of the reactants [48,60–68], surface reconstruction [42,48,50–52,60], surface roughening/retexturing [49], the deposition and then ignition of carbon on the Pt [56–59], and reversible reduction-oxidation of the Pt itself [39–41,43–45,49,50].

New spatially resolving methods (notably photoelectron emission microscopy (PEEM) [61,62,64,65] and latterly scanning tunneling microscopy (STM) [68]) started to be developed in the late 1980s and early 1990s and used to progressively detail the structural source of kinetic complexity in CO oxidation on Pt single crystal surfaces with ever greater precision [60–68].

This research culminated in 1997 with the application of STM dynamic by Ertl and co-workers that for, the first time, was able quantitatively link reaction kinetics with atomically resolved imaging of the coexisting surface phases that were responsible for the catalytic oxidation of CO [68]; a seminal and significant contribution, the result of a sustained effort over almost two decades, to the Nobel prize for chemistry awarded to Professor Gert Ertl in 2007.

However, remarkable as these achievements were, they still left numerous questions to be interrogated and answered. Almost all of these measurements were made on well-defined single crystal surfaces and at low pressures. As such they left two "gaps" that required closure: the "pressure gap", applied CO oxidation generally being achieved under total pressure of 1 atmosphere or above; and the "materials gap", technical catalysts being comprised of metal Pt nanoparticles supported upon a range of dispersants rather than well-defined Pt surfaces.

It is difficult to specify an optimal Pt particle size for CO oxidation but on surface area grounds alone, given the high cost of Pt and the concomitant desire to present as much of it to the reactive feed as possible, by and large, the sorts of dimensions aimed for would be in the 1–5 nm range (a few tens to a few thousand atoms); in other words, extremely different to the quasi infinite surfaces of Pt single crystals. As is well known on these reduced length scales many other effects may influence the properties of the nanoparticles: quantum confinement effects, the presence of numerous crystallographic faces within single particles, metal support interactions, and molecular communication between particles, along with numerous others, may all contribute to the behavior of Pt catalysts. As with the different reaction mechanisms that may be involved in CO oxidation over Pt, detailed descriptions of how and when these differing effects may be studied and where they may be quantified have been given elsewhere [69,70].

How therefore to bridge both these gaps and to validate—mechanistically speaking—the transferability of the atomic level information arrived from surface science studies on single crystal surfaces in the low pressure regime and to get to the bottom of a problem that is at first sight simple, but yet clearly contains within it a great deal of subtlety and nuance?

In the same era, the second generation of synchrotron X-ray sources (the first dedicated, rather than parasitic, resources) appeared in 1981 with the Daresbury light source in the UK, shortly followed by numerous others around the world. The appearance of these sources meant that for the first time

scientists of all persuasions might gain access to, and be able to exploit, a range of familiar (X-ray diffraction) and new (e.g., X-ray absorption spectroscopies) methods with X-ray fluxes and tunability that had previously not been available.

Techniques of this nature, that in the case of Platinum generally (though not exclusively, see for example Section 2.4) utilize X-rays of >10 keV (the Pt L_3-edge, most commonly used for XAFS and XES investigations, being at 11.564 keV), are not restricted in their application in terms of, for instance, pressure, and can be structurally deterministic on nanometric and atomic length scales.

The second generation sources were subsequently superseded by the so called "third-generation" synchrotrons the first of which was the ESRF in Grenoble, France (1994), shortly followed by the Advanced Photon Source in the USA (1996) and Spring 8 in Japan (1997). These were much more powerful and have continued to develop and augment their capacities into the 21st century. As they have done so new experimental possibilities—for instance fast UHV, and then ambient pressure, X-ray photoelectron spectroscopy (XPS), emission spectroscopies (XES), and total X-ray scattering- have been added to the canon of available probes. The 21st century has subsequently seen a proliferation of third-generation resources around the world with further gains in performance being gleaned along the way. Modern third-generation synchrotrons therefore provide an unrivalled capacity for the interrogation of catalytic systems of all types, as they are working, and on kinetically relevant timescales.

As such they have become ideal resources for the development of operando philosophy that Banares and co-workers introduced in 2002 [71,72] as a method to properly establish relevant Quantitative Structure-Reactivity relationships (QSARS) in catalysis: structurally direct X-ray techniques being highly complementary partners to global assessments of catalytic performance (e.g., MS) or laboratory based spectroscopies sensitive to chemical speciation (e.g., infrared (DRIFTS [73–79], transmission IR [80,81]) or Raman spectroscopies [82–87], for reviews see [88–91]).

These vibrational spectroscopies, along with variants that have yet to be coupled with X-ray techniques such as reflection absorption infrared spectroscopy (RAIRS), photo-elastic modulation infrared reflection absorption spectroscopy (PEM-IRRAS), and sum frequency generation (SFG), offer varying degrees of surface sensitivity and the ability to identify adsorbed species that, by and large, the bulk sensitive X-ray techniques cannot. Equally, however, and with some caveats, these methods do not directly address the structure of the particles of surfaces upon which the adsorbates exist whereas techniques such as X-ray scattering and X-ray absorption do this in a very direct manner. As such, the combination of vibrational spectroscopies with X-ray techniques, when possible, is extremely desirable in studies of catalysis as it leads to an enhanced possibility to view the working system in a more holistic manner [88–91]. Further, as we shall see the evolution of these X-ray methods has, in some cases, led to the possibility of inducing surface sensitivity (for instance in the surface variants of X-ray scattering or by adopting specific methods of data collection and a posteriori data treatment methods) where ordinarily there is none.

Indeed, the fusion of the operando methodology with the possibilities that modern day, synchrotron X-ray techniques, with or without the parallel application of adjunct probes, might be considered a fine example of the sort of interdisciplinary synthesis of the type that Langmuir hoped for back in 1915 [12] when he wrote:

> *"As yet, apparently, very few chemists have awakened to the wonderful opportunities that lie open to them on all sides when they attack the problems of chemistry by the new methods which the physicists have developed. The physicist on the other hand, in gradually beginning to extend his investigations into the field of the chemist and we may hope, if the chemist will meet him but halfway, that there will be a new physical chemistry which will have an even more far-reaching effect on our ordinary chemical conceptions than has the physical chemistry of the last decades."*

One might only hope that he might have approved of what the last two decades of X-ray based research, which I shall now try to outline in as chronological manner as possible, has allowed us to

learn regarding the mechanisms and structures that underpin the platinum catalyzed oxidation of carbon monoxide that he first studied just over 100 years ago.

2. Fast X-ray Methods as Applied to the Study of CO Oxidation over Pt Surfaces and Nanoparticulate Catalysts

Typically, our first example [92], whilst it does revolve around the application of X-rays to study the dynamic behavior of simple Pt catalysts during CO oxidation, involves neither Al_2O_3 (the support is SiO_2), or the use of a synchrotron! Indeed, it predates the term "operando" by almost ten years. However, given the subject of this review, it would be remiss of me not to include what is an elegant experiment; one that crosses the materials and pressure gaps mentioned above, and one that might set the scene for exploring how far the possibilities have come as a result of the continual development of synchrotron radiation sources since 1994.

2.1. Fast X-ray Diffraction (XRD) and Debye-Analysis of Oscillations CO Oxidation over EuroPt-1

As has been already noted, as of the early 1970s, oscillatory behavior in the notionally simple CO + O_2 catalysis over Pt in many different forms had become an object of much experimental and theoretical work [30–68]. Early measurements on supported catalysts were entirely based upon global observables such as temperature and the amount of CO_2 produced. As such, they could form the basis for mathematical descriptions of the oscillatory behavior but not give any precise insight as to the fundamental mechanisms that lay behind them. The progressive work of Ertl and co-workers [47,48,52,60–68] then slowly gained windows into this behavior using probes as PEEM, LEED, and ultimately STM, to reveal a range of possible sources of the oscillatory behavior for well-defined Pt surfaces working at low pressures: whether these same sources were at work in real supported Pt catalysts was still very much a mystery and the subject of much conjecture.

Three proposals were considered as most likely in the case of supported Pt catalysts: a model based upon adsorbate induced reconstructions of the low index faces exposed to the reactants at the surfaces of the supported Pt particles [42,48,50–52,60]; "the carbon" model, wherein carbon, resulting from the dissociation of CO could accumulate on the surface, causing transient deactivation before being cleared away to reactivate the catalyst in the presence of oxygen [56–59]; and, the redox model wherein periodic switching of the Pt between metallic Pt^0 and oxidic states, was the source of the splitting of the catalysis into high reactivity and low reactivity states [39–41,43,44,49].

To address this problem in a structurally direct manner Hartmann, Imbihl, and Vogel [92] constructed a reaction cell (shown in Figure 1a) that could fit within a Guinier X-ray diffractometer and be used to monitor the XRD patterns (within the range of reciprocal (Q ($Å^{-1}$) or 2θ degrees) space permitted by the design, the detection system, and the energy of the X-rays used (Cu Kα)). The X-rays were passed through the thin pressed sample (a 6.4 wt % Pt/SiO_2 (Europt-1) catalyst) mounted within the apparatus. The apparatus could be evacuated to 10^{-7} mbar, and heated to 1000 K whilst gases appropriate to the investigations required could be flowed over the pressed sample. The amount of reciprocal space that this set up could sample was limited but sufficient to observe the behavior of the Pt(111) reflection arising from the metallic Pt nanoparticles present initially in the catalyst.

Figure 1b outlines the experimental protocol in terms of the overall integrated intensity of the Pt(111) reflection and the sample temperature. It can be easily observed that after the preparatory procedure, and following cooling under the catalytic gas flow, the system eventually enters into periodic oscillations in both the sample temperature and the integrated intensity of the Pt(111) Bragg reflection. It can also be seen that the variations in sample temperature and the intensity of the Bragg reflection are in anti-phase (the phase angle of the changes in XRD intensity being 120 degrees in front of the temperature).

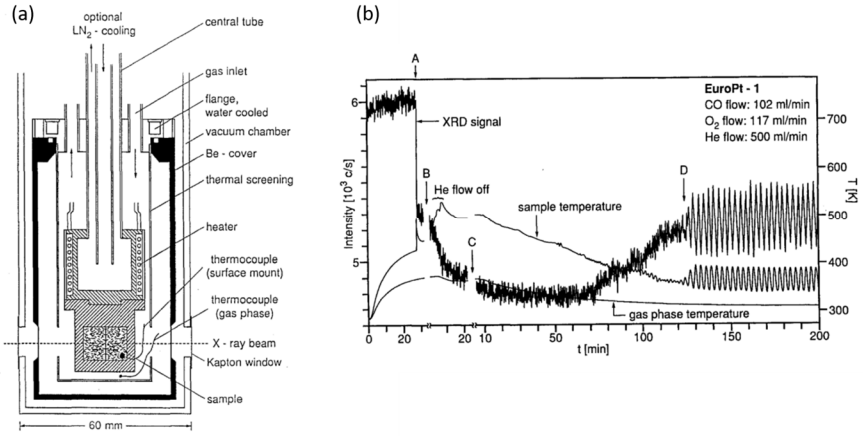

Figure 1. (**a**) Schematic of the apparatus used in [92] to permit in situ laboratory based time resolved X-ray diffraction measurements of a Pt/SiO_2 catalyst. The label (A) indicates the point where catalytic ignition occurs, (B) indicates the point where the He flow was stopped. (**b**) Temporal evolution of the catalysts as observed from the viewpoint of the integral intensity of the Pt(111) Bragg reflection from the SiO_2 supported nanoparticles. Reproduced with permission from *Catal. Letts.* **1994**, *28*, 373–381 [92]. Copyright 1994, Springer International Publishing AG.

Figure 2 then shows the results of a Debye (shape) analysis [93] of the diffraction patterns obtained at various points within the experiment shown in Figure 1b. This analysis is based on modelling the Bragg reflection in terms of face centred cubic (fcc) cubo-octahedral Pt particles of differing sizes. What is found from this exercise is that at certain points in the sample history the Pt(111) Bragg reflection can be adequately modelled using only contributions from metallic Pt phase, whereas at other points this is not the case. At these points in time contributions from oxidized forms (specifically PtO and Pt_3O_4, but not PtO_2) of Pt are required to describe the shape of the Bragg feature.

Whilst the interpretation of shape and intensity changes in single Bragg peaks fraught with potential issues, especially in the case of a nanoparticulate system, the superposition of a number of observable elements within this experiment forces the conclusion that the oscillatory behavior observed in this system is driven by redox events occurring on the Pt particles. For sure this experiment does not, of itself, really specify the oxidized structures involved and elements of the analysis could be questioned. However, the broad conclusions of this first attempt to bridge the materials and pressure gaps using a structurally direct X-ray technique on timescales commensurate with processes under study are unavoidable.

Perhaps most importantly of all this is the first structural study that pushes the globally accepted LH mechanism toward the inclusion of an MvK component to explain the oscillatory behavior in a supported catalyst system on the basis of a probe that addresses catalyst structure directly: the LH paradigm does not formally admit the possibility of a second Pt phase that is not Pt^0, being involved.

As we shall see, despite many possible reservations, these results have been, to varying degrees, validated and extended as we have learned to combine the operando philosophy with the ever increasing power of synchrotron X-ray techniques. Indeed, this early experiment could be regarded as one of the direct ancestors of some of the studies that shall be described later on in this review, especially those approaches that have exploited the scattering of high energy X-rays (vide infra) that the large third-generation synchrotrons are peerless sources of.

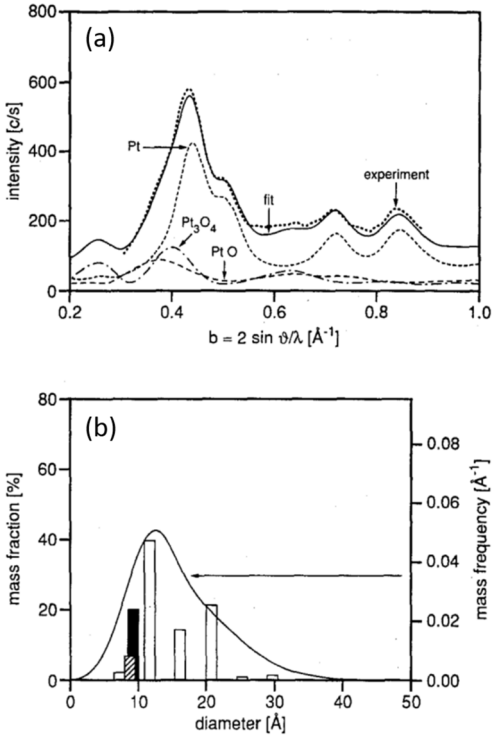

Figure 2. (**a**) The intensity profile of the Pt(111) Bragg reflection measured at point (B) in Figure 1b and showing that a reasonable fit (solid line) to the reflection requires the use of components due to oxidized phases of Pt. (**b**) The cluster size distribution use to derive the fit shown in (**a**) giving the mass fraction of the respective components used: fcc Pt nanoparticles (open bars) PtO (solid black), Pt_3O_4 (dashed bar). Reproduced with permission from *Catal. Letts.* **1994**, *28*, 373–381 [92]. Copyright 1994, Springer International Publishing AG.

2.2. A Transient Approach to CO Oxidation over Pt/Al_2O_3 Catalysts Using Fast (Energy Dispersive) X-ray Absorption Spectroscopy (DXAFS)

Some ten years after Hartmann et al.'s [92] ingenious approach to trying to uncover what lay behind the oscillatory behavior observed in compositionally simple supported Pt catalysts Carlsson et al. [94] were the first to apply the relatively new (at the time) possibility of time resolved XAFS to the study of CO oxidation by supported Pt catalysts; they also correlated the Pt L_3-edge XAFS with infrared spectroscopy albeit in separate, laboratory based, experiments.

The two possibilities for "single shot" time resolved XAFS—quick scanning (QEXAFS) and energy dispersive EXAFS (DXAFS or EDE) had appeared sometime beforehand [95,96] and had been applied to catalysts and catalytic processes previously, (EDE/DXAFS [97–100], QEXAFS [96,101–104], review [96]) but not to this particular problem; and though the first demonstration of an approach that permitted the parallel application of DRIFTS and time resolved EXAFS appeared in the same year [73], it would be some few more years before this possibility became available for catalysis users at a synchrotron beamline.

The experiment of Carlsson et al. [94] made at ID24 at the third-generation ESRF, was simply to subject the Pt catalyst to a step change in feed composition (CO to O_2), and to observe the effects this had on the catalysis using either combined DRIFTS/MS or Pt L_3-edge XAFS/MS and then to combine both sets of experiments to try and see further into the behavior of the system from the points of view of the structure of the Pt phase, the IR visible surface speciation, and the overall turnover of CO to CO_2. Their aim was to address, as quantitatively as possible, the formation of any oxidic component in the Pt and the effects this might have on CO oxidation above and beyond what might be expected from the basic LH mechanism. We might also note that in the real world application of Pt in auto

exhaust catalysts rapid changes in redox environment during operation (so called Lambda cycling) are intrinsic to operation, and that there had been reports for this catalytic reaction that enforcing periodic redox operation may improve the net performance of the catalyst [105–107].

Figure 3 summarizes some of the results of this exercise, these being: Figure 3a,b, the observed variation in the Pt L_3-edge XANES during perturbation of the catalyst at two temperatures; Figure 3c, the associated variations observed in MS (top panel) and for the energetic position of the Pt L_3-edge (bottom panel); and Figure 3d and Arrhenius plot derived from both time resolved DRIFTS and time resolved XAFS measurements.

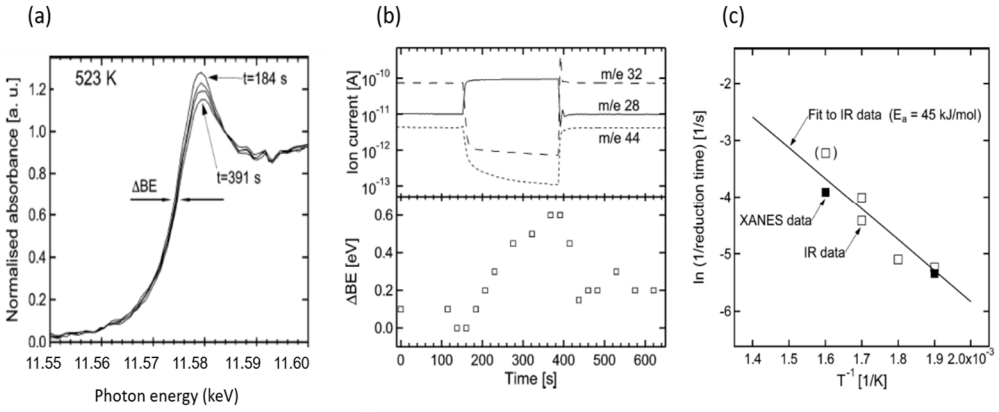

Figure 3. (**a**) Pt L_3-edge energy dispersive X-ray absorption spectroscopy using the near-edge (XANES) derived during the switching from flowing CO/Ar to O_2/Ar feeds at 523 K over a 2 wt % Pt/Al_2O_3 catalyst. (**b**) Correlation of the response in MS of O_2 (32), CO (28) and CO_2 (44) (top panel) with the binding energy shift observed in the Pt L_3-edge (bottom panel) measured at 523 K during a switching event. (**c**) Arrhenius plots for the reduction of 2 wt % Pt/Al_2O_3 under 1% CO/Ar as the a flow of O_2/Ar is switched from 5% in Ar to 0 derived from both infrared (IR) and Pt L_3-edge XANES data. Reproduced with permission from *J. Catal.* **2004**, *226*, 422–434 [94]. Copyright 2004, Elsevier.

The Pt L_3-edge during these experiments shows two subtle, but measurable, changes during these transient experiments: variation in the intensity of the Pt L_3-edge white line and the energetic position of the edge itself (0.6 eV at most). The overall shape of the Pt XANES is undeniably metallic and these changes are indicative, within certain approximations—as the detailed structure of the Pt L_3-edge XANES can also be indicative of changes in size [108–110], or indeed morphology [111]—of the oxidation of the surfaces of nanoparticles during the switch from a new reducing (CO) to net oxidizing (O_2) environment.

Once more, therefore, a process that is not admitted by the basic LH mechanism, and that is not required to understand the same reaction over Pt single crystal surfaces at low pressure is observed. However, it may be noted that, whilst the behavior of the Pt L_3-edge white line is exactly that which we would expect in switching from an O_2 containing to a CO contain feed, and consistent with redox phenomena, the augmentation of the binding energy edge position is not: upon reduction the Pt L_3-edge should move to lower binding energies not higher. This curious behavior could have a number of sources, not least of which may be the method itself; the estimated energy resolution of the experiment at the Pt L_3-edge being at best (assuming an absolute stability of the dispersive optics and a zero effect on this due to the passage of the polychromatic beam through the sample itself), around 1.4–1.74 eV [94]. However, as will be shown later using a high resolution spectroscopic approach (Section 2.5), such an effect could be caused by the effects on the XANES structure of the adsorption of molecular CO on the reduced Pt nanoparticles.

However, this observation aside, the work of Carlsson et al. results in some sort of estimate of the activation energy for the redox process involved—albeit predominantly from the IR measurements in

this case—was also arrived at and found to be acceptably consistent with that previously derived for the CO induced decomposition of oxidized Pt in a Pt powder [94].

One might note that, at this point in time, this synchrotron based dispersive XAFS investigation, whilst producing informative data on timescales required to extract kinetic data, was restricted to the analysis of Pt L_3-edge XANES rather than also permitting a direct structural analysis using the Extended X-ray absorption fine structure (EXAFS): this in spite of the fact that it had previously been demonstrated that this could be achieved using dispersive EXAFS (measured at much less powerful second-generation sources) [100,101].

The reasons for this discrepancy are many fold but suffice it so say that in approaching the development of such techniques, and their application to the study of processes *in operando*, raw power is but one of a number of considerations that need be taken into account [112,113]. As we shall see later on such limitations have now been largely overcome as a result of the continued developments of Quick scanning monochromator systems [114,115] that have taken place in the intervening years.

2.3. A Return to Pt Single Crystals: Operando Surface X-ray Diffraction (SXRD) at Elevated (Ambient) Pressures and the Role of Pt Surface Oxides

The previous examples have shown that the application of X-ray techniques, diffraction (XRD) or X-ray absorption spectroscopy (XAFS), had the potential to provide new windows into some of the complexity that lies beneath the apparently simple conversion of CO to CO_2 using O_2 over Pt. The two previous cases managed, using time resolving X-ray methods, to bridge the materials and pressure gaps that lie between the seminal works of Ertl and co-workers concerning low index Pt surfaces and the real world application of high area catalysts to this problem. They showed that elementary processes exist in real world catalysts that are not formally admitted by the basic LH concept, or observable in the low pressure/single crystal Pt situations that had dominated understanding of this catalysis in the 1980s and 1990s, specifically the presence of redox phenomena in the Pt phase under reaction conditions.

However, though alerting us to this fact in structurally direct manners, these studies were not really able to detail the nature of the structures involved and how they relate, quantitatively, to rates of catalytic reaction. However, only a year after the publication of our last example, an approach was demonstrated that achieved this objective to some good degree. To do so, a return the study of Pt single crystals was required, but one that was, by 2005, able to bridge the pressure gap and to provide a time resolved and structurally direct window into CO oxidation through the application of Surface X-ray diffraction (SXRD) at the ID 03 beamline of the ESRF [116].

A schematic of the apparatus developed for these studies is given in Figure 4 [117]. It is arranged such that UHV preparation of a single crystal sample could be achieved before the reaction chamber was filled with gas to ambient pressure and used as a batch reactor. The use of a cylindrical Be section permits the transmission of the X-rays as is required (at grazing angles of both incidence and reflection) for the SXRD experiment. We note that subsequent to the inception of this type of apparatus this idea been progressively refined, (into a UHV-elevated pressure flow reactor system [118]) that has eventually been commercialized [119].

At this point it is also worthy of note that this is a relatively large volume batch reactor that cannot, be considered as an ideal continuously stirred tank reactor (CSTR, see for instance [15]). Therefore, its ability to quantitatively link changes in surface structure with reaction kinetics will be ultimately limited by processes of diffusion of the product and reactant gases to and from the Pt surface. In this respect, that recent research has very elegantly shown that, in batch situations such as were used in our next example, diffusion limitations must be seriously considered in studies of this nature [120].

That said, in the examples that follow this limitation has not been found to prevent valid and highly insightful correlations with structure and global reactivity. Moreover, subsequent evolutions of sample environment to much lower volume flow systems (e.g., [118,119]) has gone someway to alleviating this potential bottleneck when considering quantitative kinetic evaluations.

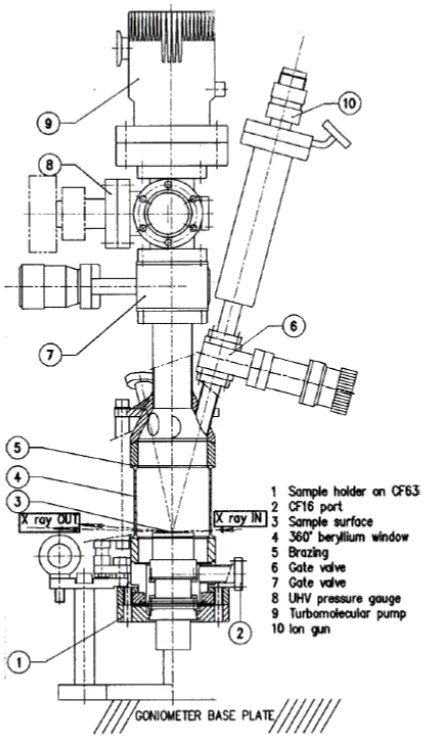

Figure 4. Schematic of the apparatus developed by Bernard et al. [114] for UHV preparation of single crystal surfaces and then Surface X-ray diffraction measurements at elevated pressures (<5 atmospheres) in batch reactor mode. Reproduced with permission from *Rev. Sci. Instr.* **1999**, *70*, 1478–1480 [114]. Copyright 1999, American Institute of Physics.

Figure 5 then summarizes the results of applying SXRD using this experimental apparatus to firstly (Figure 5a) the two differing Pt surface oxides uncovered through this approach and then (Figure 5b) the reactive relationship between the surface phases present and CO_2 evolution as either CO is pulsed into a reaction vessel that has previously been back filled O_2, or the reactor filled with a reactive CO/O_2 mixture [116].

SXRD reveals that two surface Pt-oxides may exist on Pt(110) depending on the conditions applied: an incommensurate oxide that essentially is a slightly distorted, single, α-PtO_2 layer (*c*-axis parallel to the surface) that sits upon unreconstructed Pt layers; and a commensurate (1×2) oxide that could not be observed in the absence of CO and did not correspond to other known (1×2) reconstructions of Pt(110) previously at elevated O_2 pressure observed using STM [121].

It can be seen (Figure 5b) that when the incommensurate PtO_2 layer is prepared under a back pressure of 500 mbar O_2 at 625 K, and then subjected to pulses of CO, it immediately reacts to produce CO_2, before being reformed by the excess O_2 remaining in the reactor. The gradual attenuation of the diffraction from this phase was ascribed to the induction of increased disorder (roughening) of the surface as had been previously observed using in situ STM [122]. Finally, a much longer CO pulse rapidly removes the PtO_2 layer to yield a metallic surface that shows a reduced rate of CO_2 production until the CO is switched out. When this happens the rate of CO oxidation recovers and, after a delay, the Bragg reflection due to the PtO_2 layer return is seen to reappear.

If, instead of focusing detection on a particular point in reciprocal space (to follow specifically the behavior of the hexagonal, incommensurate PtO_2), the range of reciprocal space was extended and the reaction followed again, this time starting with a CO/O_2 ratio of 1:10, then we obtain Figure 5c. This shows that eventually the highly reactive incommensurate PtO_2 phase does form, but only after ca. 20 min after the start of the reaction; and not before it is preceded by the appearance of another phase, the reflections of which correspond to the new commensurate (1×2) layer.

Two reactive (more reactive so than the metallic surface) surface oxides where therefore shown to be formed over Pt(110) at elevated pressure, and net oxidizing conditions.

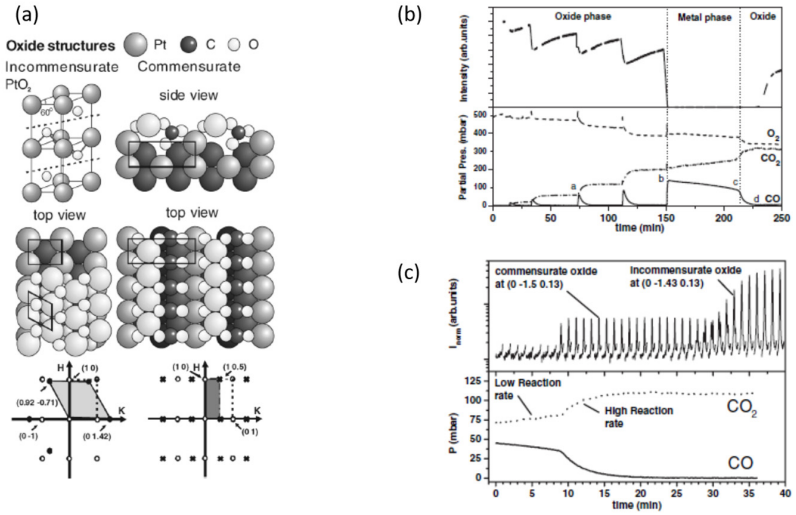

Figure 5. (**a**) The surface oxides (incommensurate and commensurate) identified by Ackermann et al. [116] to be to present during elevated pressure CO oxidation over Pt(110) using operando SXRD in the apparatus shown in Figure 4 and in both real and reciprocal space. (**b**) Correlating the mass spectrometric responses observed during CO pulsing into the O_2 backfilled reaction vessel with the X-ray diffraction intensity measured at a position in reciprocal space corresponding to the commensurate α-PtO_2 monolayer structure (0, 1.42, 0.5—see also bottom panel Figure 5a at 625 K. (**c**) Correlation of two regimes of CO oxidation catalysis with X-ray diffraction intensity measured at two positions in reciprocal space corresponding to the commensurate and incommensurate oxide structures shown in 5a and also at 625 K. Reproduced with permission from *Phys. Rev. Letts.* **2005**, *95*, 255505 [116]. Copyright 2005, American Physical Society.

The commensurate oxide only forms in the presence of significant amounts (though not too much) of CO and is eventually replaced by the incommensurate PtO_2 surface oxide when the CO/O_2 ratio diminishes to below ca. 1/50–1/100.

This ground breaking experiment therefore demonstrated that the pressure gap was indeed a very important one to span. This work reinforces and extends the conclusions of two studies already given, and other measurement/suggestions made on the basis of experiment or theory in the 1980s, that in many circumstances the LH model was inadequate a descriptor of CO oxidation by Pt under realistic conditions and that the MvK was more appropriate in many senses. This work also showed that a time resolving third-generation synchrotron approach allied to a commitment to an operando methodology could be a structurally deterministic and very powerful combination: one that was also capable of revealing elements of the surface chemistry at work—specifically the nature and reactivity of the transiently observed (1 × 2) surface oxide—that would have been impossible to study by any other means prior to this.

As a caveat we might add that, as with all experiments based upon Bragg diffraction, these sorts of studies can only yield information regarding phases that have domain sizes of sufficiently significant dimensions to yield detectable Bragg peaks. Therefore, these experiments are, to all intents, blind to the role that low Z adsorbates and any highly disordered phases might have in the catalysis being studied. In addition, surface molecular speciation is in general very difficult to be precise about when using most X-ray techniques, hence the evolution of experiments that couple X-ray methods with techniques (e.g., IR, Raman, [73–91]) that can directly address such speciation.

Whilst, as will be seen (vide infra), some assertions regarding surface disordering that may accompany the formation of ordered surface oxide phases can be derived from these sorts of

experiments, this is a fundamentally limiting factor to the use of methods founded upon Bragg diffraction, that techniques such as EXAFS, and the rapidly emerging area of total X-ray scattering/PDF studies (see Section 2.7), do not suffer from.

Lastly, with regard to this example, we note that DFT calculations regarding the structure of this commensurate (1 × 2) layer, and briefly discussed in [116] suggest, as do the circumstances under which it was observed, that this layer requires stabilization by and element derived from CO. The DFT suggested that this stabilizing element may well be a carbonate (CO_3^{2-}) species. As far as the author is aware, this has yet to be confirmed, but this is the first time that the possibility of a carbonate species was specifically invoked as a possible reactive intermediate in CO oxidation over Pt. As we shall see later, Pt carbonates might be the source of a new way to think about CO oxidation at low temperatures using Pt catalysts.

However, before we move on to other X-ray techniques have been applied to the CO oxidation over Pt surfaces and catalysts we might also consider how this operando approach views the same events occurring over Pt(111); a more densely packed, lower energy surface that has a much greater resistance to adsorbate induced surface reconstruction. Indeed, this was the surface that had been studied using STM in the low pressure regime by Ertl and co-workers as, "(it) does not involve reconstructions and has been demonstrated to follow the LH mechanism" [68]. Later theoretical work [123] had gone on to suggest that a mixture of CO covered and metallic Pt(111) and it's oxidized (α-PtO_2) counterpart should be rather active for CO oxidation as a result of phase boundaries creating new sites for reaction subject to significantly lower energetic barriers.

Figure 6a shows the results obtained during oxidation of the Pt(111) film using oxygen at elevated pressure (20 mbar O_2) and temperature (640 K) [124]. Two processes are revealed from these two measurements. Firstly, the formation of a surface oxide phase is observed that is consistent with the formation of (again) a surface α-PtO_2 phase previously shown [125,126] to be comprised of a bilayer of distorted (compressed in the *c*-axis) PtO_2.

However, accompanying the formation of the oxide observed in the H-scan, the H and L-scans both also show that, the Pt(111) surface below the growing oxide layer roughens considerably. In addition, it was found that there is a distinct pressure dependence to the oxide formation: the oxidation of this surface to yield a surface oxide could only be achieved at 640 K using pressures of O_2 > 10 mbar and that the thickness of this layer, as indicated from the diffraction, was somewhat larger (2 nm rather than 0.4) that reported by Ellinger et al. [125].

The reactivity of the surface oxide layer was then followed at 430 K (experimentation at 640 K leading to a reaction too fast to study through sequentially collecting "*H*-scans") by replacing the pure O_2 environment with a (still net oxidizing) mixture of 3 mbar CO and 18 mbar O_2 (O_2/CO = 6). The system was then followed as it developed using repeated H scans and both mass spectrometry and total pressure measurements (Figure 6c,d).

It can be seen that as soon as the CO is introduced, or at least within the time it took to complete an "*H*-scan", that the intensity of the Bragg peak (Black curve, H = 1) due to metallic Pt jumps up and (more difficult to see, H = 0.89) that from the PtO_2 surface oxide disappears. In other words, the oxide layer has been rapidly removed by the introduction of CO and the surface returned to Pt(111) with its surface order (less roughening) largely restored. At the same time the CO_2 signal jumps in MS before settling down to a slower and monotonic rate (turn over frequency ca. 10 s^{-1}).

This state of play continues essentially unchanged for ca. 2000 s. During this time the stoichiometry of the CO/O_2 mixture is changing as CO is slowly removed (best seen in the measurement of total pressure (Figure 6c, blue curve)) and the gas phase is becoming more oxidizing in nature. After ca. 2000 s the total pressure measurement indicates an increase in the velocity of the CO oxidation reaction that accelerates (to an eventual TOF ca. 100 s^{-1}) as the O_2/CO ratio increases beyond ca. 30. Eventually, beyond this point, the diffraction reports both the reappearance of the surface oxide and a re-roughening of the Pt.

This again shows just how important the pressure gap is, both in terms of the formation of the surface oxide on Pt (111), and the subsequent reactivity it shows as a function of temperature and the stoichiometry of the gas mixture applied. The authors note that at 430 K an O_2/CO ratio of 30 is required for the active (oxidized Pt) to form whereas this critical ratio decreases to just 1 between 661 and 717 K and can drop as low as 0.7 at even higher temperatures.

SXRD [127] was also successfully used to show that, at elevated pressures, and around stoichiometric reaction conditions ($1.9 < CO/O_2 < 2.2$), monoatomic steps on a vicinal (997) Pt surface can have a distinct role to play in determining the reactivity in CO oxidation.

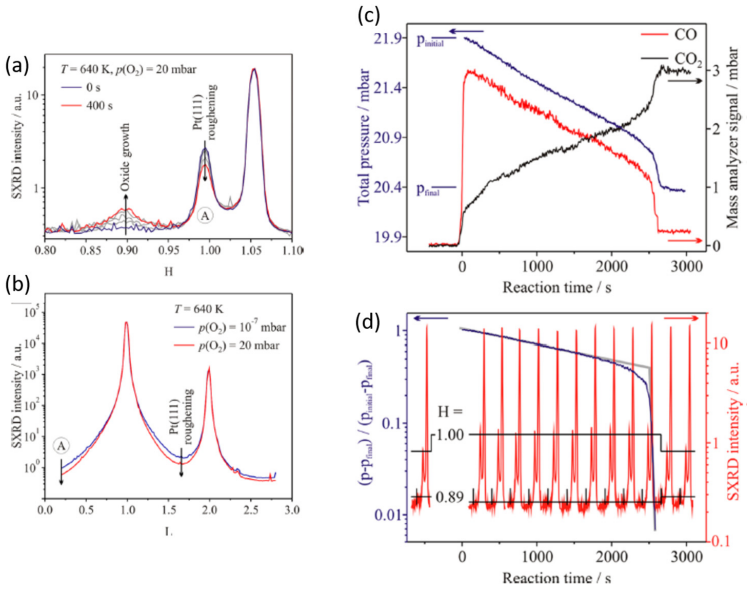

Figure 6. (**a**,**b**) Oxidation of the Pt(111) surface at 640 K as viewed by SXRD in two crystallographic directions (H and L) of reciprocal space showing both the Bragg reflection due to the growth of a α-PtO_2 surface oxide (**a**) and the effects due to the roughening of the underlying Pt surface that accompanies the formation of the surface oxide; (**c**) mass spectrometry during CO oxidation at elevated pressure (O_2/CO initial = 1/6) as a function of time; (**d**) "*H*" scans (red) collected during the CO oxidation experiment shown in (**c**) along with the variation of total pressure of the system (blue) and the two separate kinetic regimes for CO oxidation (grey lines) observed as a function of changing O_2/CO ratio. Reproduced with permission from *J. Phys. Chem. C* **2013**, *117*, 9932–9942 [124]. Copyright 2013, American Chemical Society.

Figure 7a shows, how SXRD provides a means to be sensitive to the presence of steps on the vicinal surface when a 2D imaging detector (Maxipix) is employed to measure the diffracted intensity of the X-rays. Figure 7b then shows how integrated SXRD at fixed K and L but variable H, is observed to vary as a function of the composition of 200 mbar mixtures of CO and O_2 ($2 < CO/O_2(R) < 19$) measured at 763 K. Corresponding measurements of reactivity (as a function of T and *R*) established that the maximal turnover numbers of CO attainable in this system were arrived at as of ca. 723 K and an $R = 2$ (the stoichiometric condition).

What can be seen is that, as *R* is varied either side of the stoichiometric value of 2, scattering due to the initially regularly spaced array of steps disappears. In addition, it can be seen that the starting pattern, indicative of the step density and order of the starting vicinal surface, can be largely recovered when the composition of the feed is returned to the stoichiometric value. Figure 7c then shows the dependence of the SXRD and the balance between terraces and steps on the composition of the feed ($1.9 < R < 2.2$) around the stoichiometric ($R = 2$) to show just how sensitive, and how fluid, the structure of the stepped Pt surface is to small variations of the feed composition at these elevated temperatures and pressures.

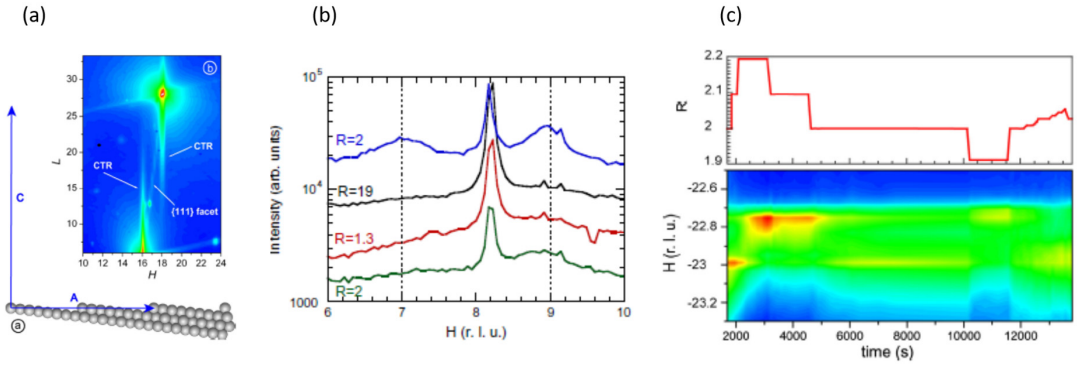

Figure 7. (**a**) Schematic illustration of the origin of diffraction features from the vicinal (997) Pt surface along with an Maxipix image of the diffraction obtained from the fresh surface showing the relevant crystal truncation rods (CTR) and scattering from the 111 surface facets. (**b**) Effect of pressures (200 mbar) of O_2 and CO at different stoichiometric ratios (R) on the Surface X-ray diffraction (SXRD) collected at fixed K and L but variable H, and at 763 K. (**c**) Temporal dependence of the SXRD as a function of small variations in (R) ($1.9 \leq R \leq 2.2$) showing the effects of the reaction environment on the balance between steps and terraces on the Pt(111) surface. Reproduced with permission from *J. Catal.* **2014**, *309*, 33–37 [127]. Copyright 2014, Elsevier.

As such, in addition redox to processes, that under net oxidizing conditions at elevated pressures ultimately lead to the formation of new and reactive surface oxide phases not observed in the low pressure regime, we can now see that the morphological response of stepped metallic Pt surface to mixtures of CO and O_2 is also a sensitive function of the composition of the gas phase. Either side of the stoichiometric (CO/O_2 ($R = 2$)) the density of ordered and well defined arrays of monoatomic steps is grossly compromised in a manner that can be related to overall CO turnover. The presence of ordered steps under these conditions must therefore be seen as central to obtaining maximal CO turnover, and that excess levels of either CO or O_2, may exact a considerable toll on the order of the surface when present in the gas phase at sufficient pressures.

2.4. Ambient Pressure XPS: The Relative Reactivity of Differing Surface Oxides in CO Oxidation over Pt Single Crystal Surfaces

Along with XRD another technique, a standard for decades in many research laboratories, has also evolved and profited from the appearance and evolution of third-generation of synchrotrons: this is X-ray photoelectron spectroscopy (XPS), originally known as ESCA (Electron spectroscopy for chemical analysis). The discovery and development of this method in the pre-synchrotron age lead to another Nobel prize, to Kai Siegbahn, in 1981.

Unlike XRD or XAFS, XPS is not, a priori, structurally direct. Instead, binding energies (E_B) of electrons are used to determine the chemical state of the element from whence they came, just as can be done in XAFS using the near-edge (XANES) structure (see, for example, Sections 2.2 and 2.5). Broadly speaking, as a result of the lower energy core-levels generally excited in XPS (compared to, for instance, XAFS) XPS has a higher level of sensitivity to the chemical state of the elements under study. For instance, XAFS will generally use the Pt L_3-edge (E_B = 11.564 keV) whereas XPS will address the Pt M (4f) edges (E_B = 70–80 eV). Moreover, XPS can also be used to address the chemical nature of adsorbates such as CO and O through their K (1s) edges (ca. 287 and 531 eV, respectively) in the same experiment.

XPS is, therefore, very sensitive to chemical environment of an atom and can be used to discriminate between subtle differences in local structure that XAFS and XRD, by and large, cannot: for instance, whether a Pt atom is part of the "bulk" of a metal or present at the surface within an extended terrace or at the edge of the monoatomic steps, the behavior of which was the subject of our last example.

XPS also brings with it an intrinsic level of surface sensitivity—due to the underlying physics of electron atom interactions that also plays a part in making EXAFS an intrinsically short range probe of local bulk structure—that is not intrinsic to XRD and XAFS as a result of energy of the X-rays, be they incident or fluorescent, applied or detected, generally used in the latter two methods.

The down side is that, as XPS relies upon the direct detection of electrons, it remained for a long time a technique that required the presence of vacuum and could not be applied at the sorts of pressures that we would equate with real world catalysis and the operando philosophy.

Latterly, however, with advances in all sort of technological areas, this limitation has, within certain limits, been overcome; and when coupled to the intrinsic power of third-generation synchrotrons XPS has become amenable to elevated pressure operation with a time resolving capacity compatible with the operando study of catalytic processes [128–131].

Indeed, prior to our last example of the application of SXRD to look into the behavior of a stepped Pt surface as a function of the composition of a feedstock, a combination of operando STM and XPS, applied over several orders of magnitude of pressure, had been used to show that CO alone could reversibly manipulate stepped Pt surfaces [132]. In this work, the flat terraces present in (557) and (332) vicinal Pt surfaces were found to be significantly roughened into nanometre size clusters as a result of CO adsorption (at pressures as high as 5×10^{-1} Torr). As with our last SXRD example, removal of the CO, or a return to a low pressure regime, resulted in a recovery of the starting surface morphology. The driving force for this behavior was suggested to be the minimization of the strongly repulsive dipolar interactions, long known from infrared spectroscopy [133], that occur between adsorbed CO molecules adsorbed at high coverages on Pt surfaces and supported Pt catalysts.

More recently these XPS studies have been augmented to study CO oxidation catalysis on low index Pt(110) [134] and Pt(111) surfaces [135], just as we have seen, in the previous section, SXRD applied to this problem. Some exemplary results, highlighting aspects of this method, are shown in Figures 8 and 9 from the study of Butcher et al. [134] regarding CO oxidation at elevated pressures on Pt(110).

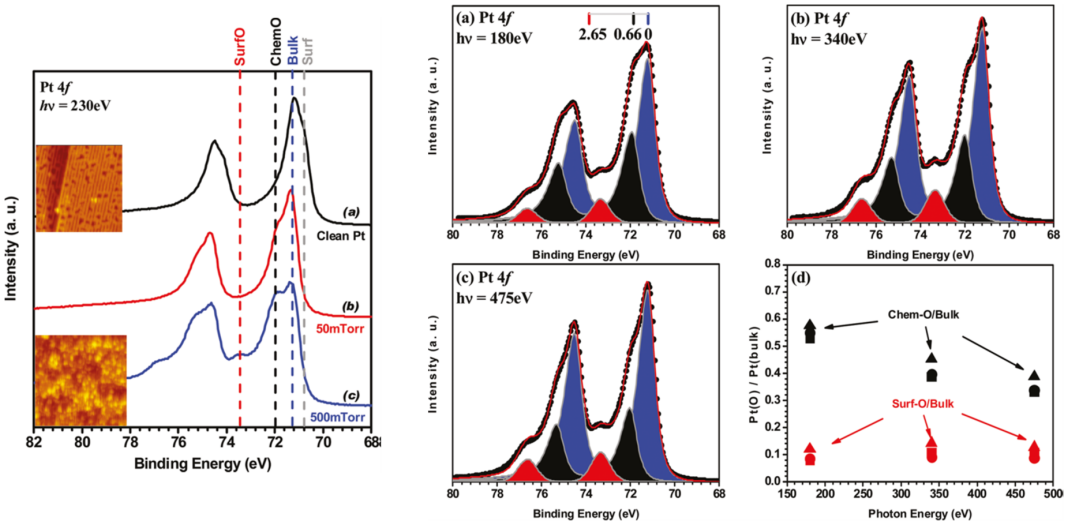

Figure 8. Left panel: Pt 4f X-ray photoelectron spectroscopies (XPS) spectra from clean Pt(110) (black), the obtained under 50 milli Torr O_2 (red), and 500 milli Torr O_2 (blue). Along with indications of the origins of the four components to the spectra. The insets show corresponding STM images of Pt(110) surfaces in two cases. **Right panels**: deconvolution of the Pt 4f spectra acquired as a function of incident X-ray energy (**a**–**c**). (**d**) The different behaviors exhibited by two of the states identified as associated with different Pt–O bonding states as a function of X-ray photon energy. The symbols ■, ●, and ▲ represent data obtained at 300, 373, and 473 K, respectively. Reproduced with permission from *J. Am. Chem. Soc.* **2011**, *133*, 20319–20325 [134]. Copyright 2011, American Chemical Society.

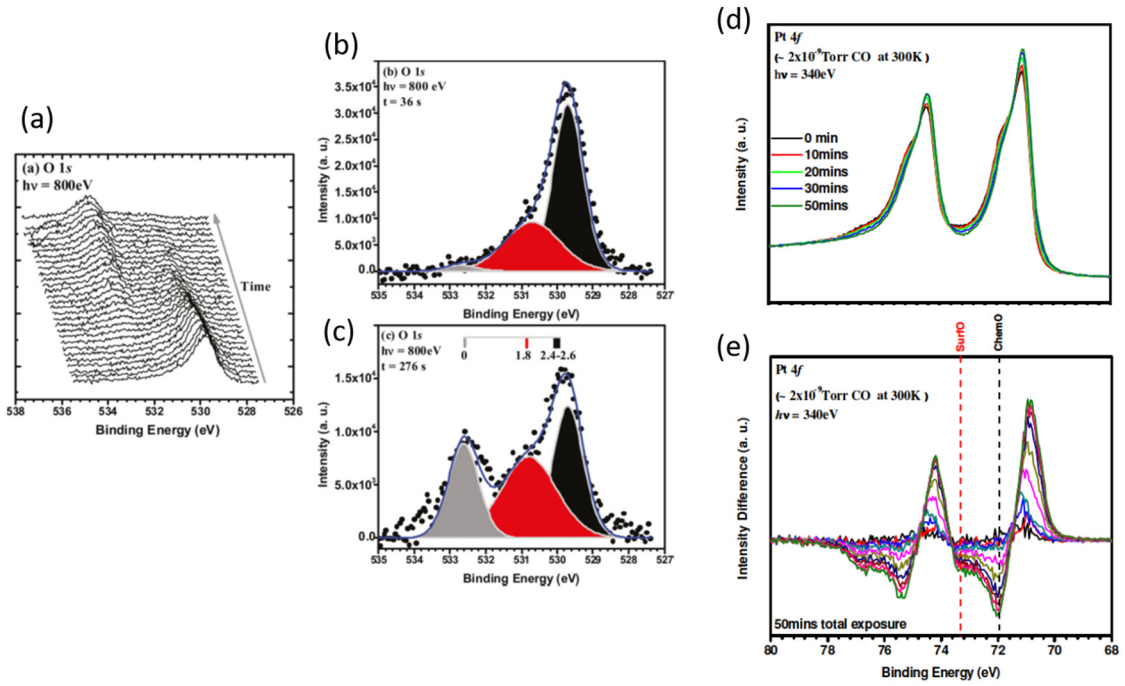

Figure 9. (**a**) Temporal variation in O 1s XPS during reaction of CO with a pre-oxidised Pt(110) surface. (**b**) and (**c**) Deconvolution of the O 1s at different states of the CO oxidation reaction into its three components at different time during reaction with CO. (**d**) and (**e**) Corresponding variations in Pt 4f XPS together (**d**) and (**e**) difference spectra made relative to the starting surface and shown the relative rates of remove of states due to chemisorbed O and those due to the removal of Pt surface oxide. Reproduced with permission from *J. Am. Chem. Soc.* **2011**, *133*, 20319–20325 [134]. Copyright 2011, American Chemical Society.

Figure 8 shows how XPS, using the Pt 4f photoelectron spectra, can be used to discriminate between Pt in different states, and then how one can use the surface sensitivity of the technique to differentiate between a signal that come from chemisorbed oxygen at the surface of the sample or from oxygen bound to Pt that corresponds to a surface oxide that has a certain projection into the surface itself.

The Pt 4f photoelectron spectrum can be deconvoluted into four separate components indicative of different Pt states: surface, bulk, surface attached to chemisorbed O, and coordinated to O but within a surface oxide. By raising the energy of the X-rays applied the kinetic energy of the photoelectrons ejected from the Pt surface increases. In the range of kinetic energy being probed (as dictated by the binding energy of the Pt 4f photoelectron) the inelastic mean free path of the electron is also increasing and contributions from Pt further into the surface become more significant as the incident X-ray energy is augmented. Therefore, a truly surface phase, such as chemisorbed O, will become less significant to the whole spectrum as the kinetic energy of the photoelectrons increases whereas a phase that has some extension into the bulk, will, within limits, show no relative change within the spectrum as the X-ray energy is varied.

As is evident from panel 8 (Figure 8d) the Pt state that has 0.65 eV greater binding energy than that from the bulk can be shown to be a genuinely surface (chemisorbed O) state using this method. On the other hand the Pt state whose binding energy is over 2.5 eV greater than the Pt bulk is not purely two dimensional but has a component that extends into the selvedge, i.e., a surface oxide the structure of which can be inferred through reference to elevated pressure STM (insets to the left panel in Figure 8) measurements or the SXRD (vide supra) previously considered (Section 2.3).

Figure 9 then shows how XPS permits a surface reaction to be followed from the perspectives of both the Pt substrate and the different types of oxygen present upon it as they are exposed to CO.

Figure 9a shows representative O1s spectra collected every 12 s from a Pt(110) surface covered in chemisorbed O alone and shows the removal of this O and its eventual replacement with adsorbed CO. Figure 9b,c show changes in the relative population of three O species (molecular CO, chemisorbed CO, and O existing within PtO_2 at 0, 1.8 and 2.4–26 eV relative binding energies) during CO exposure at different times. Panels (d) and (e) then show how the Pt 4f spectra also change during CO oxidation with changes due to the removal of the chemisorbed O and PtO_2 (−ve features) indicated in the difference spectra shown in (e) along with concurrent formation of Pt^0 (+ve features).

One might note that the pressure of CO used was only 10^{-6} Torr, most likely to slow the reaction down such that it might successfully be followed using XPS, and to avoid the possibility of X-ray induced artefacts in the measurement that the authors note (especially in the oxidation of the Pt surface itself), describe, and subsequently take action to avoid.

X-rays in general, but especially in this energy regime, have a significant potential to modify chemistry and this is an increasingly important source of error, especially when considering kinetics and reaction mechanisms and we shall return to this issue toward the end of this review.

In comparison to our previous examples this is experiment that is still somewhat rooted in the low pressure regime. Nonetheless, when addressing the reactivity of the surface oxide—a phase that can only be induced in Pt surfaces through using substantially higher pressure of O_2 (Figure 8)—this is a study of relevance within the operando paradigm; a hybrid approach that does ultimately permit the relative reactivity of different surfaces phases (chemisorbed O and surface oxide) for the conversion of CO to CO_2 over Pt.

In the case of Pt(110) the reactivity of the α-PtO_2 phase formed at elevated pressure under O_2, and chemisorbed oxygen was found, to be roughly similar, with the latter being found to be slightly more reactive though the difference is less than a factor of two at the temperatures used (270–275 K).

However, in a follow up study, using a Pt(111) [135] surface, rather than Pt(110), and remembering the rather different behaviors of Pt(110) and Pt(111) previously observed through the application of SXRD to CO oxidation over these surfaces, a rather different story was forthcoming from XPS. On the Pt(111) surface a second, PtO like phase was known from previous studies to be able to co-exist with both the α-PtO_2, and chemisorbed O phases [126]. All three phases of O adsorbed at Pt (111) were characterized using both XPS and polarization dependent O K-edge XANES [135].

These phases and their relative reactivity are indicated in Figure 10. Differences in reactivity that exist between, for example, the α-PtO_2 phase, be it present as a perfect film (red circles) or islands coexisting with a surface PtO phase (green squares), and chemisorbed oxygen existing on an unreconstructed Pt(111) surface (blue triangles), are considerably greater than found on Pt(110). It might be noted that this schematic shows a situation that would correspond to the classical LH mechanism (chemisorbed O) and two possibilities that would conform to MvK mechanisms (the PtO_2 and PtO) wherein the O to be reacted away by CO has become incorporated into the Pt surface to form a new reactive phase.

Finally, I note that in [134] the Pt 4f XPS from 1.5 nm Pt nanoparticles (NP) was also measured and compared with spectra derived from the α-PtO_2/Pt(110) case. The authors found that the binding energy of the component fitted to an oxidized branch of the Pt 4f spectrum showed the same binding energy as that derived for the α-PtO_2 surface oxide. They therefore concluded "the surface oxide formed under high-pressure oxygen exposure is similar to the NP oxide". We shall return to this issue further in the article.

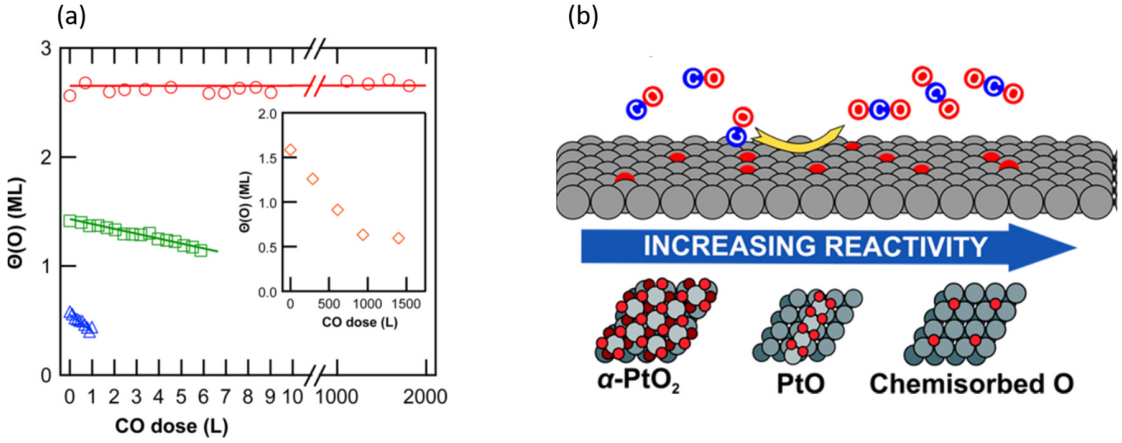

Figure 10. (**a**) Relative reactivity of different coverages of oxygen on Pt(111): red circles = a completely oxidized PtO_2/Pt(111) surface; green squares, a surface partially covered with a PtO_2/PtO surface oxides; blue triangles, a surface covered only with chemisorbed O only with no formation of surface oxide. (**b**) a schematic representation of the derived relative reactivity of the chemisorbed O, and PtO and PtO_2 surface oxides as derived from time resolved XPS. The complete (ca. 2.8 mL) α-PtO_2 structure corresponds to the does above ca. 1000 L as indicated in the inset to Figure 10. Both the chemisorbed O and PtO structure can be formed at lower coverages alongside domains of the α-PtO_2 surface oxide at lower doses and their relative reactivities assessed in a single shot using XPS. See [135]. Reproduced with permission from *J. Am. Chem. Soc.* **2014**, *136*, 6340–6347 [135]. Copyright 2011, American Chemical Society.

2.5. High Energy Resolution XANES (HERFD) Studies of the Nature of Pt Active in CO Oxidation over Pt/Al_2O_3 Catalysts

We have previously seen (Section 2.4) that energy dispersive Pt L_3-edge XANES yielded the first time resolving X-ray absorption based insight into CO oxidation over Pt/Al_2O_3 catalysts, and one that added directly to the mounting evidence of the time that the basic LH reaction mechanism needed to be revised to include redox phenomena that could substantially affect the Pt phase.

Of itself, however, a standard XANES measurement made at the Pt L_3-edge is held hostage to the limitations imposed upon it by the large core-hole lifetime inherent to the Pt once ionized. This causes an inherent broadening of the spectral features that reduces the level of insight obtainable from such a measurement.

As early as 1991, however [136], it was shown that this sort of limitation could be ameliorated by using a crystal detector to measure a specific fluorescence line and obtain an energy resolution less than that of the intrinsic core-hole width. Sometime later it was then demonstrated by De Groot and co-workers [137] that one could measure the Pt L_3-edge with a resolution of 2 eV, and in doing so could see details of the Pt L_3-edge structure that had lain previously hidden. However, to achieve this enhanced resolving power, a significant cost had to be paid in respect of the photon fluxes detetable in the fluorescence measurement. As such, more powerful sources and more efficient detectors were required to extend this approach to low loaded catalysts, rather than bulk materials, and then to achieve the time resolution required to following catalytic processes in a reasonable manner.

These duly arrived in the early 2000s and the enhanced resolving power of HERFD (high energy resolution fluorescence detection) spectroscopy entered into the canon of X-ray methods that could be used to address the behavior of supported metal catalysts in a study of supported Au systems [138]. In the same year, Safonova et al. [139] turned their attentions to Pt to show that the increased sensitivity to the structure of the Pt L_3-edge XANES could even be used to gain insight into the nature of CO adsorbtion at the surface of supported Pt nanoparticles.

Two years later the first example of HERFD being used to follow the development of a Pt catalyst engaged in the oxidation of CO followed [140]. Figure 11 shows the enhanced resolution obtained at the Pt L_3-edge (Figure 11b) that the HERFD method results in as compared to a traditional XANES measurement (Figure 11a) (see also Section 2.2) for a 5 wt % Pt/Al_2O_3 sample thermally treated under three different environments: H_2/He (473 K—black), helium (473 K—red) containing trace levels of O_2, and finally 1% CO in He (298 K—blue). Various elements of the XANES (for instance, the edge position and white line) are better resolved, both energetically and in relative intensity, in the HERFD spectrum, and in the case of the CO treated sample, the white line is resolved into two components where the conventional XANES resolves only one: calculations indicated that this could be explained by the predominant mode of CO adsorption being into a linear atop site, with the second newly observable XANES feature the result of d–2π* overlap for which the linear atop bonding geometry has the greatest metal to ligand charge transfer characteristic [140].

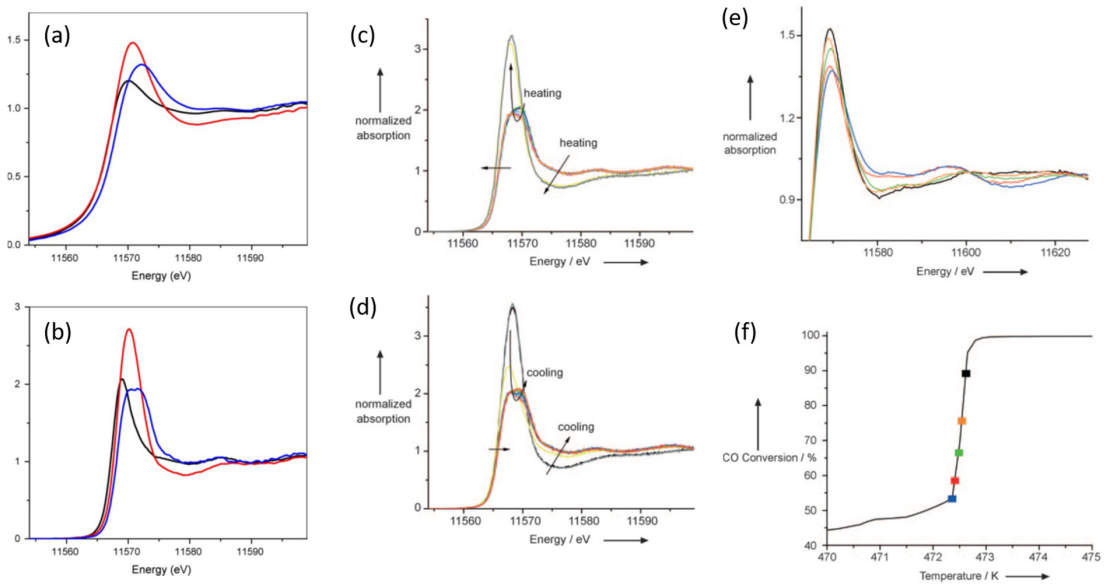

Figure 11. (**a**) Pt L_3-edge XANES from 2 wt % Pt/Al_2O_3 catalysts obtained using standard XAFS in transmission. (**b**) Pt L_3-edge XANES from supported Pt catalysts obtained using fluorescence yield HERFD XAFS. In both cases: red = He, black = H_2, and under 1% CO all at 473 K. (**c**) and (**d**) variation in time resolved operando Pt L_3-edge HERFD as a function heating (**c**) and cooling (**d**) under a $CO/O_2 = 1$ feedstock. (**e**) and (**f**) evolution of Pt L_3-edge HERFD during catalysts light off under a $CO/O_2 = 1$ flow. In this panel the color of the circles decorating the CO oxidation light off curve correspond to the coloration of the spectra shown in panel (**e**). Reproduced with permission from *Angew. Chem. Int. Ed.* **2008**, *47*, 9260–9264 [140]. Copyright 2008, John Wiley and Sons.

The middle panel in Figure 11 then shows HERFD derived during the heating and cooling a 2 wt % powder catalyst under a catalytic feed of a CO/O_2 ratio of 1, showing in detail the reversible changes in oxidation state and speciation of the Pt during this experiment. The last panel then shows in more detail how the changes in the Pt L_3-edge white line (top panel), related to the degree of CO turnover achieved (bottom panel). The same behavior was shown to occur in the range of feeds used ($1 < O_2/CO < 5$) through with increasing O_2 content to the feed the light off temperature decreased ca. 40 K in both heating and cooling cycles between which a hysteresis of 9–16 K was also observed.

Further experimentation [141,142] established that, within a narrow range of sizes ca. 7.5–20 Å average diameter), that light off of the catalysts was always accompanied by sudden and significant oxidation of the Pt nanoparticles, and that in the "high activity" state the Pt surface have to be considered as being covered in an oxide of a disordered and defective nature, the thickness of which depends upon the Pt particle size and the nature of the support.

2.6. Oscillations Again: Spatio-Temporal Operando Quick EXAFS Investigations in Plug Flow Microreactors

Most of the investigations in this review have, up until now, used methods that have aimed to bridge materials and pressure gaps to further understanding of the basic structures and events that characterize the oxidation of CO on surfaces and nanoparticles, by maintaining them under "static" pressures (in the batch reactor sense) or flowing gases over the materials in question rather than through them. This situation is unavoidable in the study of flat surfaces, yet, within the *operando* philosophy, the functional ideal that should be aimed for when dealing with high area catalysts is to attain what is known as "plug flow". Put simply this is a state of affairs where in the applied feed should flow evenly through the catalysts bed in such a manner that radial gradients are avoided and a space velocity or a contact time may be properly established (see, for instance, [15]).

It is obvious that the (now generally abandoned) practice of using pressed samples of ill-defined porosity around which an applied gas mix is allowed to flow (see Sections 2.1 and 2.2) is, from the perspective of reaction kinetics and QSARS, a far from an ideal situation that is very unlikely to conform to the plug flow paradigm (for an excellent paper regarding this aspect of reactor design and sample presentation see [143]).

Apart from permitting the establishment of a contact time/space velocity, the plug flow paradigm also introduces a further element of practical interest: that of axial variation in structure and reactivity as the feedstock passes along the catalyst bed.

In a plug flow situation, as soon as the reactive gas mixture passes the inlet of the catalyst bed, the feed starts to change composition as a result of the catalysis itself. As such, the catalyst that exists further down into the bed in the direction of flow does not experience the same feed composition to a degree that is dependent upon the activity of the catalyst. From an applied point of view, this is an important consideration in terms of optimizing the use of the catalysts and the conditions (of space velocity for example) under which they are best run.

By and large the spatial variation of structure and reactivity within a catalyst bed was for a very long time rather ignored, most likely as the probes generally available to quantify what was going on within such reactors were only able to integrate over the total volume of the reactor. Recently, however, there has been a considerable surge of interest in resolving spatially how the catalysts and the catalysis proceeds within the flow conditions imposed by the plug flow paradigm as solutions to achieving spatial resolution *in operando* (such as IR and Raman) have been demonstrated [144–148].

The X-ray beams that third-generation synchrotrons produce, as well as being intrinsically powerful, are also excellently adapted to the spatial probing of materials chemistry and easily capable of providing spatially resolved information as to the state of a catalyst within a working catalyst bed. In the mid 2000s, therefore, papers started to appear that made use of this property to study the axial variation in the structure of the supported metal catalysts using quick scanning [149,150] or energy dispersive EXAFS [151].

Since then this type of approach has been applied to the study of the behavior of Pt/Al_2O_3 catalysts beds, and specifically when various types of oscillatory behavior are also being observed by global measurements of performance such as MS. The next two examples [152,153] once again utilize the time resolving nature of QEXAFS, with its intrinsic ability to sample relatively small volumes within the much larger volume of a larger catalyst bed, alongside other methods that sample the working system in different ways: the ever present workhorse of MS, that integrates over the entirety of the catalyst bed, and methods based on infrared; spectroscopy applied in a non-spatially resolving, but surface functionality specific, manner [152], and imaging IR thermography that can reveal axial temperature variations within a catalyst bed [153].

Figure 12 outlines the results of a study of oscillatory behavior observed in 2 wt % Pt/Al_2O_3 catalysts as it evolves under an oxidizing (O_2/CO = 20) reactive feed. Figure 12a shows IR and MS results obtained from a pellet (pressed sample) reactor. As the sample is heated one can see the emergence of catalytic reactivity (MS) and changes in the levels of bridged and linear CO species associated with a metallic Pt phase. As catalysis ensues the levels of these species are observed to

decrease yet, periodically, they are restored to higher levels as, at the same time, overall conversion transiently diminishes. This pattern of behavior continues, with ever decreasing intensity, to a quasi (small oscillations in reactivity and surface functionality still be observable) steady state of high conversion above ca. 380 K.

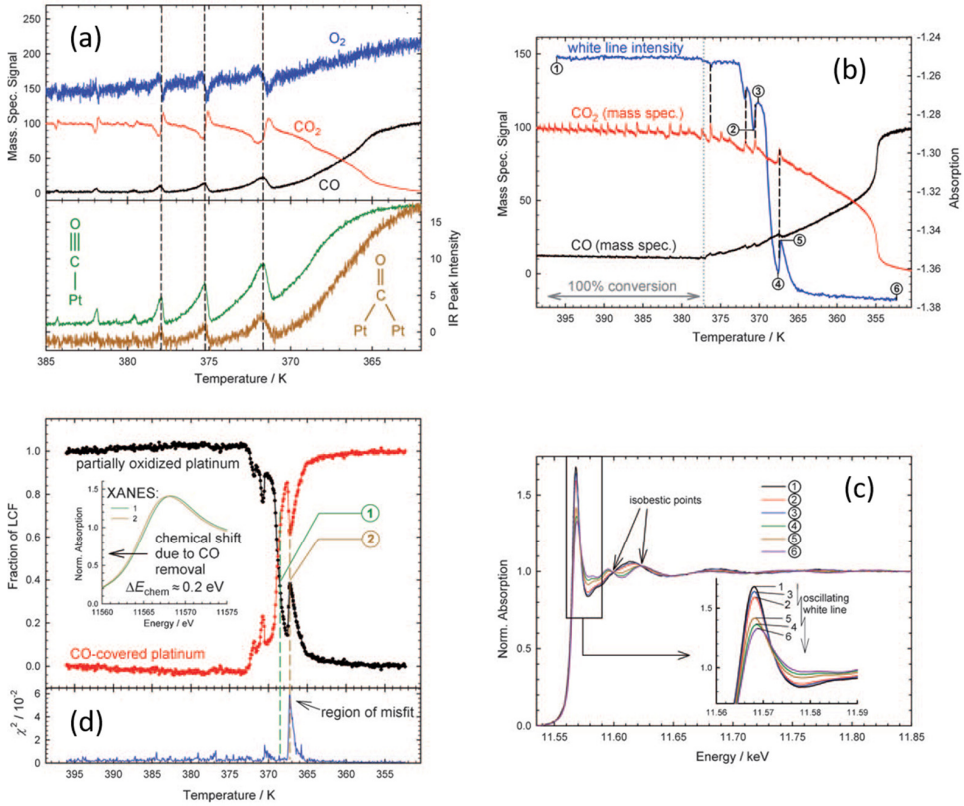

Figure 12. (**a**) Variation in O_2, CO, and CO_2 signals observed in MS (upper panel) with infrared bands corresponding to linear and bridged CO species measured in a pellet reactor as a function of temperature. (**b**) Pt L_3-edge white line intensity (blue) variations measure 1 mm into the in inlet of a plug flow reactor containing a 2 wt % Pt/Al_2O_3 catalysts under a reactive CO/O_2 feed (CO/O_2 = 1:19) alongside online MS for CO (black) and CO_2 (red) as a function of temperatures. (**c**) Pt L_3-edge XANES spectra at the points indicated (1–5) in (**b**). (**d**) The results of LCF fitting of the time resolved Pt L_3-edge XANES obtained from the plug flow reactor experiment shown in (**c**) derived from fitting combinations due to CO covered and surface oxidized Pt spectra. Reproduced with permission from. *ChemCatChem.* **2010**, *2*, 653–657 [152]. Copyright 2010, John Wiley and Sons.

Figure 12b then repeats this experiment again from the view point MS, but this time correlated to the changes in Pt L_3-edge white line absorption observed using transmission QEXAFS made through a tubular plug flow reactor and at the inlet to the catalyst bed itself: Figure 12c shows the normalized Pt L_3-edge spectra highlighting how they appear at various points in the oscillatory development of the catalyst. Figure 12d then shows the results of fitting the Pt L_3-edge XANES as a linear combination fitting (LCF) of the spectra derived from the initially reduced catalyst and one that has been fully oxidized.

These results show that the results obtained from employing a pressed sample in the pellet reactor, whilst qualitatively similar to those derived from the plug flow system, are not the same, specifically in terms of the temperature dependence of the evolution of the Pt catalyst and the catalytic activity it displays. No doubt this is a direct result of the manner in which the sample is presented in each case [145]. However, in both cases oscillatory chemistry is observed and clearly linked to the levels of

molecular CO present at the surface of the Pt catalysts and to redox behavior occurring in the Pt phase (from the Pt L_3-edge XAFS).

As with our first, diffraction based example from 1994 [92], an explicit link between oscillatory phenomena and the switching between more reduced and more oxidized forms of Pt within the working catalyst is established. We further see that under these net oxidizing conditions high CO turnover is associated with a Pt phase that is (according to the LCF fitting) around 100% surface oxidized, at least in respect of the reference spectra used to arrive at this determination. Lastly we might note the evolution of the quality of time resolved XANES from that obtained around 2004 using dispersive EXAFS (Section 2.2), to that obtainable in a single shot using the fast scanning monochromators, that by 2010 were in place at the SuperXAS beamline at the Swiss light source, and which since then have been evolved even further (vide infra, [114,115]).

This experiment was then augmented by sampling the XAFS at different axial positions along the microreactor from the inlet to the outlet. The conclusions reached from this further study are summarized in Figure 13.

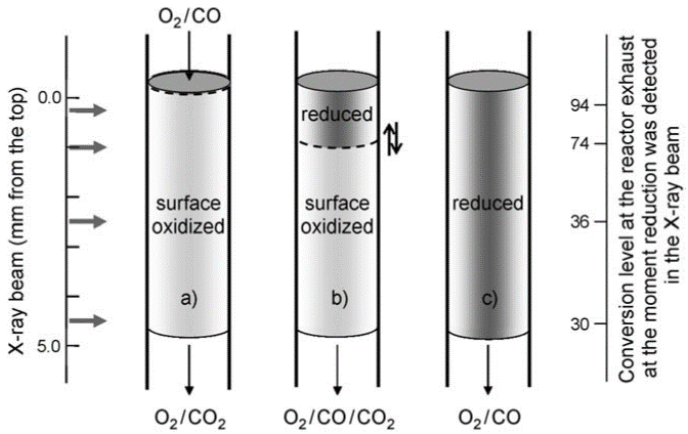

Figure 13. A schematic summary of the results derived in [152] and pertaining to Figure 12. Before extinction of the oscillatory behavior spatially resolved XAFS leads to the conclusion that the Pt in the catalysts is essentially surface oxidized throughout. Post extinction of the oscillatory behavior the bed is now seen to be uniformly reduced and poisoned by CO. During extinction of the oscillatory behavior a large gradient was observed between reduced and oxidized Pt. Reproduced with permission from *ChemCatChem* **2010**, *2*, 653–657 [152]. Copyright 2010, John Wiley and Sons.

What was deduced from this exercise was that, prior to extinction of the oscillations, the catalyst was largely surface oxidized along the entire length of the bed. Post extinction a more reduced and CO poisoned state dominated. In between times, and during the extinction events themselves, a stark gradient in the state of the catalysts was detected wherein the front (inlet) part of the bed was found to be reduced whilst the rest remained oxidized. The implication was that oscillations not only involve redox events in the Pt phase but that, in a plug flow situation, their appearance and disappearance is also accompanied by a reactive wave front that travels the length of the bed from inlet to outlet according to variations in gas composition and temperature due to the catalysis itself.

These studies were recently extended by Gänzler et al. [153] who investigated 4 wt % catalysts of average particle size very similar to that used in the previous example. In this case however, an elegant combination of imaging thermography was added to the use of time resolved EXAFS to gain even greater insight into the structural-reactive behavior of a working catalyst bed.

Figure 14a shows the conversion of CO (ppm) versus temperature as this catalyst was heated under feed compositions of O_2/CO of 100:1 and 10:1. In the former case oscillations in CO conversion are observed as of ca. 120 C; in the latter as of 150 C. The magnitudes of the oscillations are seen to be greatest in the most oxidizing (O_2/CO of 100:1) of the two flows.

Figure 14b then shows thermal images of the beds exposed to the most oxidizing feed as a function of increasing temperature. What can be observed is that, as a function of total CO conversion and catalyst temperature, well defined "hotspots" can be seen to form at different positions within the bed. At the lowest temperature/conversion they are primarily observed at the very end of the bed and work their way back toward the inlet; at the next temperature they start in the center of the bed; and at the highest temperature they are found more towards the reactor inlet but still, over time, work their way slightly toward the inlet.

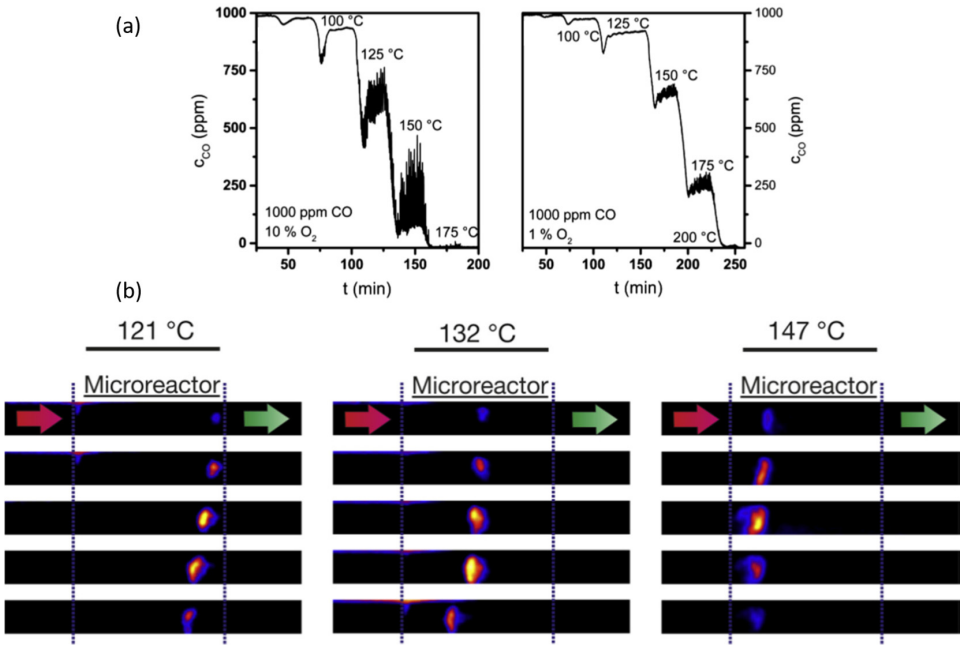

Figure 14. (**a**) CO conversion measured in a plug flow reaction using mass spectrometry as a function of temperature and for two different CO/O_2 feeds: left panel, O_2/CO = 100:1; right panel, O_2/CO = 10:1. (**b**) Imaging thermography showing the axial formation of reactive hot spots at different temperatures in a plug flow reactor and for O_2/CO = 100:1 and under conditions of reaction oscillation. Reproduced with permission from *J. Catal.* **2015**, *328*, 216–224 [153]. Copyright 2015, Elsevier.

Figure 15 then summarizes the results obtained from repeating these measurements at discrete axial positions along the catalyst bed and correlating this with the total activity of the system observed using MS.

The hotspots are indicative of activity (CO oxidation being a highly exothermic reaction ($\Delta H = -282$ kJ·mol^{-1}) [154]) and their observation suggests that the majority of the catalysis, and the source of the oscillatory chemistry, is occurring only at rather localized positions within the catalyst bed.

What is revealed by these investigations is a rather complex picture of the behavior of the Pt in this system that the MS only averages over. The inlet of the bed is shown to comprise of ostensibly metallic Pt (EXAFS) that displays no evidence of variation at all from the LCA analysis of the XANES.

Around the center of the bed (point (2)) we can see that this situation has changed: small and regular oscillations in the LCA-fitting are now observable (period ca. 120 s) and the FT of the EXAFS has clearly changed in a manner that indicates a greater level of oxidation that then briefly increases during the period of oscillation.

Moving forward to point (3), around three-quarters of the way along the bed, the EXAFS has changed again to suggest an even higher degree of oxidation in the Pt phase. The Fourier transforms are now (for the most part) dominated by Pt–O interactions rather than Pt–Pt with the latter almost disappearing during the new periods of oscillation.

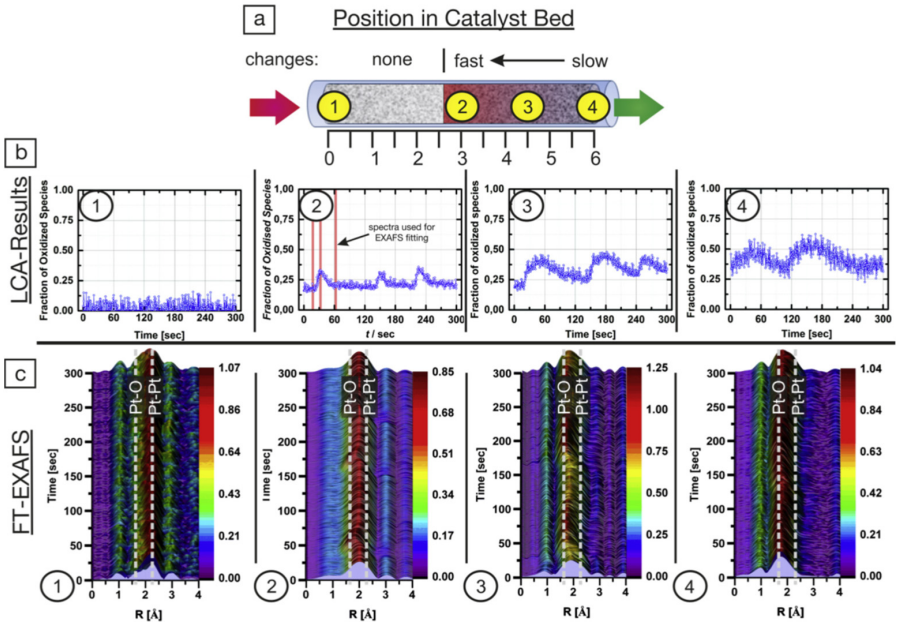

Figure 15. (**a**) Schematic describing both the axial positions used for the acquisition of time resolved Pt L_3-edge XAFS further described in (**b**,**c**) along with indications of the types of temporal change observed during experimentation. (**b**) Results of LCF fitting of the Pt L_3-edge XANES acquired at each position noted in (**a**) in terms of the fraction of oxidized Pt species present. (**c**) Non-phase corrected Fourier transforms of the k^2-weighted EXAFS data obtained from Pt L_3-edge QEXAFS at each position within the bed during oscillatory behavior observed by the MS and located (axially) using imaging thermography. Reproduced with permission from *J. Catal.* **2015**, *328*, 216–224 [153]. Copyright 2015, Elsevier.

This is reflected in the LCF of the Pt XANES that now has a baseline of with 25% of the Pt being seen as oxidized that then rises to between 40% and 50% during periods of oscillation; periods that are now seen to have become temporally broader though still retaining a period of ca. 120 s. Lastly at the very outlet of the bed (4) we again observe oscillatory behavior in the LCF that has continued to broaden (though maintaining its period) and attain levels of >50% of the Pt being oxidized.

What this combination of time resolved XAFS and imaging thermography is very adeptly showing may be summarized as follows. Firstly, a blind reliance upon a technique such as MS that integrates over the whole volume of the catalyst bed, or even an advanced X-ray technique such as QEXAFS that targets only small volumes within the reactor, could be very misleading in trying to understand the behavior of a complex system: much of the chemistry is revealed to be rather localized within the reactor at positions that depend upon the applied circumstances. Imaging thermography is also shown to be an ideal way for this sort of (exothermic) catalytic problem to be observed and then used to inform the sampling of the catalytic reaction from the local order and chemical state viewpoints provided by the QEXAFS.

This elegant combination of methods also shows that under the rather oxidizing conditions studied, over oxidation of the Pt phase can be just as much of an issue for reactivity as too little; at this point we may recall the conclusions of both SXRD and XPS from Pt surfaces that perfectly formed surface oxide layers are not at all reactive for CO oxidation (Sections 2.3 and 2.4).

The working catalyst bed is also resolved into a spatial entity wherein the Pt phase present is graduated axially from the front of the bed—where the Pt particles are reduced and largely poisoned by CO—through to a second heavily oxidized phase that is also largely inactive. In between these two extremes lies a small sweet spot that is the source of the oscillatory behavior observed in MS and the transient increase in CO_2 production.

The nature of this active phase, within the limits of description afforded by the EXAFS, appears to be a metallic phase that is to some degree, most likely around and about a monolayer's worth, oxidized. These results, derived from almost a reaction engineering point of view, are therefore broadly consistent with the evolving picture of reactivity in this system, in terms of the optimal surface phases required for CO conversion to CO_2—as very precisely delineated by some of the surface science studies (Sections 2.4 and 2.5) already described. Which brings us to our next example: one that asks the question as to whether the structural specificity that studies based upon well characterized single crystal surfaces can be achieved for nanoparticulate, real world catalysts operating under realistic conditions?

2.7. Time Resolved High Energy X-ray Total Scattering/Pair Distribution Analysis as Applied to CO Oxidation over 1 wt % Pt/Al_2O_3: Identifying a Reactive Surface Oxide in a Real Catalyst

In the previous sections we have, by degrees, seen how the application of modern synchrotron surface X-ray diffraction and X-ray spectroscopies have been used to bridge the materials and pressure gaps that remained after Ertl's seminal works on Pt single crystals. We have seen how fast SXRD and ambient pressure XPS have provided new routes to specify, with high levels of structural and kinetic precision, the roles of surface oxides in facilitating CO conversion over single crystals, and confirming a shift in mechanistic paradigm from the pure LH mechanism to one that is more formally based in the MvK.

But what of real nano-particulate systems? We have already seen that, starting from the XRD work of Hartmann et al. [92] and the subsequent application of fast XAFS—in both Quick scanning [140–144,152,153] and energy dispersive variations [94]—has established some sort of accord with those single studies made at elevated pressures; they too have confirmed the dominant participation of oxidized Pt phases in CO oxidation in a range of circumstances, and specifically as the main drivers for oscillatory behavior.

However, whilst Pt L_3-edge XANES, HERFD, and EXAFS measurements made on high area nano-particulate catalysts have been very successful in determining the generalities of the chemical states of the Pt and how they interconvert under relevant conditions and timescales, they have been unable to achieve the level of structural precision that, for instance, SXRD studies have been able to attain.

This state of affairs is regrettably intrinsic to the EXAFS approach, which is not, a priori, surface sensitive, and dominated by the physics of photoelectron-atom scattering: limited photoelectron inelastic mean free paths, the $1/R^2$ dependence of the scattering intensity, where R is the mean interatomic separation, and the dampening effects of both static and dynamic disorder, all conspire to limit the depth of structural information that can reasonably be retrieved from heterogeneous supported catalysts using this method. As such, the unequivocal determination of the structure of these transient and active phases has not been forthcoming from these methods: phrases such as "PtO_2 like" abound, though in being realistic regarding the limitations of the XAFS method, in the case of Pt at least, this is absolutely reasonable.

How then might we resolve this impasse in a manner that allows an operando approach to CO oxidation for high area, nanoparticulate, Pt catalysts to be adopted and, at the same time, can yield the sort of structural detail obtainable from SXRD for nanoparticles supported upon a high area alumina support?

The answer to this question, at least in part, is to use high energy total X-ray scattering coupled to pair distribution function (PDF) analysis. The recent emergence of time resolved high energy X-ray scattering/PDF is a fine example of just how rapidly third-generation synchrotrons have evolved in the 21st century (specifically in terms of insertion device and detector technology) to offer researchers of all persuasions completely new ways of looking at a variety of problems.

The term "new" is somewhat misleading as the first examples of a PDF approach to solving the structure of materials that have little or no long range order can be traced back to 1934 [155,156] in

Warren's work on amorphous SiO_2, and seminal works by Rosalind Franklin regarding the structure of graphite in 1950 [157,158]. PDF therefore predates XAFS, XES and XPS by come considerable margin. Indeed, from a time predating the advent of dedicated synchrotrons, certain insightful, not to say brave, souls were already trying to apply this method to the study of supported metal catalysts. (See, for instance, [159] and reference therein).

As with EXAFS the PDF method is not a surface sensitive technique. However, it differs considerably in regard to the basic physics that underpins it: the former relies upon the scattering, by surrounding atoms, of X-ray induced photoelectron, whilst PDF is founded upon the scattering of the X-rays themselves. If one can obtain enough of this X-ray scattering (reciprocal space) then, as with EXAFS, a Fourier transform to yield a pair distribution function (PDF) can be obtained that contains within it all the pairwise scattering events that result from the structure of the material over the length scales before which such signals can be measured.

Importantly, and in comparison to SXRD or conventional Bragg diffraction, there is no requirement whatsoever for any long range order to be present in the sample for this method to work; and, in comparison to XAFS, the scattering of high energy X-rays is not subject to the same restrictions that limit the field of view of photoelectrons around an emitting atom, and can therefore provide information that admits the possibility of more detailed structural refinement.

However, to do this well one needs to be able to collect a great deal of reciprocal space with a high statistical quality to the data. As such, until less than 10 years ago, for reasons that are beyond the scope of this review, the very idea that one could make PDF measurements on the timescale of seconds or less, let alone on low loaded supported metal catalysts, would have been absurd.

Three things had to happen to make this possible: suitable advances in insertion device technology, specifically undulators, for high energy X-rays; a new generation of fast imaging detectors that can work at high (>60 keV) X-ray energies; and, most crucially, the wit and wherewithal to put these elements together. These disparate factors first came together at sector 11 of the Advanced Photon Source in the US as of around 2007 [160].

As long ago as 1987, Sinfelt and co-workers [161] had shown, using the Stanford Synchrotron Radiation Laboratory (SSRL), that the X-ray scattering due to supported Pt nanoparticles could be separated from that due to the support to access the structure of the supported particles. They used an "anomalous" scattering" approach based on varying the energy of the X-rays around the Pt L_3 -edge to achieve this, with a single scan taking ca. 1000 min. The advances made by Chupas and co-workers, working at much higher (>60 keV) X-ray energies reduced this to seconds and showed that the same isolation of the scattering due to a supported Pt phase could be achieved using simple difference method based on independently measuring the scattering response from the support and subtracting it from that due to the metal loaded catalyst [162].

A few years later our next example of the operando application of synchrotron methods to the catalytic oxidation of CO over Pt made use of this new capacity to identify the structure of a reactive surface oxide formed over a working nano-particulate Pt catalyst [163]. In doing so, materials and pressure gaps were spanned and a direct structural-reactive link between the behavior of Pt single crystal surfaces (most specifically Pt(110) [116]), and their supported nanosize counterparts under relevant operating conditions, was demonstrated.

To achieve this a 1 wt % Pt/Al_2O_3 catalyst, characterized using TEM as having relatively narrow particle size distribution centered around ca. 2 nm average particle diameter, was subjected to alternating flows (25 $mL{\cdot}min^{-1}$) of stoichiometric (stoich: CO/O_2 = 2:1) and net-oxidizing (ox: CO/O_2 = 1:5) flows at 500 K within a plug flow microreactor [164]. At the same time high energy scattering patterns were collected at rates of 1–4 Hz as the progress of the catalysis was monitored by mass spectrometry. Figure 16 shows difference—that is to say after subtraction of reference measurements made through a bed of the Al_2O_3 support at the same temperature—PDF obtained from this approach at various points in the redox cycling.

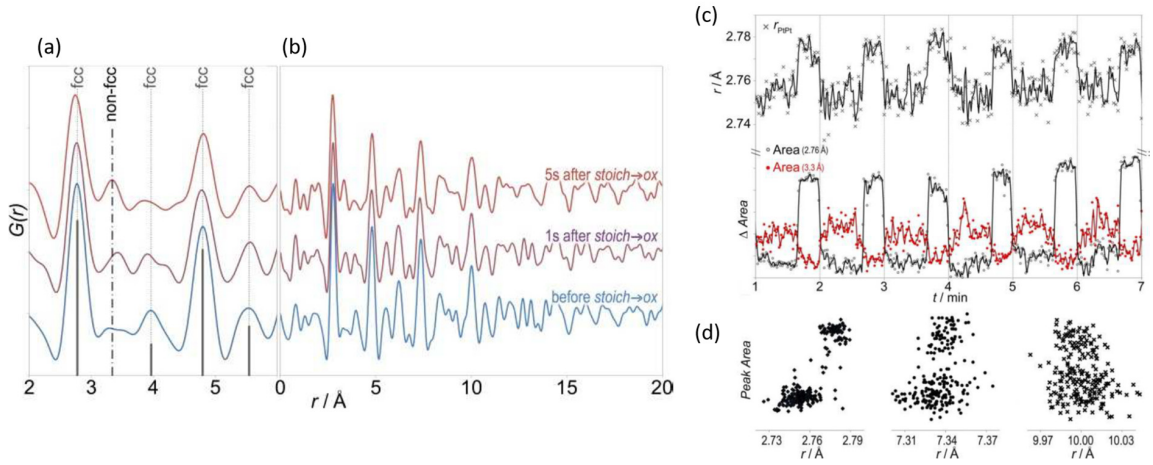

Figure 16. (**a**,**b**) difference PDFs for a 1 wt % Pt/Al_2O_3 catalysts working *in operando* at 473 K under periodic operation under alternating flows of $2CO/O_2$ (stoich) and $CO/5O_2$ (ox) as indicated in (**b**). (**a**) shows a close up of 0–6 Å in the PDF, and indicated scattering features due to fcc Pt and those that are not expected from the fcc Pt structure, whilst (**b**) shows the entire PDF from 0–20 Å. (**c**) Variations observed during periodic operation in (top) the bond distance for the first shell PtPt scattering interaction in the Pt nanoparticles, and (bottom) the corresponding variations in the integrated areas of the first shell Pt feature at 2.75 Å and of the non-fcc scattering peak at 3.3 Å. (**d**) correlations for different fcc scattering features between their fitted position (r/Å) and their integrated intensity. Reproduced with permission from *J. Am. Chem. Soc.* **2012**, 134, 5036–5039 [163]. Copyright 2012, American Chemical Society.

The ability of PDF to see far beyond what may be observed by EXAFS is immediately clear. Structural details, that in this experiment are dominated by Pt–Pt interactions, and that can be fitted to a progression of PtPt scattering events expected from a nanoparticulate fcc Pt phase, are very evident. It is also evident that, as a function of the applied feed, the intensity of these features is subject to modulation. Moreover, from the close up of the low r/(Å) parts of the patterns shown in Figure 16a, after the flow has been switched from a stoichiometric to an oxidizing flow, a new scattering interaction, that is not expected from an fcc structure is observed to appear and grow.

Figure 16c,d then show the behavior of differing structural elements extracted from the time resolved PDF: the anti-phase relationship between the intensity of the first fcc PtPt scattering interaction (2.76 Å) with the much weaker, non-fcc scattering at ca. 3.3 Å; the shift in PtPt bondlength observed to occur in the first fcc PtPt shell; and then (**d**) the variation in areas of a number of fcc scattering features up to an r/(Å) of ca. 10 Å that clearly show a partitioning of the reactive system into two states and (from MS (not shown)) two reactive branches, according to the environment being experienced by the catalyst.

Further analysis, that reveals the nature of the oxidic surface phase and its relation to the catalysis, is shown in Figure 17. Figure 17a shows the PDF, together with a fits to the data using spherical particles that are on average 2 nm in diameter. Figure 17b then shows the results of applying a further difference between these two extremes to reveal a new pattern of scattering interactions that contains the structural identity of the difference between the Pt states; that is to say the scattering pattern due to a surface oxide.

It can be shown [163] that if one propagates the basic two dimensional unit cell shown in Figure 17b then all of the scattering peaks (save for three—that then can be shown to relate to the relationship between the PtO_2 layer and the fcc structure of the Pt nanoparticle normal to its surfaces) can be accounted for by the formation of the surface oxide shown schematically in Figure 17c that we can immediately recognize as the incommensurate α-PtO_2 surface oxide first observed *in operando* by Ackermann et al. using SXRD [116]. Moreover, we can also see from Figure 17d that the yield of CO_2

depends on the presence of this phase; the more we see the surface oxide the more CO_2 we obtain even though the partial pressure of CO in the oxidizing cycle is five times less that in the stoichiometric. MS [163] shows that the "steady state" production of CO_2 obtained in the oxidizing cycle, wherein the surface oxide is formed and persists, is considerably larger than that obtained under the stoichiometric flow, and that the highest levels of CO_2 production occur upon the switch from the oxidizing to the stoichiometric. This switch in feed is accompanied by a sharp spike of CO_2 production as the α-PtO_2 surface oxide is rapidly reacted away as the partial pressure of the CO rises. The implication is that the surface oxide is at least an order of magnitude more reactive that the metallic surface under these conditions.

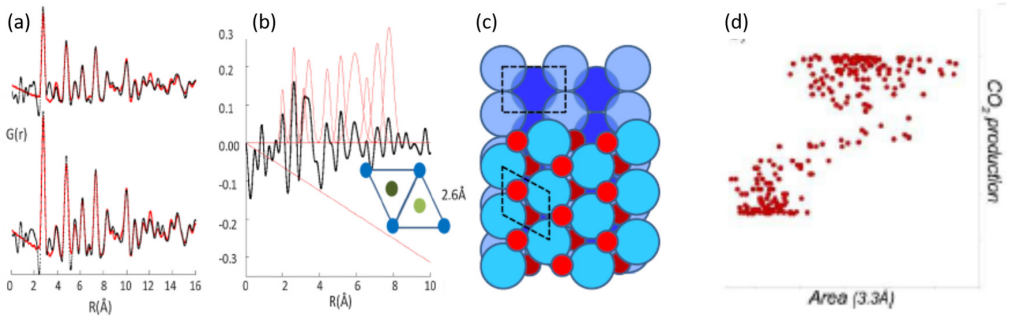

Figure 17. (**a**) Difference PDFs derived from 1 wt % Pt/Al_2O_3 taken from the ends of the stoich ($2CO/O_2$) cycle (bottom) and the ox ($CO/5O_2$) cycle (top) together with fits made using PDFGui (http://www.diffpy.org/products/pdfgui.html) for spherical nanoparticles of ca. 20 Å in diameter. (**b**) Subtraction of the patterns shown in (**a**) to reveal the scattering differences between the two catalyst states present in the stoich and ox cases. The red curves are those fitted to the data. (**c**) The PtO_2 adlayer structure derived from the pattern of scattering features derived by the difference shown in (**d**) Correlation of the non-fcc scattering feature with the levels of CO_2 measured by online MS. Reproduced with permission from *J. Am. Chem. Soc.* **2012**, 134, 5036–5039 [163]. Copyright 2012, American Chemical Society.

As such this experiment succeeded in bridging both materials and pressure gaps and was able to provide detailed structural-activity relationships that had previously been the sole preserve of studies made on low index Pt metal surfaces.

We shall see later that this sort of experiment, along with other scattering approaches that strongly favor the use of high energy X-rays, and that hold within them even greater promise in the unravelling the detailed structure of the surface phases that are responsible for catalysis over supported metal nanoparticles, should benefit enormously from ongoing upgrades of third-generation synchrotrons. However, to end the experimental part of this review, we shall go back to the use of time resolved XAFS, allied to MS and infrared spectroscopy, to consider how combined application of these methods can help to demonstrate an entirely new perspective regarding the possibility of inducing simple Pt/Al_2O_3 catalysts to catalyze CO oxidation at temperatures that are forbidden by the LH mechanism as a result of the intrinsic character of the interaction of CO with Pt surfaces.

3. A New Mechanistic Possibility for CO Oxidation at Room Temperature Using "Simple" Pt/Al_2O_3 Catalysts?

Thus far, and for the entire history of CO oxidation over Pt, a metallic Pt phase, be it single crystal, wire, or as nanoparticles, has always taken center stage. Whether as the host to adsorbed CO and O, which are then be converted to CO_2 without undue perturbation of the underlying Pt (the basic LH mechanism), or as the support for reactive surface Pt oxides that, a metallic Pt phase has always been present and thought of as essential.

However, recent years have seen a growing understanding that isolated metal atoms supported on a variety of inorganic dispersants can catalyze a number of reactions. Such atomically disperse metal atoms might display reactive behavior that is different to both extended surfaces and nanoparticles, or conventional organo-metallic species (be they in solution, or tethered to, or absorbed upon a support material).

Amongst these systems atomic Pt adsorbed upon Al_2O_3 and its behavior in oxidation processes has garnered some considerable interest. From a basis of theoretical studies of the structural-electronic properties of transition metals adsorbed upon θ-Al_2O_3 surfaces [165], Narula and co-workers have gone on to show experimentally that isolated Pt atoms adsorbed upon Al_2O_3 show a conspicuous activity for NO oxidation by O_2 [166]; they then turned their attention to the CO oxidation using O_2 [167]. In this paper, they synthesized and characterized catalysts wherein atomic Pt was present in a majority, and then showed (using infrared spectroscopy and DFT calculations) that these species, when placed in contact with CO, could form isolated Pt(CO_3^{2-}) species. Moreover, and invoking concepts from organometallic chemistry, they then theoretically constructed an entire catalytic cycle founded solely upon CO and O_2 reacting with isolated atomic Pt and producing CO_2 via a transiently formed Pt(CO_3^{2-}); in doing so the necessity for any extended Pt phase, be it metallic or surface oxide, is completely avoided. This novel mechanism is shown in Figure 18.

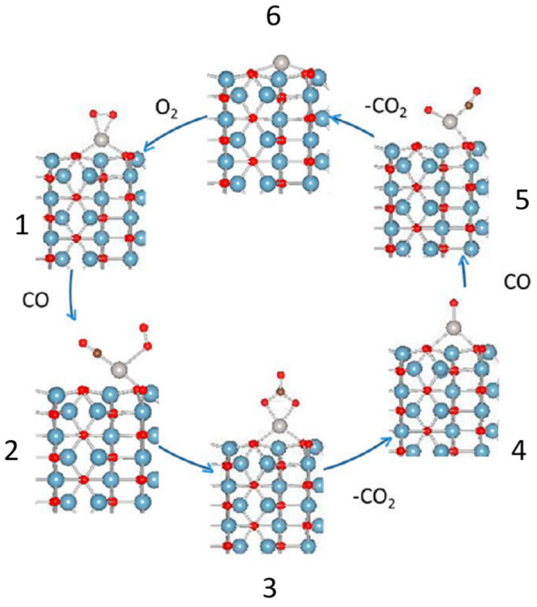

Figure 18. A catalytic cycle derived theoretically by Moses-DeBusk et al. [167] for the oxidation of CO by O_2 mediated solely by isolated Pt atoms supported upon a theta-Al_2O_3 surface and involving the transient formation of a bidentate Pt(CO_3^{2-}) species (VI). Grey = Pt, red = O, brown = C, blue = Al. **1** shows the starting oxidized Pt atom adsorbed upon the Al_2O_3 to which CO may add to eventually form an adsorbed bidentate carbonate (**3**). This carbonate then decomposes that loses CO_2 to form a new adsorbed PtO (**4**) that can react with a second CO molecule to eventually release a second CO_2 molecule and form a third atomic Pt species (**6**) to which O_2 can add. Reproduced with permission from *J. Am. Chem. Soc.* **2013**, *135*, 12634–12645 [167]. Copyright 2013, American Chemical Society.

The implications of such a mechanism are clear. A mechanism of this sort would not be subject to the fundamental limitations imposed by the LH mechanism that arise as a result of the poisoning of any Pt surface by molecular CO at low temperatures, simply as there are no extended such surface to be poisoned in the first place.

Subsequently Newton and co-workers [168,169] took a commercially available 5 wt % Pt/Al_2O_3 (Johnson Matthey, Reading, UK, Type 94, average Pt particle size ca. 3 nm (TEM)) to investigate

whether a carbonate mediated route to CO conversion was in fact possible and whether it might be able to induce such chemistry at ambient temperature.

They used a combination of sub-second time resolved Pt L_3-edge QEXAFS, DRIFTS, and Mass spectrometry and a novel DRIFTS/EXAFS cell [77] developed expressly for these types of measurements. The periodic-operation approach is shown at the top of Figure 19. The sample was purged in He, reduced (to 573 K) under flowing 5% H_2/He before being cooled back to RT and purged again with He. The sample was then alternately exposed to flowing 5% CO/He or O_2/He during which DRIFTS/MS, or XAS/MS data was collected. The lower half of this figure (Figure 8a–c) shows how the catalyst behaves in terms of CO_2 production, and some of the speciation concurrently observed using infrared spectroscopy (DRIFTS).

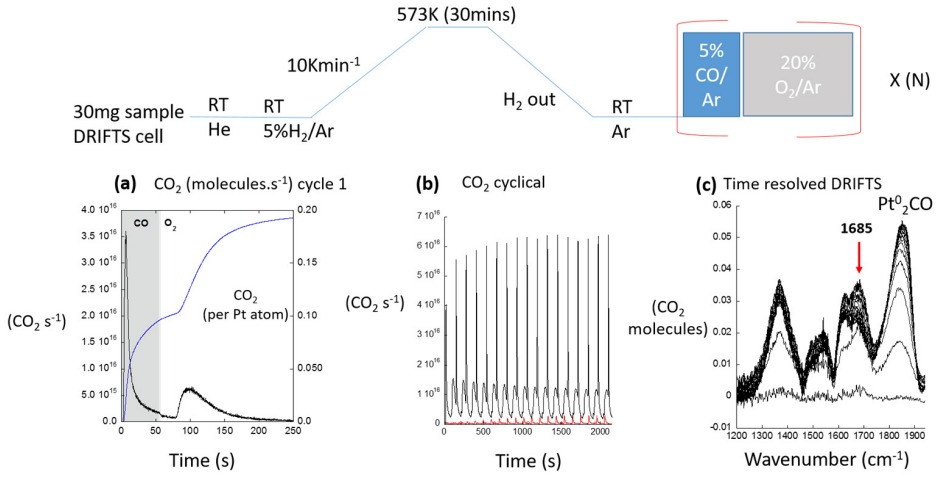

Figure 19. Top: experiment approach adopted in [168,169] to investigate CO oxidation at ambient temperature over a 5 wt % Pt/Al_2O_3 catalyst (Type 94, Johnson Matthey). Bottom: (**a**) CO_2 production during a single cycle of periodic redox operation expressed as molecules $CO_2 \cdot s^{-1}$ (left axis) and as CO_2 atoms per Pt atom in the catalyst. (**b**) CO production over a sequence of redox cycles over the T-94 catalyst at RT (black) and an unloaded Al_2O_3 sample (red). (**c**) Representative DRIFTS spectra in the 1240–1940 cm^{-1} region during a CO cycle. The bridging CO species on reduced Pt is indicated, as is the band (at ca. 1685 cm^{-1}) that amongst the carbonate species observed is the only one whose temporal behavior precisely matches that observed in MS for the production of CO_2. Adapted from *Nat. Comms.* **2015**, *6*, 8675 [168]. Copyright 2015, Nature Publishing Group and *J. Am. Chem. Soc.* **2016**, 138, 13930–13940 [169]. Copyright 2016, American Chemical Society.

As can be seen, from Figure 19a, when this catalyst is exposed to 5% CO at RT a very fast but transient evolution of CO_2 is observed. Subsequent switching of the flow to 20% O_2 also produces CO_2, though in a very different, much slower, manner. Most importantly this behavior can be seen to be repeatable (Figure 19b) and indicates that a catalytic cycle can be achieved at room temperature over a "simple" Pt/Al_2O_3 catalyst.

The LH mechanism says this cannot happen: any metallic Pt phase present would be completely covered, and therefore poisoned, by adsorbed CO under these conditions. Indeed, the time resolved DRIFTS (c), clearly shows the expected, and spectroscopically dominant, appearance of linear (not shown in Figure 19c) and bridged CO species (indicated as $Pt^0{}_2CO$ in Figure 19c) that do indeed rapidly cover the metallic Pt component of this catalyst under CO; it also shows that these are then removed (through desorption) under O_2. Importantly this latter event is observed to have to occur before we again observe CO_2 in the oxygen cycle.

However, alongside these familiar [133] IR signatures for CO adsorbed upon Pt metal surfaces, a number other bands in the 1300–1700 cm^{-1} range are also seen to appear. For the most part these are carbonates directly associable with the Al_2O_3 and are observed to predominantly accumulate, storing

CO, rather than reacting to yield CO_2. The most prominent exception to this general observation is the broad IR band identified in Figure 19c at ca. 1685 cm^{-1}. This band appears and (largely) disappears in concert with the two different branches of CO_2 production. Moreover, this band exists precisely in the middle of the region expected, on the basis of the experiment and calculations made by Moses-DeBusk et al. [167], for Pt-carbonates species. Quantification of the CO_2 production using MS indicates that the CO_2 produced corresponds to 10%–15% (given the augmentation of CO_2 production subsequent to the first cycle) of the Pt atoms contained in the catalyst bed.

Examples of the time resolved (4 spectra per second) Pt L_3-edge XAFS are given in Figure 20 that highlight changes in the XANES observed during the cycling and also the type of data quality that a state of the art, quick scanning monochromator system coupled to fast ion chambers, [114,115] can now produce. This is of considerable importance as the changes in the XANES that signal redox events in this system that are accompanying the reactive chemistry are small (see also Section 2.2) and rapid (especially in the CO cycle). Observing them, such that a quantitative link between the redox behavior of the Pt, changes of surface functionality (DRIFTS), and reactivity (MS), might be established, would not be possible if the datasets obtained were not of as high quality.

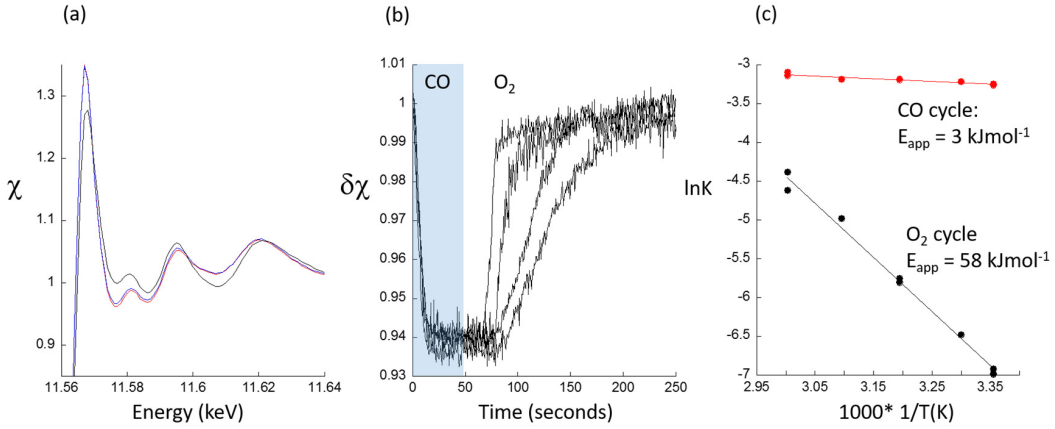

Figure 20. (**a**) Close up view of the Pt L_3-edge XANES obtained at a rate of 4 Hz per spectrum during periodic redox operation over the T-94 catalyst at room temperature. (**b**) Temporal changes in integrated white line intensity on the Pt L_3-edge XANES during single redox (CO/O_2) cycles carried out at temperatures between 298 and 333 K. (**c**) Arrhenius plots derived from the time resolved XANES for the redox events observed to be occurring in the Pt XANES that may be directly correlated to CO_2 production in the CO cycle (red) and O_2 cycles (black). Reproduced from *Nat. Comms.* **2015**, *6*, 8675 [168]. Copyright 2015, Nature Publishing Group and *J. Am. Chem. Soc.* **2016**, *138*, 13930–13940 [169]. Copyright 2016, American Chemical Society.

All of the applied techniques can be used to derive estimates of the apparent activation energies for the two branches of the CO_2 production, and the results derived from the Pt L_3-edge XANES are shown in Figure 20c. This shows that under CO the reduction of a portion of the Pt, corresponding to the formation and turnover of the carbonate is subject to a very low apparent activation energy (E_{app}); a fact confirmed by analyses of the MS and DRIFTS that all sample the catalyst bed in different manners. By contrast the re-oxidation of the Pt reduced in the CO cycle, by O_2, and the second phase of carbonate turnover, is characterized by an E_{app} of ca. 56.5 $kJ \cdot mol^{-1}$ (when averaged over the three applied methods).

This latter value is consistent with the reaction to form CO_2 occurring under O_2 being rate limited by desorption of molecular CO from the nanoparticulate component of the catalyst. In the limit of saturation CO coverage, heats of desorption for CO adsorbed at high coverages, and over a wide range of Pt dispersions, fall in the 54–63 $kJ \cdot mol^{-1}$ range [170]; the same is true for Pt single crystal surfaces

at saturation coverage of CO ((111) 60 kJ·mol^{-1} [171] and (110) 70 kJ·mol^{-1}) [172] obtained at low CO pressures.

From these central observations, made from perspectives of the net CO_2 production (MS), the infrared visible surface speciation, and the redox events occurring in the Pt component of the catalyst (Pt L_3-edge XAFS), a novel mechanism, that involves the participation of both atomic Pt species (that provide the sites for carbonate formation and turnover) and Pt nanoparticles (that supply the dissociated O required to re-oxidized the atomic Pt sites to close the catalytic cycle once CO has been desorbed), has been proposed [168,169] and detailed in Figure 21.

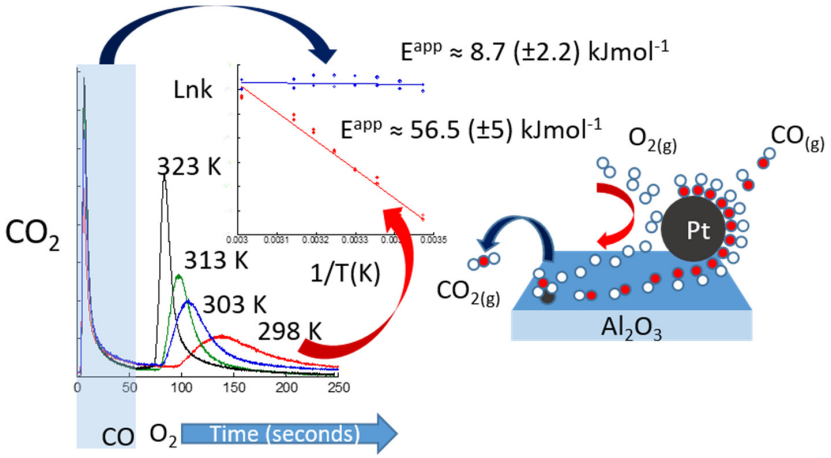

Figure 21. Mechanism for the low temperature oxidation of CO_2 derived from the combined application of time resolved XAFS, DRIFTS, and MS [168,169]. Isolated Pt atoms are suggested to be the active sites for the formation of reactive carbonate species (DRIFTS). The sites that form these carbonates must be reactivated through the participation of the nanoparticulate Pt also present that acts to supply oxygen to the atomic Pt sites once CO has desorbed from them. Reproduced with permission from *J. Am. Chem. Soc.* **2016**, *138*, 13930–13940 [169]. Copyright 2016, American Chemical Society.

Whilst, on the one hand, this mechanism is still hobbled by the same inhibition by CO adsorbed upon Pt nanoparticles and surfaces that has always fundamentally limited the application of simple Pt catalysts for CO turnover at low temperatures, this work has demonstrated that highly reactive carbonates exist and can react with CO at ambient temperature and below.

At present this can only be turned into a workable catalytic cycle by adopting a periodic approach to catalytic operation. However, the application of state of the art XAFS allied with MS and DRIFTS, in an appropriately adapted, operando manner, has permitted quantification of a novel mechanistic possibility and shown us what needs to be achieved to realize a Pt catalyst that can be used for steady state CO conversion at ambient temperatures.

4. A Brief Survey of Other Available X-ray Techniques, a Posteriori Methods of Data Treatment, and Caveats Relating X-ray Induced Effects *in Operando* Catalysis

4.1. XAFS and XES

Having detailed, as chronologically as possible, the evolution of our understanding of CO oxidation over Pt surfaces and simple supported catalysts through the fusion of operando methods with modern X-ray probes, and to some degree the evolution of the probes themselves, we might consider whether there are other X-ray methods and approaches that have yet to be brought to bear on the specific system that this review has devoted itself to.

As might be deduced from what has been shown previously, the capacities of time resolved XAFS has grown greatly in the last twenty years and quick scanning XAFS is no longer limited to

the interrogation of Pt L_3-edge XANES: for reasonable Pt loadings (ca. 1 wt % or greater) analyzable EXAFS on sub second time scales is now very much achievable for catalysts based on simple and "light" supports such as Al_2O_3.

A similar case can be made for emission spectroscopies especially for catalysis wherein the reactive reversibility of a catalyst can be used to obtained greater statistics through averaging in feed cycling experiments. New XES variants have also emerged, one of which deserves specific mention, that of high energy resolution off-resonant spectroscopy (HEROS) [173,174] that has also shown to have the ability to be applied in a time resolving manner to shed different insight into catalysis such as CO oxidation over Pt/Al_2O_3.

The essence of this approach is to apply monochromatic X-rays just below the edge of interest (in our case the Pt L_3-edge) and to use a bent crystal detection mechanism to collect the fluorescence yields in an energy dispersive manner. This result in fluorescence spectra, that have no self absorbtion issues to be accounted for and their shape can be analytically modelled. The details are beyond of the scope of this review and the interested reader is referred elsewhere [174,175] but this method has recently been applied to the dynamic study of the behavior Pt/Al_2O_3 catalysts under conditions of periodic gas switching.

It might further be surmised that a clear and present way to increase our fundamental understanding of the QSARS that underpin the catalytic conversion of CO to CO_2 by Pt is to make much more use of size and shape selected Pt nanoparticles. Examples of static XAFS fused with this of sort of approach have been undertaken [175] and it is clear that by starting with nanoparticles of a known size and shape then a good deal of uncertainty in the association with structure and structural change, that is endemic to samples that are heterogeneous in more ways than one, can be removed and more specific insight obtained. There is growing evidence (for instance [175]) that such fusion of more advanced synthetic methods with an operando approach and state of the art fast XAFS (or any other technique for that matter), could be a very powerful combination, though at the time of writing the author is not aware of such an approach taken for the particular catalytic case that is the scope of this review.

4.2. Methods Based Upon the Scattering of X-rays: SAXS, GISAXS, and High Energy Scattering Techniques —SXRD and Total X-ray Scattering/PDF

4.2.1. SAXS and GISAXS

Of the commonly known X-ray scattering methods that had yet to be applied to the particular catalytic problem that this review seeks to deal with is that of small angle scattering (SAXS) and its surface variant (GISAXS). This method complements XAFS and other scattering methods in its sensitivity to particle size distributions and morphological change (see for instance [159]) and these days it may be operated *in operando* and on sub-second timescales. That this method could indeed be used to considerable effect has also been demonstrated in a 2012 GISAXS study of the behavior of Pt nanoparticles supported upon Mg(001) in the presence of CO at pressures in the range 10^{-6}–10^{3} Pa [176].

What this study revealed was that Pt particles of the order of 1 nm diameter were disrupted to form carbonyls that were then readily assimilated into particles of ca. 2 nm in yet a further example of just how fluid Pt surfaces and nanoparticles can become under the influence of CO at elevated pressure. However, it remains to be seen what sort of new and dynamic insight into the behavior of supported Pt nanoparticles under conditions of CO oxidation this approach might reveal.

4.2.2. Approaches Using High Energy (>50 keV): SXRD and Total X-ray Scattering/PDF

High energy scattering methods are also coming of age, as hopefully the study shown in Section 2.7 has made clear in the case of supported Pt catalysts for fast PDF studies. However, SXRD [177,178] made upon metal surfaces and a sophisticated variant of it due to Stierle and co-workers [179–182]

using high energy X-rays to investigate supported nanoparticles has much to offer; and there are good reasons to think that in the near future both high energy PDF, XRD and even high energy SAXS measurements are going to be able to play ever more important roles in the wider scheme of catalytic science.

Amongst the many advantages the high energy X-rays have over those of a more conventional energy regime is that for a given solid angle of detection one obtains much more reciprocal space information; a situation that inevitably leads to the potential restoration of more precise structural information. When the system under study is a catalytic one, the corollary of this is that ever more exact relations can be achieved between structure, reactivity, and selectivity.

If one then combines this general idea with a combinatorial (graduated particle sizes [180] or compositions [182]) as Stierle and co-workers have succeeded in doing, then a very powerful, structurally deterministic operando approach rises. Importantly in these cases, crystal truncation rods that arise from the arrays of selected and supported metal nanoparticles used in such studies, become measurable. From these, precise assertions regarding the morphology—perhaps the most difficult aspect of nanoparticle structure to be precise about—and structural behavior of these nanoparticles *in operando* (using the evolution of the reactor due to Ferrer et al. in its commercialized flow version [118,119]) becomes possible. Indeed, in [182] this has even been achieved for arrays of PtRh nanoparticles undergoing CO oxidation to show that the more platinum rich these nanoparticles are the more structurally labile they become in terms of morphology and sintering, and that this structural fluidity is related to the energy released into the particles by the CO oxidation events themselves.

Beyond these new developments there is the ever evolving technology of the synchrotrons themselves to consider. Most of the large synchrotrons, that by their very nature provide the best sources of high energy (>50 keV) X-rays, are undergoing upgrades; and one of the biggest beneficiaries of these upgrades will be in the high energy regime. For instance, ID 15 at the ESRF is predicted to have ca. 70 times more flux density (at ca. 70 keV) as a result of the proposed reconfiguration of the ESRF lattice and the institution of new insertion devices [183]. Together with a new generation of fast imaging detectors adapted to work at these energies the potential gains for fast and structurally definitive SXRD on surfaces, or PDF studies of working catalysts of all sorts, could be enormous. The opportunities that await researchers into catalysis and materials chemistry in this area therefore could be considerable; opportunities to reconsider previous experimental limitations and create new experimental approaches that will allow even greater insight to be attained as to how catalysts function and how they might be manipulated and tailored to ever greater applied effect.

4.3. A Posteriori Approaches to Data Treatment and What They May Have to Offer

Thus far in this review we have seen a considerable augmentation in the ability of X-ray techniques of various types to be applied in *operando* situations; and as a consequence, new insights of fundamental and applied importance have arisen.

However, whilst this review is primarily occupied within delineating this evolution from an experimental perspective—and indeed for a particular example taken from within the catalytic canon—we might also ask how our ability to analyze the data now obtainable (which, by definition, in highly time resolved experimentation can be copious) has also advanced.

This consideration can be divided into two parts: the ability to reliably process large datasets as a preamble to analysis; and more advanced modes of analysis itself that may extract deeper insight and make the best use of the data now obtainable.

For the initial processing of large datasets, be they of a spectroscopic or scattering nature, solutions have often evolved locally at individual beamlines or as more general analysis packages that may be sometimes freely available. In the second category, methods of advanced analysis, then we might point to three significant areas: the recent and increasing awareness within the catalytic community of modulation excitation spectroscopy analysis (MES) [184], and more advanced approaches toward the modelling of XANES and EXAFS data that can provide deeper insight or resolve problems that

more conventional approaches struggle with. Within the time resolved, structural-kinetic, remit of this review by far the most important of these, if only as it is a method that is independent of the applied probe method, is MES, though we also note some other advanced methods in relation to getting the most from X-ray spectroscopy.

4.3.1. Modulation Excitation Spectroscopy (MES).

MES, using phase sensitive detection (PSD), is founded upon the principle that the behavior of a system that may be reversibly perturbed (for instance redox cycling) can then be analyzed on the basis that an applied square wave perturbation may be expressed as Fourier series wherein the square wave is viewed as an infinite summation of odd-frequency sine functions [184–187]. Almost by definition, therefore, any decent (i.e., continually reformed) catalytic system should be amenable to this form of experimentation and subsequent analysis.

Whilst the mathematical basis of this approach [184–187] is well beyond the scope of this review the major benefits of this method may be summarized as follows. In the first instance it permits a considerable enhancement in the sensitivity of any given technique to changes that are related to the applied perturbation and can therefore reveal aspects of the chemistry at hand that are otherwise invisible. A corollary of this is that for a nanoparticulate catalyst wherein the catalysis occurs at the surface of the particles whilst the bulk remains relatively unperturbed by the surface chemistry it can induce a surface sensitivity where none is native to the applied methods. In its fullest application it may also permit a complete kinetic (frequency response) analysis of the processes under study.

The infrared spectroscopic community were the first to adopt this type of approach to studying catalysis [183–189] and hence the soubriquet MES. However, this is an a posteriori method that is not limited to spectroscopic techniques; providing the requisite reversible modulation may be realized, any data, be it spectroscopic or scattering in nature, may be subsequently handled in this manner. As such, in recent years, the MES approach has started to be adopted by the X-ray community that studies a wide range of materials that includes catalysts. Since its first application in considering the dynamic responses of Rh and Pd catalysts under modulated feed conditions using dispersive XAFS [190], it has subsequently been utilized to enhance the ability of X-ray scattering techniques to see into dynamic catalyst behavior [191–200].

However, and as with all methods MES comes with caveats, checks, and balances beyond the basic requirement for a quantitative reversibility in the process under study. The depth of information that may be retrieved from an MES experiment is subject to limitations imposed by how the experiment was carried out and the technique applied. Again, whilst the mathematics are beyond this review, and as with any analysis based upon Fourier series or transforms, the more data you have the more robust subsequent analysis may be. This is well known in EXAFS and in PDF analysis. In the case of MES the two most important considerations are the number of modulations over which the data may be analyzed and density of data that can be collected within the modulations themselves; as it is these that will determine the range of frequencies (or harmonics) within the modulations that can be accessed by the subsequent analysis. As such for fast chemical transformations occurring over catalysts rapid and stable sampling of the catalysis by the probe used is very much a requirement; and one that can be met by many X-ray techniques available at modern synchrotrons.

It is also the case that the MES method yields difference patterns or spectra that whilst extremely informative can be problematic to quantitatively analyze. In the case of X-ray spectroscopy it has been shown that such quantitative structural analysis can be restored from MES-EXAFS data [191], and the work of Chernyshov et al. has done the same [195–197], for the analysis of X-ray diffraction data. For the moment, however, MES is predominantly used as a qualitative enhancer of the sensitivity of the basic XAFS or XRD based experiment. To the author's knowledge, quantitative restoration of reaction kinetics using the full frequency response capacity of MES has yet to be demonstrated for X-ray based experiments, though examples do exist in the world of infrared spectroscopy (see for instance [186]).

That said it seems only a matter of time before this potentially powerful method is more fully adopted and codified for more general and in depth study of catalysis using X-ray methods if only for the fact that the required X-ray methods and capacity are in place at beamlines around the world.

4.3.2. Modelling of Near Edge Structure (XANES) and Wavelet Analysis in X-ray Spectroscopy

More In-Depth Use of XANES: Analysis and Modelling

As we have seen, when using operando methods based upon X-ray absorption, information regarding the structure and behavior of the system under study may be derived from both XANES and EXAFS regions of the spectrum. More often than not, however, in time resolved study it is the XANES region that forms the basis of comprehending the nature of the changes occurring in the system. The XANES region potentially contains a huge amount of information (both structural and electronic) regarding the system under study and its composition; it has even been theoretically shown, in the case of Pt, that standard Pt L_3-edge XANES can be sensitive to aspects of the structure of very small Pt particles such as morphology [111]. However, the relative ease with which XANES may be obtained (compared to reliably analyzable EXAFS) is in direct opposition to its complexity and therefore the extent to which it is used is, more often than not, in more qualitative or semi-quantitative manners.

For example, in some of the examples given in this review we have seen that the application of linear combinations of well-chosen standard spectra can start to quantify the relative amounts of oxidation present in a working system (Section 2.6). Thus, quantified they can be directly related to aspects of reactive behavior and point out situations wherein a simple linear combinations of spectra fails to account for the detailed behavior of the XANES.

However, one might ask whether we can go further and extract more specific information: the answer to this question is an undeniable "yes": but a "yes" that is very much qualified by the intrinsic complexity of the XANES region and, in the case of Pt, intrinsically large core-hole lifetimes; though, as we have, seen (Section 2.5) high energy resolution methods can do something about within certain limits.

It has been shown that, by combining HERFD with the theoretical modelling capability of the FEFF8.2 (The FEFF Project, University of Washington, Seattle, WA, USA, 2001) [141] resource for XAFS analysis, the features revealed by HERFD for supported Pt nanoparticles exposed to CO could be explained through the dominant adsorption of linearly bound CO in an atop configuration. As an exemplar this is proof that the XANES may be used in a manner that can identify the nature of some types of surface speciation as well as the oxidation states present in a Pt catalyst. Equally, however, it could be argued that of itself, this information could be arrived at in a more detailed manner (especially in a highly time resolved situation) using infrared spectroscopy combined with XAFS and for which many approaches have now been demonstrated [73–81].

To move beyond information that could be obtained by other means, other methods do present themselves. Of these we might point to methods based upon principal component analyses (PCA) [200,201] and those based upon theoretical calculation of the XANES spectra based upon a variety of approaches.

Of these two very different possibilities only the former has thus far been used to extract otherwise non accessible information regarding the dynamic (and particle size dependent) behavior of a working catalyst, and for Pd rather than Pt [201].

By and large the methods of explicitly calculating XANES structure [202–208], are clearly becoming very powerful. Generally, however, they are rooted in the modeling of discrete molecules rather than extended structures such as the nanoparticles for which this review has its major remit. One might also note that their application requires suitable time resolved datasets: thus far, to the author's knowledge, such a fusion of time resolved operando experimentation with these advanced theoretical methods has not been demonstrated. In a more general catalytic sense, however, the continued improvement of these methods, along with an increased usage of time resolved operando

XAFS and XES, will eventually result in their fusion to yield a far more precise understanding of catalysts of many types that we have obtained to date.

Wavelet (WT) Analysis as Applied to EXAFS

In conventional EXAFS analysis certain combinations of atom types can be hard to distinguish and their satisfactory localization within a coordination sphere may remain impossible to determine even after extensive analysis. In terms of the specific catalysis dealt with in this review this is not an issue. However, bearing in mind the much wider field of catalysis in general and even catalysts based upon Pt but whose function may be determine by other elements, WT analysis of EXAFS [209–212], that has not received a great deal of attention from the catalysis world, is worthy of mention as an analytical method than can enhance a time resolved operando experiment. The essence of the approach is based upon the use of non-infinite sine functions that add extra degrees of freedom to the fitting of the EXAFS. The result is that R space and K space may be correlated in a two dimensional manner to more clearly reveal the scattering interactions present within the system under study.

In [212], for example, this approach is used to identify isolated Pt^{IV} sites in $Mg(In)(Al)O_x$ catalysts and the subsequent formation of PtIn alloy nanoparticles after reduction. Whilst this method does not get around the general inability of XAS to distinguish scattering from neighbouring elements in the periodic table, it does add a new dimension to how the scattering information contained within an EXAFS experiment can be revealed such that a more detailed physical understanding may be arrived at.

It remains to be seen, however, whether this method can be successfully applied to the large datasets that arise from time resolved study that often come with reduced data quality compared to a standard scanning EXAFS experiment. As we have seen, however, advances in the technology behind Quick scanning EXAFS [114,115] continue to reduce this deficit and with it the magnitude of the trade-off that exists between data quality and high time resolution.

4.4. Potential Pitfalls and Caveats: X-ray Induced Effects in Catalytic Study

Aside designing experiments that conform, as optimally as possible, to the conditions that catalysts might actually experience during real operation, the use of X-ray probes brings with it another consideration: that the probe should not influence what is to be measured.

Unfortunately, for all their utility, X-rays can interact with matter in various unwanted ways that can change the systems under study and lead to erroneous conclusions being drawn. These may result from the deposition of thermal energy into the samples as a result of the absorption of the X-rays by the sample or as a result of electrons emitted as by product of X-ray absorption and scattering by the sample or the reaction media. The latter can have wide ranging transformative effects including the degradation of the sample itself whilst both of these effects can have a significant influence on rates of reaction and therefore derived kinetics.

As already mentioned (Section 2.4) such effects were noted and steps taken to avoid them [134,135]. Indeed, amongst the various reports of X-ray induced effects in a variety of materials and catalytic situations [213–215], we might specifically note X-ray induced oxidation of even a gold foil in elevated pressure XPS [215]. Given the nobility of Au surfaces this study highlights just how pernicious such problems can be. Moreover, given the modern trend for ever higher brilliance and power densities of X-ray beams, this is an issue that may only get worse and practitioners of operando study must always be on the lookout for unwanted beam related effects.

However, the propensity for any experiment to be sensitive to such artefacts is a complex matter for which catch-all rules cannot readily be established. Whether any given experiment might be susceptible to X-ray induced artefacts is a function of the nature of the sample, the reaction medium, and the brilliance of the X-rays, but also the energy of the applied X-rays themselves.

As a (very) general rule of thumb such problems are going to be far more likely encountered the lower the energies of the applied X-rays are. This may sound somewhat counter intuitive but the higher the energy of the X-rays the less likely they are to be absorbed to heat the sample, or lead to the

formation of potentially system altering electrons: the cross sections for X-ray excitation fall away very rapidly the further one is away from an elemental absorption edge.

Therefore we might surmise that techniques such as XPS, or microscopies wherein the power density of the X-ray beam can be extremely high, will always be more susceptible to the unwanted effects than, for instance, conventional EXAFS (that operates at generally higher energies and with relatively large X-ray beams), or high energy diffraction and total X-ray scattering PDF where the absorption of X-rays (at energies > 50 keV) is minimized by definition as the X-ray energies themselves are very far away from most elemental adsorbtion edges.

5. Conclusions

The last twenty years have seen a massive growth in the abilities of synchrotron sources. On roughly the same sort of timescales we have seen a much keener effort on many sides to observe catalytic systems, whether they be models based upon metal or oxide surfaces, or real catalysts operating at high pressures and temperature, under well-defined conditions that are parameterized according to the processes under study, and in a fashion that gets as close as possible to that situation that Banares [71,72] coined as "operando". For sure approaches that sought to do this predated the term, but the idea has acted as a considerable stimulus to the development of new methods and combinations of methods—that are not only efficient but internally self-consistent—that attempt to attain this ideal; and to do so they have required the effective collaboration of a very diverse array of people and knowledge bases. This is no more the case when considering catalysis experiments at synchrotrons whose implementation and successful conclusion require wide-ranging competences and knowledge to be brought together.

In terms of the remit of this review therefore, what have we learned from an exercise that started around twenty years ago, at a time when research into the catalytic oxidation of CO over Pt surface and simple catalysts was already eighty or so years old?

The two most prominent issues that modern synchrotron methods allied to the operando philosophy have resolved are the importance of the pressure gap and the dominant roles that redox phenomena in the Pt component and reactive surface oxides can have. These are not formally considered in the traditional LH mechanism, and were not observed to be present in the low pressure single crystal regimes that did so much to enhance our atomic level understanding of surface chemistry in the eighties and nineties. However, right from the first of the examples given in this review a rather different picture has emerged. As soon as one bridges the pressure gap we find that redox phenomena in the Pt phase can very much dominate proceedings and lie at the very heart of some of the complex phenomena (such as oscillatory behavior) longtime observed in this system. At the very least, therefore, Langmuir's model needs revision to include these surface oxides and a component that, formally speaking, is of the Mars–van Krevelen type.

The other gap, the materials gap, has appeared of lesser importance in this particular system. Within the range of operando X-ray experimentation achieved in this area there appears a remarkable level of consistency regarding the appearance and roles of Pt surface oxides, whether they be formed on Pt single crystals or on nanoparticulate catalysts; and we have even seen the transferability of one surface oxide structure observed on Pt single crystals [116] to the Pt nanoparticle in a Pt/Al_2O_3 catalyst [163]. Surface based diffraction methods have also highlighted roles of surface roughness and surface steps may have to play as a function of feedstock in their conversion, such is the apparent malleability of Pt in the presence of CO. In this latter case, whether such specific insight may be eventually attained for real nanoparticulate systems, where the fundamental roles of particle morphology and changes in it are still very much open questions that are extremely difficult to measure and be precise about, remains to be seen.

However, it is the surface oxides and the potential for redox events involving the Pt that we can now see as playing a deterministic role in CO oxidation. In this respect a recent move to considering spatial effects, using fast X-ray techniques in plug flow situations [152,153] has added another, reaction engineering based, element, to the study of CO oxidation by Pt.

Lastly, an example [168,169] that would confirm a recently made hypothesis [167] that low temperature CO turnover can be affect by Pt carbonates, most likely present as isolated atoms at the surface of an alumina, has arisen from operando, multi-technique, experimentation, even though at present the evidence suggests that Pt nanoparticles are still required to help regenerate these atomic sites.

What the future might have in store for this particular piece of surface chemistry cannot be readily surmised. But for this, and many other examples of catalysis, be they gas-solid, liquid-solid or homogeneous, I hope that this little tour through a well-trodden pasture has shown that modern synchrotron sources, many of which will be upgraded in the new future, offer a great deal to catalytic scientists that is well worth the effort.

Acknowledgments: I should like to thank: the Department of Physics at the University of Warwick, UK, for the provision of a visiting scientist position that permitted the experiments in Section 3 to be carried out; the Royal Society of Chemistry for a Journals grant (09 01 639) that permitted the PDF measurements described in Section 2.6 to be undertaken; the Advanced Photon Source at Argonne National Laboratory, USA, for a visiting scientist position that allowed the analysis of those results, and the development of a combined PDF/DRIFTS/MS experiment for the dynamic operando study of working catalysts at Sector 11 of the Advanced Photon Source (APS) [78]; and the Swiss light Source for a visiting position that permitted the experiments described in Section 3 [168,169] to be made.

Above all I should like to thank my collaborators for their long standing support in these and future studies into room temperature CO oxidation—Peter J. Chupas and Karena W. Chapman at the APS, Marco Di Michiel at ID 15 at the ESRF, Davide Ferri at the Paul Scherrer Institute, Switzerland, and Maarten Nachtegaal at the SuperXAS beamline, Swiss Light Source, also at the Paul Scherrer Institute, Switzerland.

Conflicts of Interest: The author declares no conflict of interest.

References

1. Rogers, T.H.; Piggot, C.S.; Balke, W.H.; Jennings, J.M. The catalytic oxidation of carbon monoxide. *J. Am. Chem. Soc.* **1921**, *43*, 1743. [CrossRef]
2. Merrill, D.R.; Scalione, C.C. The Catalytic oxidation of carbon monoxide at ordinary temperatures. *J. Am. Chem. Soc.* **1921**, *43*, 1982–2002. [CrossRef]
3. Lamb, A.B.; Bray, W.C.; Frazer, J.C.W. The removal of carbon dioxide from air. *Ind. Eng. Chem.* **1920**, *12*, 213–221. [CrossRef]
4. Platinum. Available online: http://www.rsc.org/periodic-table/element/78/platinum (accessed on 12 February 2017).
5. Platinum Quaterly Q4. Available online: https://www.platinuminvestment.com/files/WPIC_Platinum_Quarterly_Q4_2014.pdf (accessed on 12 February 2017).
6. Dallabetta, R.A.; McCune, R.C.; Sprys, J.W. Relative importance of thermal and chemical deactivation of noble-metal automotive oxidation catalysts. *Ind. Eng. Chem. Prod. Res. Dev.* **1976**, *15*, 169–172. [CrossRef]
7. Lamy, C.; Leger, J.M. Electrocatalytic oxidation of small organic materials at platinum single crystal surfaces. *J. Chim. Phys. Phys. Chim. Biol.* **1991**, *88*, 1649–1671.
8. Carrette, L.; Friedrich, K.A.; Stimming, U. Fuel cells: Principles, types, fuels, and applications. *Chem. Phys. Chem.* **2000**, *1*, 162–193. [PubMed]
9. Markovic, N.M.; Ross, P.N. Surface science studies of model fuel cell electrocatalysts. *Surf. Sci. Rep.* **2002**, *45*, 121–229. [CrossRef]
10. Cheng, X.; Shi, Z.; Glass, M.; Zhang, L.; Zhang, J.J.; Song, D.T.; Liu, Z.S.; Wang, H.J.; Shen, J. A review of PEM hydrogen fuel cell contamination: Impacts, mechanisms, and mitigation. *J. Power Sources* **2007**, *165*, 739–756. [CrossRef]
11. Langmuir, I. Chemical reactions at low pressures. *J. Am. Chem. Soc.* **1915**, *37*, 1139–1167. [CrossRef]
12. Langmuir, I. The mechanism of the catalytic action of platinum in the reactions $2CO + O_2 = CO_2$, and $2H_2 + O_2$. *Trans. Faraday Soc.* **1922**, *17*, 621–654. [CrossRef]
13. Eley, D.D.; Rideal, E.K. Parahydrogen conversion on Tungsten. *Nature* **1940**, *146*, 401–402. [CrossRef]
14. Mars, P.; van Krevelen, D.W. Oxidations carried out by means of vanadium oxide catalysts. *Chem. Eng. Sci. Spec. Suppl.* **1954**, *3*, 41–50. [CrossRef]
15. Laidler, K.J. *Chemical Kinetics*; Harper & Row: New York, NY, USA, 1987.

16. Royer, S.; Duprez, D. Catalytic oxidation of carbon monoxide over transition metal oxides. *ChemCatChem* **2011**, *3*, 24–65. [CrossRef]
17. Haruta, M. Size- and support-dependency in the catalysis of gold. *Catal. Today* **1997**, *36*, 153–166. [CrossRef]
18. Thormählen, P.; Skoglundh, M.; Fridell, E.; Andersson, B. Low-temperature CO oxidation over platinum and cobalt oxide catalysts. *J. Catal.* **1999**, *188*, 300–310. [CrossRef]
19. Bond, G.C.; Thompson, D.T. Catalysis by gold. *Catal. Rev. Sci. Eng.* **1999**, *41*, 319–388. [CrossRef]
20. Carretin, S.; Concepcion, P.; Corma, A.; Nieto, J.M.L.; Puntes, V.F. Nanocrystalline CeO_2 increases the activity of Au for CO oxidation by two orders of magnitude. *Angew. Chem. Int. Ed.* **2004**, *43*, 2538–2540. [CrossRef] [PubMed]
21. Hashmi, A.S.K.; Hutchings, G.J. Gold catalysis. *Angew. Chem. Int. Ed.* **2006**, *45*, 7896–7936. [CrossRef] [PubMed]
22. Yao, Y.Y. The oxidation of hydrocarbons and CO over metal oxides: III. Co_3O_4. *J. Catal.* **1974**, *33*, 108–122. [CrossRef]
23. Perti, D.; Kabel, R.L. Kinetics of CO oxidation over Co_3O_4/γ-Al_2O_3. Part I: Steady state. *AIChE J.* **1985**, *31*, 1420–1426. [CrossRef]
24. Xie, X.; Liu, Z.-Q.; Haruta, M.; Shen, W. Low-temperature oxidation of CO catalysed by Co_3O_4 nanorods. *Nature* **2009**, *458*, 746–749. [CrossRef] [PubMed]
25. Vayssilov, G.N.; Lykhach, Y.; Migani, A.; Staudt, T.; Petrova, G.P.; Tsud, N.; Skala, T.; Bruix, A.; Illas, F.; Prince, K.C.; et al. Support nanostructure boosts oxygen transfer to catalytically active platinum nanoparticles. *Nat. Mater.* **2011**, *10*, 310–315. [CrossRef] [PubMed]
26. Qiao, B.; Wang, A.; Yang, X.F.; Allard, L.F.; Jiang, Z.; Cui, Y.T.; Liu, J.Y.; Li, J.; Zhang, T. Single-atom catalysis of CO oxidation using Pt_1/FeO_x. *Nat. Chem.* **2011**, *3*, 634–641. [CrossRef] [PubMed]
27. Chen, G.X.; Zhao, Y.; Fu, G.; Duschene, P.N.; Gu, L.; Zheng, Y.P.; Weng, X.F.; Chen, M.S.; Zhang, P.; Pao, C.W.; et al. Interfacial effects in iron-nickel hydroxide—Platinum nanoparticles enhance catalytic oxidation. *Science* **2014**, *344*, 495–499. [CrossRef] [PubMed]
28. Peterson, E.J.; De La Riva, A.T.; Lin, S.; Johnson, R.S.; Guo, H.; Miller, H.T.; Kwak, J.H.; Peden, C.H.F.; Kiefer, B.; Allard, L.F.; et al. Low-temperature carbon monoxide oxidation catalysed by regenerable atomically dispersed palladium on alumina. *Nat. Commun.* **2014**, *5*, 4885. [CrossRef] [PubMed]
29. Guan, H.; Lin, J.; Qiao, B.; Yang, X.; Li, L.; Miao, S.; Liu, J.; Wang, A.; Wang, X.; Zhang, T. Catalytically active Rh sub-nanoclusters on TiO_2 for CO oxidation at cryogenic temperatures. *Angew. Chem. Int. Ed.* **2016**, *55*, 2820–2824. [CrossRef] [PubMed]
30. Jakubith, M. Isothermal oscillation in CO-oxidation on platinum mesh. *Chem. Ing. Tech.* **1970**, *42*, 943.
31. Hugo, P.; Jakubith, M. Dynamic behaviour and kinetics of carbon-monoxide on platinum catalysts. *Chem. Ing. Tech.* **1972**, *44*, 383. [CrossRef]
32. Beusch, H.; Wicke, E.; Fieguth, P. Thermally and kinetically produced instabilities in reaction behaviour of individual catalyst grains. *Chem. Ing. Tech.* **1972**, *44*, 445. [CrossRef]
33. Dauchot, J.P.; Vancaken, J. Oscillations during catalytic oxidation of carbon monoxide. *Nat. Phys. Sci.* **1973**, *246*, 61–63. [CrossRef]
34. McCarthy, E.; Zaharadnik, J.; Kuczynski, G.C.; Carberry, J.J. Some unique aspects of CO oxidation on supported Pt. *J. Catal.* **1975**, *39*, 29–35. [CrossRef]
35. Sheintuch, M.; Schmitz, R.A. Oscillations in catalytic reactions. *Catal. Rev. Sci. Eng.* **1977**, *15*, 107–172. [CrossRef]
36. Varghese, P.; Carberry, J.J.; Wolf, E.E. Spurious limit-cycles and related phenomena during CO oxidation on supported platinum. *J. Catal.* **1978**, *55*, 76–87. [CrossRef]
37. Slin'ko, M.G.; Slin'ko, M.M. Self-oscillations of heterogeneous catalytic reaction rates. *Catal. Rev. Sci. Eng.* **1978**, *17*, 119–153. [CrossRef]
38. Plichta, R.T.; Schmitz, R.A. Oscillations in the oxidation of carbon-monoxide on a platinum foil. *Chem. Eng. Commun.* **1979**, *3*, 387–398. [CrossRef]
39. Turner, J.E.; Sales, B.C.; Maple, M.B. Oscillatory oxidation of a Pt catalyst. *Surf. Sci.* **1981**, *103*, 54–74. [CrossRef]
40. Sales, B.C.; Turner, J.E.; Maple, M.B. The oxidation and CO reduction kinetics of a platinum surface. *Surf. Sci.* **1981**, *112*, 272–280. [CrossRef]

41. Sales, B.C.; Turner, J.E.; Maple, M.B. Oscillatory oxidation of CO over Pt, Pd, and Ir catalysts—Theory. *Surf. Sci.* **1982**, *114*, 381–394. [CrossRef]
42. Ertl, G.; Norton, P.R.; Rustig, J. Kinetic oscillations in the platinum-catalyzed oxidation of CO. *Phys. Rev. Lett.* **1982**, *42*, 177–180. [CrossRef]
43. Turner, J.E.; Maple, M.B. Oxide formation and reduction over Pt, Pr, and Ir—A driving mechanism oscillations in the CO oxidation reaction. *Surf. Sci.* **1984**, *147*, 647–662. [CrossRef]
44. Tsai, P.K.; Wu, M.G.; Maple, M.B. Oscillatory oxidation of CO over Pt at pressures from 10 to 760 Torr. *J. Catal.* **1991**, *127*, 512–523. [CrossRef]
45. Lynch, D.T.; Wanke, S.E. Oscillations during CO oxidation over supported metal catalysts: I. Influence of catalyst history on activity. *J. Catal.* **1984**, *88*, 333–344. [CrossRef]
46. Lynch, D.T.; Wanke, S.E. Oscillations during CO oxidation over supported metal catalysts: II. Effects of reactor operating conditions on oscillatory behaviour for a Pt-Pd/Al_2O_3 catalyst. *J. Catal.* **1984**, *88*, 345–354. [CrossRef]
47. Imbihl, R.; Cox, M.P.; Ertl, G. Kinetic oscillations in the catalytic CO oxidation on Pt(100)—Theory. *J. Chem. Phys.* **1985**, *83*, 1578–1587. [CrossRef]
48. Cox, M.P.; Ertl, G.; Imbihl, R.P. Spatial self-organization of surface-structure during and oscillating catalytic reaction. *Phys. Rev. Lett.* **1985**, *54*, 1725–1728. [CrossRef] [PubMed]
49. Galwey, A.K.; Gray, P.; Griffiths, J.F.; Hasko, S.M. Surface retexturing of Pt wires during the catalytic oxidation of CO. *Nature* **1985**, *313*, 668–671. [CrossRef]
50. Yeates, R.C.; Turner, J.E.; Gellman, A.J.; Somorjai, G.A. The oscillatory behaviour of the CO oxidation reaction at atmospheric pressure over platinum single crystals—Surface analysis and pressure dependent mechanisms. *Surf. Sci.* **1985**, *149*, 175–190. [CrossRef]
51. Lynch, D.T.; Emig, G.; Wanke, S.E. Oscillations during CO oxidation over supported metal catalysts: III. Mathematical modelling of the observed phenomena. *J. Catal.* **1986**, *97*, 456–468. [CrossRef]
52. Imbihl, R.; Cox, M.P.; Ertl, G. Kinetic oscillations in the catalytic CO oxidation on Pt(100)—Experiments. *J. Chem. Phys.* **1986**, *84*, 3519–3534. [CrossRef]
53. Razon, L.F.; Chang, S.-M.; Schmitz, R.A. Chaos during the oxidation of carbon monoxide on platinum—Experiments and analysis. *Chem. Eng. Sci.* **1986**, *41*, 1561–1576. [CrossRef]
54. Razon, L.F.; Schmitz, R.A. Intrinsically instable behaviour during the oxidation of carbon monoxide on platinum. *Catal. Rev. Sci. Eng.* **1986**, *28*, 89–164. [CrossRef]
55. Razon, L.F.; Schmitz, R.A. Multiplicities and instabilities in chemically reacting systems. *Catal. Rev. Sci. Eng.* **1987**, *42*, 1005–1047. [CrossRef]
56. Burrows, V.A.; Sundaresan, S.; Chabal, Y.J.; Christman, S.B. Studies of self-sustained reaction rate oscillations: I. Real-time infrared measurements during oscillatory oxidation of carbon-monoxide on platinum. *Surf. Sci.* **1985**, *160*, 122–138. [CrossRef]
57. Burrows, V.A.; Sundaresan, S.; Chabal, Y.J.; Christmann, S.B. Studies of self-sustained reaction rate oscillations: II. The role of carbon and oxides in the oscillatory oxidation of carbon-monoxide on platinum. *Surf. Sci.* **1987**, *180*, 110–135. [CrossRef]
58. Collins, N.A.; Sundaresan, S.; Chabal, Y.J. Studies of self-sustained reaction rate oscillations: III. The carbon model. *Surf. Sci.* **1987**, *180*, 136–152. [CrossRef]
59. Schuth, F.; Wicke, E. IR spectroscopic investigations during oscillations of the CO/NO and CO/O_2 reaction on Pt and Pt catalysts: I. Platinum. *Ber. Bunsenges. Phys. Chem.* **1989**, *93*, 191–201. [CrossRef]
60. Eiswirth, M.; Moller, P.; Wetzl, K.; Imbihl, R.; Ertl, G. Mechanisms of spatial self-organisation in isothermal kinetic oscillations during the catalytic CO oxidation on Pt single crystal surfaces. *J. Chem. Phys.* **1989**, *90*, 510–521. [CrossRef]
61. Ertl, G. Oscillatory kinetics and spatio-temporal self-organisation in reactions at solid surfaces. *Science* **1991**, *254*, 1750–1755. [CrossRef] [PubMed]
62. Engel, W.; Kordesch, M.E.; Rotermund, H.H.; Kubala, S.; von Oertzen, A. A UHV compatible photoelectron emission microscope for applications in surface science. *Ultramicroscopy* **1991**, *36*, 148–153. [CrossRef]
63. Rotermund, H.H.; Engel, W.; Kordesch, M.; Ertl, G. Imaging of spatiotemporal pattern evolution during carbon-monoxide oxidation on platinum. *Nature* **1990**, *343*, 355–357. [CrossRef]
64. Krischer, K.; Eiswirth, M.; Ertl, G. Oscillatory CO oxidation on Pt(110)—Modelling of temporal self-organisation. *J. Chem. Phys.* **1992**, *96*, 9161–9172. [CrossRef]

65. Lauterbach, J.; Haas, G.; Rotermund, H.H.; Ertl, G. Spatio temporal pattern formation on polycrystalline platinum surfaces during catalytic CO oxidation. *Surf. Sci.* **1993**, *294*, 116–130. [CrossRef]
66. Gorodetskll, V.; Lauterbach, J.; Rotermund, H.H.; Block, J.H.; Ertl, G. Coupling between adjacent crystal places in heterogeneous catalysis by propagating reaction-diffusion waves. *Nature* **1994**, *370*, 276–279. [CrossRef]
67. Eiswirth, M.; Burger, J.; Strasser, P.; Ertl, G. Oscillating Langmuir-Hinshelwood mechanisms. *J. Phys. Chem.* **1996**, *100*, 19118–19123. [CrossRef]
68. Winterlin, J.; Volkening, S.; Janssens, T.V.W.; Zambelli, T.; Ertl, G. Atomic and macroscopic reaction rates of a surface catalysed reaction. *Science* **1997**, *278*, 1931–1934. [CrossRef]
69. Che, M.; Bennett, C.O. The influence of particle size on the catalytic properties of supported metals. *Adv. Catal.* **1989**, *36*, 55–172.
70. Cuenya, B.R. Synthesis and catalytic properties of metal nanoparticles: Size, shape, support composition, and oxidation effects. *Thin Solid Films* **2010**, *518*, 3127–3150. [CrossRef]
71. Guerrero-Perez, M.O.; Banares, M.A. Operando Raman study of alumina supported Sb-V-O catalyst during propene ammoxidation to acrylonitrile with on-line activity measurement. *Chem. Commun.* **2002**, 1292–1293. [CrossRef]
72. Banares, M.A.; Guerrero-Perez, M.O.; Fierro, J.L.G.; Cortez, G.G. Raman spectroscopy during catalytic operations with on-line activity measurement (operando spectroscopy): A method for understanding the active centres of cations supported on porous materials. *J. Mater. Chem.* **2002**, *12*, 3337–3342. [CrossRef]
73. Newton, M.A.; Jyoti, B.; Dent, A.J.; Fiddy, S.G.; Evans, J. Synchronous, time resolved, diffuse reflectance FT-IR, energy dispersive EXAFS (EDE) and mass spectrometric investigation of Rh catalysts during NO reduction by CO. *Chem. Commun.* **2004**, 2382–2384. [CrossRef] [PubMed]
74. Marinkovic, N.S.; Wang, Q.; Frenkel, A.I. In situ diffuse reflectance IR spectroscopy and X-ray absorption spectroscopy for fast catalytic processes. *J. Synchrotron Radiat.* **2011**, *18*, 447–455. [CrossRef] [PubMed]
75. Newton, M.A.; Di MIchiel, M.; Kubacka, A.; Fernández-García, M. Combining time resolved hard X-ray diffraction (XRD) and diffuse reflectance infrared spectroscopy (DRIFTS) to illuminate CO dissociation and transient carbon storage by supported Pd nanoparticles during CO/NO cycling. *J. Am. Chem. Soc.* **2010**, *132*, 4540–4541. [CrossRef] [PubMed]
76. Newton, M.A.; Di Michiel, M.; Kubacka, A.; Iglesias-Juez, A.; Fernández-García, M. Seeing oxygen storage and release in action and elucidating synergies between noble metal nanoparticles and promoter oxides. *Angew. Chem. Int. Ed.* **2012**, *51*, 2363–2367. [CrossRef] [PubMed]
77. Chiarello, G.L.; Nachtegaal, M.; Marchionni, V.; Quaroni, L.; Ferri, D. Adding diffuse reflectance infrared Fourier transform spectroscopy capability to extended X-ray absorption fine structure in a new cell to study solid catalysts in combination with a modulation approach. *Rev. Sci. Instrum.* **2014**, *85*, 074102. [CrossRef] [PubMed]
78. Beyer, K.A.; Zhao, H.; Borkiewicz, O.J.; Newton, M.A.; Chupas, P.J.; Chapman, K.W. Simultaneous diffuse reflection infrared spectroscopy and X-ray pair distribution function measurements. *J. Appl. Cryst.* **2014**, *47*, 95–101. [CrossRef]
79. Brieger, C.; Melke, J.; van der Bosch, N.; Reinholz, U.; Riesemeier, H.; Buzanich, A.G.; Kayarkatte, M.K.; Derr, I.; Schökel, A.; Roth, C. A combined in-situ XAS-DRIFTS study unraveling adsorbate induced changes on the Pt nanoparticle structure. *J. Catal.* **2016**, *339*, 57–67. [CrossRef]
80. Bando, K.K.; Wada, T.; Miyamoto, T.; Miyazaki, K.; Takakusagi, S.; Gott, T.; Yamaguchi, A.; Nomura, M.; Oyama, S.T.; Asakura, K. In situ FTIR and XANES studies of thiophene hydrodesulpurisation on Ni_2P/MCM-41. *J. Phys. C* **2009**, *190*, 012158.
81. Bando, K.K.; Wada, T.; Miymoto, T.; Miyazaki, K.; Takakusgi, S.; Koike, Y.; Inada, Y.; Nomura, M.; Yamaguchi, A.; Oyama, S.T.; et al. Combined in situ QXAFS and FTIR analysis of a Ni phosphide catalyst under hydrodesulphurisation conditions. *J. Catal.* **2012**, *286*, 165–171. [CrossRef]
82. Beale, A.M.; van der Eerden, A.M.J.; Kervinen, K.; Newton, M.A.; Weckhuysen, B.M. Adding a third dimension to operando spectroscopy: A combined UV-Vis, Raman, and XAFS set up to study heterogeneous catalysts under working conditions. *Chem. Commun.* **2005**, 3015–3017. [CrossRef] [PubMed]
83. Briois, V.; Belin, S.; Villain, F.; Bouamrane, F.; Lucas, H.; Lescouezec, R.; Julve, M.; Verdaguer, M.; Tokumoto, M.S.; Santilli, C.V.; et al. New insights for materials science characterisation using different complentary techniques combined with X-ray absorption spectroscopy. *Phys. Scr.* **2005**, *T115*, 38–44. [CrossRef]

84. Briois, V.; Lutzenkirchen-Hecht, D.; Villain, F.; Fonda, E.; Belin, S.; Griesebock, B.; Frahm, R. Time-resolved study of the oxidation of ethanol by cerium(IV) using combined Quick-EXAFS, UV-Vis, and Raman spectroscopies. *J. Phys. Chem. A* **2005**, *109*, 320–329. [CrossRef] [PubMed]
85. Grandjean, D.; Beale, A.M.; Petukhov, A.V.; Weckhuysen, B.M. Unraveling the crystallisation mechanism of CoAPO-5 molecular seives under hydrothermal conditions. *J. Am. Chem. Soc.* **2005**, *127*, 14454–14465. [CrossRef] [PubMed]
86. De Smit, E.; Cinquini, F.; Beale, A.M.; Safonova, O.V.; van Beek, W.; Sautet, P.; Weckhuysen, B.M. Stability and reactibity of ε-χ-θ iron carbide catalyst phases in Fischer-Tropsch synthesis: Controlling μ_c. *J. Am. Chem. Soc.* **2010**, *132*, 14928–14941. [CrossRef] [PubMed]
87. Iglesias-Juez, A.; Beale, A.M.; Maajien, L.; Weng, T.C.; Glatzel, P.; Weckhuysen, B.M. A combined in situ time resolved UV-Vis, Raman, and high energy resolution X-ray absorption spectroscopy study on the deactivation behaviour of Pt and Pt-Sn propane dehydrogenation catalyts under industrial reaction conditions. *J. Catal.* **2010**, *276*, 268–279. [CrossRef]
88. Newton, M.A.; van Beek, W. Combining vibrational spectroscopies with synchrotron based X-ray techniques for the in situ study of heterogeneous catalysts: A view from a bridge. *Chem. Soc. Rev.* **2010**, *39*, 4845–4863. [CrossRef] [PubMed]
89. Bentrup, U. Combining in situ characterisation methods in on set-up: Looking with ore eyes into the intricate chemistry of the synthesis and working of heterogeneous catalysts. *Chem. Soc. Rev.* **2010**, *39*, 4718–4730. [CrossRef] [PubMed]
90. Newton, M.A.; Fernandez-Garcia, M. Combining infrared spectroscopy with X-ray techniques for the investigation of working heterogeneous catalysts. In *In-Situ Characterization of Heterogeneous Catalysts*; Chupas, P.J., Hanson, J., Rodriguez, J.A., Eds.; Wiley: Hoboken, NJ, USA, 2013; Chapter 14; pp. 369–409.
91. Van Beek, W.; Ruiz-Martinez, J.; Milanesio, M. XRD-Raman and modulation excitation spectroscopy. In *In-Situ Characterization of Heterogeneous Catalysts*; Chupas, P.J., Hanson, J., Rodriguez, J.A., Eds.; Wiley: Hoboken, NJ, USA, 2013; Chapter 15; pp. 411–440.
92. Hartmann, N.; Imbihl, R.; Vogel, W. Experimental evidence for an oxidation/reduction mechanism in rate oscillations of catalytic CO oxidation on Platinum. *Catal. Lett.* **1994**, *28*, 373–381. [CrossRef]
93. Gnutzmann, V.; Vogel, W. Structural sensitivity of the standard Pt/SiO_2 catalyst EuroPt-1 to hydrogen and oxygen exposure by in situ X-ray diffraction. *J. Phys. Chem.* **1990**, *94*, 4991–4997. [CrossRef]
94. Carlsson, P.-A.; Österlund, L.; Thormählen, P.; Palmqvist, A.; Fridell, E.; Jansson, J.; Skoglundh, M. A transient FTIR and XANES study of CO oxidation over Pt/Al_2O_3 catalysts. *J. Catal.* **2004**, *226*, 422–434. [CrossRef]
95. Phizackerley, R.P.; Rek, Z.U.; Stephenson, G.B.; Conradson, S.D.; Hodgson, K.O.; Matsushita, T.; Oyanagi, H. An energy dispersive spectrometer for the rapid measurement of X-ray absorption spectra using synchrotron radiation. *J. Appl. Cryst.* **1983**, *16*, 220–232. [CrossRef]
96. Frahm, R. QEXAFS—X-ray absorption studies in seconds. *Physica B* **1989**, *158*, 342–343. [CrossRef]
97. Couves, J.W.; Thomas, J.M.; Waller, D.; Jones, R.H.; Dent, A.J.; Derbyshire, G.E.; Greaves, G.N. Tracing the conversion of aurichalcite to a copper catalyst by combined X-ray absorption and diffraction. *Nature* **1991**, *354*, 465–468. [CrossRef]
98. Coulston, G.W.; Bare, S.R.; Kung, H.; Birkeland, K.; Bethke, G.K.; Harlow, R.; Herron, N.; Lee, P. The kinetic significance of V^{5+} in *n*-butane oxidation catalysed by vanadium phosphates. *Science* **1997**, *275*, 191–193. [CrossRef] [PubMed]
99. Ressler, T.; Hagelstein, M.; Hatje, U.; Metz, W. In situ X-ray absorption spectroscopy studies on chemical oscillations in the CO/O_2 system on supported Pd catalysts. *J. Phys. Chem. B* **1997**, *101*, 6680–6687. [CrossRef]
100. Fiddy, S.G.; Newton, M.A.; Dent, A.J.; Salvini, G.; Corker, J.M.; Turin, S.; Campbell, T.; Evans, J. In situ energy dispersive EXAFS (EDE) of low loaded $Pt(acac)_2/H_I$ SiO_2 catalyst precursors on a timescale of seconds and below. *Chem. Commun.* **1999**, 851–852. [CrossRef]
101. Newton, M.A.; Dent, A.J.; Evans, J. Bringing time resolution to EXAFS: Recent developments and application to chemical systems. *Chem. Soc. Rev.* **2002**, *31*, 83–95. [CrossRef] [PubMed]
102. Clausen, B.S.; Grabaek, L.; Steffensen, G.; Hansen, P.L.; Topsoe, H. A combined QEXAFS XRD method for online in situ studies of catalysts—Examples of dynamics measurements of Cu based methanol catalysts. *Catal. Lett.* **1993**, *20*, 23–26. [CrossRef]
103. Als-Nielsen, J.; Grubel, G.; Clausen, B.S. QEXAFS in seconds at an undulator source. *Nucl. Instrum. Methods B* **1995**, *97*, 522–525. [CrossRef]

104. Grunwaldt, J.D.; Molenbroek, A.M.; Topsoe, N.Y.; Topsoe, H.; Clausen, B.S. In situ investigations of structural changes in Cu/ZnO catalysts. *J. Catal.* **2000**, *194*, 452–460. [CrossRef]
105. Graham, W.R.C.; Lynch, D.T. CO oxidation on Pt—Variable phasing of inputs during forced composition cycling. *AICHe* **1990**, *36*, 1796–1806. [CrossRef]
106. Carlsson, P.-A.; Skoglundh, M.; Fridell, E.; Jobson, E.; Andersson, B. Induced low temperature catalytic ignition by transient changes in the gas composition. *Catal. Today* **2001**, *73*, 307–313. [CrossRef]
107. Carlsson, P.-A.; Thormahlen, P.; Skoglundh, M.; Persson, H.; Fridell, E.; Jobson, E.; Andersson, B. Periodic control for improved low temperature catalytic activity. *Top. Catal.* **2001**, *16*, 343–347. [CrossRef]
108. Bazin, D.; Sayers, S.; Rehr, J.J.; Mottet, C. Numerical simulation of the platinum L_{III} edge white line relative to nanometer scale clusters. *J. Phys. Chem. B* **1997**, *101*, 5332–5336. [CrossRef]
109. Nagai, Y.; Hirabayashi, T.; Dohmae, K.; Takagi, N.; Minami, H.; Shinjoh, S.; Matsumoto, S. Sintering inhibition mechanism of platinum supported on ceria-based and Pt-oxide-support interaction. *J. Catal.* **2006**, *242*, 103–109. [CrossRef]
110. Nagai, Y.; Dohmae, K.; Ikeda, Y.; Takagi, N.; Tanabe, T.; Hara, N.; Guilera, G.; Pascarelli, S.; Newton, M.A.; Kuno, O.; et al. In situ redsiperson Pt autoexhaust catalsts; an online approach to increasing catalyst lifetimes. *Angew. Chem. Int. Ed.* **2008**, *48*, 9303–9306. [CrossRef] [PubMed]
111. Ankudinov, A.L.; Rehr, J.J.; Low, J.J.; Bare, S.R. Sensitivity of Pt X-ray absorption near edge structure to the morphology of small Pt clusters. *J. Chem. Phys.* **2002**, *116*, 1911–1919. [CrossRef]
112. Newton, M.A. Beamsize related phenomena and effective normalisation in energy dispersive EXAFS for the study of heterogeneous catalysts, powder materials, and the processes they mediate: Observations, and (some) solutions. *J. Synchrotron Radiat.* **2007**, *14*, 372–381. [CrossRef] [PubMed]
113. Newton, M.A.; Dent, A.J. Energy dispersive EXAFS: Principles, application, and possibilities for the understanding the dynamic behaviour of heterogeneous catalysts. In *In-Situ Characterization of Heterogeneous Catalysts*; Chupas, P.J., Hanson, J., Rodriguez, J.A., Eds.; Wiley: Hoboken, NJ, USA, 2013; Chapter 3; pp. 75–118.
114. Mueller, O.; Nachtegaal, M.; Just, J.; Luetzenkirchen-Hecht, D.; Frahm, R. Quick-EXAFS setup at the SuperXAS beamline for in situ X-ray absorption spectroscopy with 10 ms time resolution. *J. Synchrotron Radiat.* **2016**, *23*, 260–266. [CrossRef] [PubMed]
115. Mueller, O.; Luetzenkirchen-Hecht, D.; Frahm, R. Quick scanning monochromator for millisecond in situ and *in operando* X-ray absorption spectroscopy. *Rev. Sci. Instrum.* **2015**, *86*, 093905. [CrossRef] [PubMed]
116. Ackermann, M.D.; Pedersen, T.M.; Hendriksen, B.L.M.; Robach, O.; Bobaru, S.C.; Popa, I.; Quiros, C.; Kim, H.; Hammer, B.; Ferrer, S.; et al. Structure and reactivity of surface oxides on Pt(110) during catalytic CO oxidation. *Phys. Rev. Lett.* **2005**, *95*, 255505. [CrossRef] [PubMed]
117. Bernard, P.; Peters, K.; Alvarez, J.; Ferrer, S. Ultrahigh vacuum high pressure chamber for surface X-ray diffraction experiments. *Rev. Sci. Instrum.* **1999**, *70*, 1478–1480. [CrossRef]
118. Balmes, O.; van Rijn, R.; Wermeille, D.; Resta, A.; Petit, L.; Isern, H.; Dufrane, T.; Felici, R. The ID 03 surface diffraction beamline for in situ investigations of catalytic reactions at surfaces. *Catal. Today* **2009**, *145*, 220–226. [CrossRef]
119. High Pressure SXRD Reactor. Available online: http://lpmwww.physics.leidenuniv.nl/uploads/datasheets/sxrd_flyer_web.pdf (accessed on 12 February 2017).
120. Blomberg, S.; Zhou, J.; Gustafson, J.; Zetterberg, J.; Lundgren, E. 2D and 3D imaging of the gas phase close to an operating model catalyst by planar laser induced fluorescence. *J. Phys. Condens. Matter* **2016**, *28*, 453002. [CrossRef] [PubMed]
121. Li, W.X.; Österlund, L.; Vestergaard, E.K.; Vang, R.T.; Matthiesen, J.; Pedersen, T.M.; Laegsgaard, E.; Hammer, B.; Besenbacher, F. Oxidation of Pt(110). *Phys. Rev. Lett.* **2004**, *93*, 146104. [CrossRef] [PubMed]
122. Hendriksen, B.L.M.; Frenken, J.M.W. CO oxidation on Pt(110) scanning tunnelling microscopy inside a high pressure flow reactor. *Phys. Rev. Lett.* **2002**, *89*, 046101. [CrossRef] [PubMed]
123. Li, W.; Hammer, B. Reactivity of a gas/metal/metal-oxide three phase boundary: CO oxidation at the Pt(111)-$c(4 \times 2)$-2CO/α-PtO_2 phase boundary. *Chem. Phys. Lett.* **2005**, *492*, 183–186. [CrossRef]
124. Farkas, A.; Zalewska-Wierzbicka, K.; Bachmann, C.; Goritzka, J.; Langsdorf, D.; Balmes, O.; Janek, J.; Over, H. High pressure carbon monoxide oxidation over platinum (111). *J. Phys. Chem. C* **2013**, *117*, 9932–9942. [CrossRef]

125. Ellinger, C.; Stierle, A.; Robinson, I.K.; Nefedov, A. Atmospheric pressure oxidation of Pt(111). *J. Phys. C* **2008**, *20*, 184013. [CrossRef]
126. Miller, D.J.; Öberg, H.; Kaya, S.; Casalongue, H.S.; Fribel, D.; Anniyev, T.; Ogasawara, H.; Bluhm, H.; Pettersson, L.G.M.; Nilsson, A. Oxidation of Pt(111) under near-ambient conditions. *Phys. Rev. Lett.* **2011**, *107*, 195502. [CrossRef] [PubMed]
127. Balmes, O.; Prevot, G.; Torrelles, X.; Lundgren, E.; Ferrer, S. Generation of surface steps on Pt(977) induced by the catalytic oxidation of CO. *J. Catal.* **2014**, *309*, 33–37. [CrossRef]
128. Salmeron, M.; Schlogl, R. Ambient pressure photoelectron spectroscopy: A new tool for surface science and nanotechnology. *Surf. Sci. Rep.* **2008**, *63*, 169–199. [CrossRef]
129. Knop-Gericke, A.; Kleimenov, E.; Haevacker, M.; Blume, R.; Teschner, D.; Zafeiratos, S.; Schlogl, R.; Bukhtivarov, V.I.; Kaichev, V.V.; Prosvirin, I.P.; et al. X-ray photoelectron spectroscopy for investigation of heterogeneous catalytic processes. *Adv. Catal.* **2009**, *52*, 213–272.
130. Papp, C.; Steinruck, H.-P. In situ high resolution X-ray photoelectron spectroscopy—Fundamental insights into surface reactions. *Surf. Sci. Rep.* **2013**, *68*, 446–487. [CrossRef]
131. Toyoshima, R.; Kondoh, H. In-situ observations of catalytic surface reactions with soft X-rays under working conditions. *J. Phys. C* **2015**, *27*, 083003. [CrossRef] [PubMed]
132. Tao, F.; Dag, S.; Wang, L.-W.; Liu, Z.; Butcher, D.R.; Bluhm, H.; Salmeron, M.; Somorjai, G.A. Breakup of stepped platinum surfaces by high CO coverage. *Science* **2010**, *327*, 850–853. [CrossRef] [PubMed]
133. Hollins, P. Influence of surface defects on the infrared spectra of adsorbed species. *Surf. Sci. Rep.* **1992**, *16*, 51–94. [CrossRef]
134. Butcher, D.R.; Grass, M.E.; Zeng, Z.; Aksoy, F.; Bluhm, H.; Li, W.X.; Mun, B.S.; Somorjai, G.A.; Liu, Z. In situ oxidation study of Pt(110) and its interaction with CO. *J. Am. Chem. Soc.* **2011**, *133*, 20319–20325. [CrossRef] [PubMed]
135. Miller, D.; Casalongue, H.S.; Bluhm, H.; Ogasawara, H.; Nilsson, A.; Kaya, S. Different reactivity of the various platinum oxides and chemisorbed oxygen in CO oxidation on Pt(111). *J. Am. Chem. Soc.* **2014**, *136*, 6340–6347. [CrossRef] [PubMed]
136. Hamalainen, K.; Siddons, D.P.; Hastings, J.B.; Berman, L.E. Elimination of the inner-shell lifetime broadening in X-ray absorption spectroscopy. *Phys. Rev. Lett.* **1991**, *67*, 2850–2853. [CrossRef] [PubMed]
137. DeGroot, F.M.F.; Krisch, K.H.; Vogel, J. Spectral sharpening of the Pt L edges by high resolution X-ray emission. *Phys. Rev. B* **2002**, *66*, 195112. [CrossRef]
138. Van Bokhoven, J.A.; Louis, C.; Miller, J.T.; Tromp, M.; Safonova, O.V.; Glatzel, P. Activation of oxygen on gold/alumina catalysts: In situ high energy resolution fluorescence and time resolved X-ray spectroscopy. *Angew. Chem. Int. Ed.* **2006**, *45*, 4651–4654. [CrossRef] [PubMed]
139. Safonova, O.V.; Tromp, M.; van Bokhoven, J.A.; DeGroot, F.M.F.; Evans, J.; Glatzel, P. Identification of CO adsorption sites in supported Pt catalysts using high energy resolution fluorescence detection X-ray spectroscopy. *J. Phys. Chem. B* **2006**, *110*, 16162–16164. [CrossRef] [PubMed]
140. Singh, J.; Alayon, E.M.C.; Tromp, M.M.; Safonova, O.V.; Glatzel, P.; Nachtegaal, M.; Frahm, R.; van Bokhoven, J.A. Generating highly active partially oxidized platinum during oxidation of carbon monoxide over Pt/Al_2O_3. *Angew. Chem. Int. Ed.* **2008**, *47*, 9260–9264. [CrossRef] [PubMed]
141. Singh, J.; Tromp, M.; Safonova, O.V.; Glatzel, P.; van Bokhoven, J.A. In situ XAS with high-energy resolution: The changing structure of platinum during the oxidation of carbon monoxide. *Catal. Today* **2009**, *145*, 300–306. [CrossRef]
142. Singh, J.; van Bokhoven, J.A. Structure of alumina supported platinum catalysts of different particle size during CO oxidation using in situ IR and HERFD XAS. *Catal. Today* **2010**, *155*, 199–205. [CrossRef]
143. Grunwaldt, J.D.; Caravati, M.; Hannemann, S.; Baiker, A. X-ray absorption spectroscopy under reaction conditions: Suitability of different reaction cells for combined characterisation and time resolved studies. *Phys. Chem. Chem. Phys.* **2004**, *6*, 3037–3057. [CrossRef]
144. Urakawa, A.; Maeda, N.; Baiker, A. Space and time resolved combined DRIFT Raman spectroscopy: Monitoring dynamic surface and bulk processes during NO_x storage. *Angew. Chem. Int. Ed.* **2008**, *47*, 9256–9259. [CrossRef] [PubMed]
145. Urakawa, A.; Baiker, A. Space resolved profiling relevant in heterogeneous catalysis. *Top. Catal.* **2009**, *52*, 1312–1322. [CrossRef]

146. Korup, O.; Mavlyankariev, S.; Geske, M.; Goldsmith, C.F.; Horn, R. Measurement and analysis of spatial reactor profiles in high temperature catalysis research. *Chem. Eng. Proc.* **2011**, *50*, 998–1009. [CrossRef]
147. Touitou, J.J.; Morgan, K.; Burch, R.; Hardacre, C.; Goguet, A. An in situ spatially resolved method to probe gas phase reactions through a fixed bed catalyst. *Catal. Sci. Technol.* **2012**, *2*, 1811–1813. [CrossRef]
148. Morgan, K.; Touitou, J.J.; Choi, J.S.; Coney, C.; Hardacre, C.; Pihl, J.A.; Stere, C.E.; Kim, M.Y.; Stewart, C.; Goguet, A.; et al. Evolution and enabling capacities of spatially resolved techniques for the characterisation of heterogeneously catalysed reactions. *ACS Catal.* **2016**, *6*, 1356–1381. [CrossRef]
149. Grunwaldt, J.D.; Baiker, A. Axial variation of the oxidation state of Pt-Rh/Al_2O_3 during partial methane oxidation in affixed bed reactor: An in situ X-ray absorption spectroscopy study. *Catal. Lett.* **2005**, *99*, 5–12. [CrossRef]
150. Grunwaldt, J.D.; Wagner, J.B.; Dunin-Borkowski, R.E. Imaging catalysts at work: A hierarchical approach from the macro- to the meso- and nano-scale. *ChemCatChem* **2013**, *5*, 62–80. [CrossRef]
151. Newton, M.A.; Jyoti, B.; Dent, A.J.; Diaz-Moreno, S.; Fiddy, S.G.; Evans, J. Rapid monitoring of the nature and interconversion of supported catalyst phases and their influence upon performance: CO oxidation to CO_2 by γ-Al_2O_3 supported Rh catalysts. *Chem. Eur. J.* **2006**, *12*, 1975–1985. [CrossRef]
152. Singh, J.; Nachtegaal, M.; Alayon, E.M.C.; Stötzel, J.; van Bokhoven, J.A. Dynamic structure changes of a heterogeneous catalyst within a reactor: Oscillations in CO oxidation over a supported platinum catalyst. *ChemCatChem* **2010**, *2*, 653–657. [CrossRef]
153. Gänzler, A.M.; Casapu, M.; Boubnov, A.; Müller, O.; Conrad, S.; Lichtenberg, H.; Frahm, R.; Grunwaldt, J.D. Operando spatially and time-resolved X-ray absorption spectroscopy and infrared thermography during oscillatory CO oxidation. *J. Catal.* **2015**, *328*, 216–224. [CrossRef]
154. Campbell, C.T.; Ertl, G.; Kuipers, H.; Segner, J. A molecular beam study of the catalytic oxidation of CO on a Pt(111) surface. *J. Phys. Chem.* **1980**, *73*, 5862–5873. [CrossRef]
155. Warren, B.E. X-ray determination of the stricture of a glass. *J. Am. Ceram. Soc.* **1934**, *17*, 249–254. [CrossRef]
156. Warren, B.E.; Krutter, H.; Morningstar, O. Fourier analysis of X-ray patterns of vitreous SiO_2 and B_2O_2. *J. Am. Ceram. Soc.* **1936**, *19*, 202–206. [CrossRef]
157. Franklin, R.E. The interpretation of diffuse X-ray diagrams of carbon. *Acta Cryst.* **1950**, *3*, 107–121. [CrossRef]
158. Franklin, R.E. The structure of graphitic carbons. *Acta Cryst.* **1951**, *4*, 253. [CrossRef]
159. Gallezot, P. X-ray techniques in catalysis. In *Catalysis*; Anderson, J.R., Boudart, M., Eds.; Springer: Beriln/Heidelberg, Germany, 1979; Chapter 4; pp. 221–273.
160. Chupas, P.J.; Chapman, K.W.; Lee, P.L. Applications of an amorphous silicon detector for high resolution, high sensitivity and pair distribution function measurements. *J. Appl. Cryst.* **2007**, *40*, 463–470. [CrossRef]
161. Liang, K.S.; Laderman, S.S.; Sinfelt, J.H. Structural study of small catalytic particles using differential anomalous scattering. *J. Chem. Phys.* **1987**, *86*, 2352–2355. [CrossRef]
162. Chupas, P.J.; Chapman, K.W.; Jennings, G.; Lee, P.L.; Grey, C.P. Watching nanoparticles grow: The mechanism and kinetics for the formation of TiO_2 supported platinum nanoparticles. *J. Am. Chem. Soc.* **2007**, *129*, 13822. [CrossRef] [PubMed]
163. Newton, M.A.; Chapman, K.W.; Thompsett, D.; Chupas, P.J. Chasing changing nanoparticles with time-resolved pair distribution function measurements. *J. Am. Chem. Soc.* **2012**, *134*, 5036–5039. [CrossRef]
164. Chupas, P.J.; Chapman, K.W.; Kurtz, C.; Hanson, J.C.; Lee, P.L.; Grey, C.P. A versatile sample environment for non-ambient X-ray scattering experiments. *J. Appl. Cryst.* **2008**, *41*, 822–824. [CrossRef]
165. Narula, C.K.; Stocks, G.M. Ab initio density functional calculations of adsorption of transition metals on the θ-Al_2O_3 (010) surface. *J. Phys. Chem. C* **2012**, *116*, 5628–5636. [CrossRef]
166. Narula, C.K.; Allard, L.F.; Stocks, G.M.; Moses-Debusk, M. Remarkable NO oxidation on single supported platinum atoms. *Sci. Rep.* **2014**, *4*, 7238. [CrossRef] [PubMed]
167. Moses-DeBusk, M.; Yoon, M.; Allard, L.F.; Mullins, D.R.; Wu, Z.L.; Yang, X.F.; Veith, G.; Stocks, G.M.; Narula, C.K. CO oxidation on supported single Pt atoms: Experimental and ab initio density functional studies of CO interaction with Pt atom on θ-Al_2O_3 (010) surface. *J. Am. Chem. Soc.* **2013**, *135*, 12634–12645. [CrossRef] [PubMed]
168. Newton, M.A.; Ferri, D.; Smolentsev, G.; Marchionni, V.; Nachtegaal, M. Room temperature carbon monoxide oxidation by oxygen over Pt/Al_2O_3 mediated by reactive platinum carbonates. *Nat. Commun.* **2015**, *6*, 8675. [CrossRef] [PubMed]

169. Newton, M.A.; Ferri, D.; Smolentsev, G.; Marchionni, V.; Nachtegaal, M. Kinetic studies of Pt carbonate mediated, room temperature, oxidation of carbon monoxide by oxygen over Pt/Al_2O_3 using combined, time resolved, XAFS, DRIFTS and mass spectrometry. *J. Am. Chem. Soc.* **2016**, *138*, 13930–13940. [CrossRef] [PubMed]
170. Allian, D.; Takanabe, K.; Fujdala, L.; Hao, X.; Truex, T.; Cai, J.; Buda, C.; Neurock, M.; Iglesia, E. Chemisorption of CO and mechnism of CO oxidation on supported metal nanoclusters. *J. Am. Chem. Soc.* **2011**, *133*, 4498–4517. [CrossRef]
171. Wartnaby, C.E.; Stuck, A.; Yeo, Y.Y.; King, D.A. Microcalorimetric heats of adsorption of CO, NO, and oxygen on Pt(110). *J. Phys. Chem.* **1996**, *100*, 12483–12488. [CrossRef]
172. Yeo, Y.Y.; Vattuone, L.; King, D.A. Calorimetric heats for CO and oxygen adsorption and for the catalytic CO oxidation reaction on Pt(111). *J. Chem. Phys.* **1997**, *106*, 392–401. [CrossRef]
173. Szlacheto, J.; Ferri, D.; Marchionni, V.; Kambolis, A.; Safonova, O.V.; Milne, C.J.; Kröcher, O.; Nachtegaal, M.; Sá, J. Subsecond and in situ chemical speciation of Pt/Al_2O_3 during oxidation-reduction cycles monitored by high-energy resolution off-resonant X-ray spectroscopy. *J. Am. Chem. Soc.* **2013**, *135*, 19071–19074. [CrossRef] [PubMed]
174. Blachuki, W.; Szlachetko, J.; Hoszowska, J.; Dousse, J.C.; Kayser, Y.; Nachtegaal, M.; Sa, J. High energy resolution off-resonant spectroscopy for X-ray absorption spectra free of self-absorption effects. *Phys. Rev. Lett.* **2014**, *112*, 173003. [CrossRef] [PubMed]
175. Mostafa, S.; Behafarid, D.; Croy, J.R.; Ono, L.K.; Li, L.; Yang, J.C.; Frenkel, A.I.; Roldan-Cuenya, B. Shape-dependent catalytic properties of Pt nanoparticles. *J. Am. Chem. Soc.* **2010**, *132*, 15714–15719. [CrossRef] [PubMed]
176. Chaâbane, N.; Lazzari, R.; Jupille, J.; Renaud, G.; Soares, E.A. CO-induced scavenging of supported Pt nanoclusters: A GISAXS study. *J. Phys. Chem. C* **2012**, *116*, 23362–23370. [CrossRef]
177. Gustafson, J.; Shipilin, M.; Zhang, C.; Stierle, A.; Hejral, U.; Ruett, U.; Gutowski, O.; Carlsson, P.A.; Skoglundh, M.; Lundgren, E. High-energy surface X-ray diffraction for fast surface structure determination. *Science* **2014**, *343*, 758–761. [CrossRef] [PubMed]
178. Shipilin, M.; Gustafson, J.; Zhang, C.; Merte, L.R.; Stierle, A.; Hejral, U.; Ruett, U.; Gutowski, O.; Skoglundh, M.; Carlsson, P.A.; et al. Transient structures of PdO during CO oxidation over Pd(100). *J. Phys. Chem. C* **2015**, *119*, 15469–15476. [CrossRef]
179. Nolte, P.; Stierle, A.; Jin-Phillipp, N.Y.; Kasper, N.; Schulli, T.U.; Dosch, H. Shape changes of supported Rh nanoparticles during oxidation and reduction cycles. *Science* **2008**, *321*, 1654–1658. [CrossRef] [PubMed]
180. Nolte, P.; Stierle, A.; Kasper, N.; Jin-Phillipp, N.Y.; Reichert, H.; Ruhm, A.; Okasinski, J.; Dosch, H.; Schoder, S. Combinatorial high-energy X-ray microbeam study of the size-dependent oxidation of Pd nanoparticles on MgO(100). *Phys. Rev. B* **2008**, *77*, 115444. [CrossRef]
181. Nolte, P.; Stierle, A.; Kasper, N.; Jin-Phillipp, N.Y.; Jeutter, N.; Dosch, H. Reversible shape changes of Pd nanoparticles on MgO(100). *Nano Lett.* **2011**, *11*, 4697–4700. [CrossRef] [PubMed]
182. Heiral, U.; Muller, P.; Balmes, O.; Pontoni, D.; Stierle, A. Tracking the shape-dependent sintering of platinum-rhodium model catalysts under operando conditions. *Nat. Commun.* **2016**, *7*, 10964.
183. Di Michiel, M. (ESRF) Private Communication, 2016.
184. Baurecht, D.; Fringeli, U.P. Quantitative modulated excitation Fourier transform infrared spectroscopy. *Rev. Sci. Instrum.* **2001**, *72*, 3782–3792. [CrossRef]
185. Urakawa, A.; Wirz, R.; Burgi, T.; Baiker, A. ATR-IR flow-through cell for concentration modulation excitation spectroscopy: Diffusion experiments and simulations. *J. Phys. Chem. B* **2003**, *107*, 13061–13068. [CrossRef]
186. Urakawa, A.; Burgi, T.; Schlapfer, H.P.; Baiker, A. Simultaneous in situ monitoring of surface and gas species and surface properties by modulation excitation polarization-modulation infrared reflection-absorption spectroscopy: CO oxidation over Pt film. *J. Chem. Phys.* **2006**, *124*, 054717. [CrossRef] [PubMed]
187. Urakawa, A.; Burgi, T.; Baiker, A. Sensitivity enhancement and dynamic behavior analysis by modulation excitation spectroscopy: Principle and application in heterogeneous catalysis. *Chem. Eng. Sci.* **2008**, *63*, 4902–4909. [CrossRef]
188. Burgi, T.; Baiker, A. In situ infrared spectroscopy of catalytic solid-liquid interfaces using phase-sensitive detection: Enantioselective hydrogenation of a pyrone over Pd/TiO_2. *J. Phys. Chem. B* **2002**, *106*, 10649–10658. [CrossRef]

189. Ferri, D.; Kumar, M.S.; Eyssler, A.; Korsak, O.; Hug, P.; Weidenkaff, A.; Newton, M.A. First steps in combining concentration modulation techniques with synchronous dispersive EXAFS/DRIFTS/mass spectrometry for in situ time resolved study of heterogeneous catalysts. *Phys. Chem. Chem. Phys.* **2010**, *12*, 5634–5646. [CrossRef] [PubMed]
190. Ferri, D.; Newton, M.A.; Nachtegaal, M. Modulation excitation X-ray absorption spectroscopy to probe surface species on heterogeneous catalysts. *Top. Catal.* **2011**, *54*, 1070–1078. [CrossRef]
191. Koenig, C.F.J.; van Bokhoven, J.A.; Schildhauer, T.J.; Nachtegaal, M. Quantitative analysis of modulated excitation X-ray absorption spectra: Enhanced precision of EXAFS fitting. *J. Phys. Chem. C* **2012**, *116*, 19857–19866. [CrossRef]
192. Marchionni, V.; Newton, M.A.; Kambolis, A.; Kumar, S.M.; Weidenkaff, A.; Ferri, D. A modulated excitation ED-EXAFS/DRIFTS study of hydrothermal ageing of Rh/Al_2O_3. *Catal. Today* **2014**, *229*, 80–87. [CrossRef]
193. Nilsson, J.; Carlsson, P.A.; Fouladvand, S.; Martin, N.M.; Gustafson, J.; Newton, M.A.; Lundgren, E.; Grönbeck, H.; Skoglundh, M. Chemistry of supported palladium nanoparticles during methane oxidation. *ACS Catal.* **2015**, *5*, 2481–2489. [CrossRef]
194. Urakawa, A.; Van Beek, W.; Monrabal-Capilla, M.; Galan-Mascaros, J.R.; Palin, L.; Milanesio, M. Combined, modulation enhanced X-ray powder diffraction and Raman spectroscopic study of structural transitions in the spin crossover material $[Fe(Htrz)_2(trz)](BF_4)$. *J. Phys. Chem. C* **2011**, *115*, 1323–1329. [CrossRef]
195. Chernyshov, D.; Van Beek, W.; Emerich, H.; Milanesio, M.; Urakawa, A.; Viterbo, D.; Palin, L.; Caliandro, R. Kinematic diffraction on a structure with periodically varying scattering function. *Acta Crystallogr. A* **2011**, *67*, 327–335. [CrossRef] [PubMed]
196. Chernyshov, D.; Dyadin, V.; Van Beek, W.; Urakawa, A. Frequency analysis for modulation-enhanced powder diffraction. *Acta Crystallogr. A* **2016**, *72*, 500–506. [CrossRef] [PubMed]
197. Voronov, A.; Urakawa, A.; Van Beek, W.; Tsakoumis, N.E.; Emerich, H.; Ronning, M. Multivariate curve resolution applied to in situ X-ray absorption spectroscopy data: An efficient tool for data processing and analysis. *Anal. Chim. Acta* **2014**, *840*, 20–27. [CrossRef] [PubMed]
198. Ferri, D.; Newton, M.A.; Di Michiel, M.; Chiarello, G.L.; Yoon, S.; Lu, Y.; Andrieux, J.; Kumar, M.S.; Weidenkaff, A. Synchrotron hard X-ray methods coupled to phase sensitive analysis to characterize aging of solid catalysts with enhanced sensitivity. *Phys. Chem. Chem. Phys.* **2013**, *15*, 8629–8639. [CrossRef] [PubMed]
199. Ferri, D.; Newton, M.A.; Di Michiel, M.; Chiarello, G.L.; Yoon, S.; Lu, Y.; Andrieux, J. Seeing further into the dynamic structure of complex solid catalysts using X-ray diffraction combined with modulated excitation spectroscopy. *Angew. Chem. Int. Ed.* **2014**, *53*, 8890–8894. [CrossRef] [PubMed]
200. Fernández-Garcia, M. XANES analysis of catalytic systems under reaction conditions. *Catal. Rev. Sci. Eng.* **2002**, *44*, 59–121. [CrossRef]
201. Iglesias-Juez, A.; Kubacka, A.; Fernández-Garcia, M.; Di Michiel, M.; Newton, M.A. Nanoparticulate Pd supported catalysts: Size-dependent formation of Pd(I)/Pd(0) and their role in CO elimination. *J. Am. Chem. Soc.* **2011**, *133*, 4484–4489. [CrossRef] [PubMed]
202. Ankudinov, A.L.; Ravel, B.; Rehr, J.J.; Conradson, S.D. Real-space multiple-scattering calculation and interpretation of X-ray-absorption near-edge structure. *Phys. Rev. B* **1998**, *58*, 7565–7576. [CrossRef]
203. Ankudinov, A.L.; Bouldin, C.E.; Rehr, J.J.; Sims, J.; Hung, H. Parallel calculation of electron multiple scattering using Lanczos algorithms. *Phys. Rev. B* **2002**, *65*, 104107. [CrossRef]
204. Rehr, J.J.; Ankudinov, A.L. Progress in the theory and interpretation of XANES. *Coord. Chem. Rev.* **2005**, *249*, 131–140. [CrossRef]
205. Smolentsev, G.; Soldatov, A. Quantitative local structure refinement from XANES: Multi-dimensional interpolation approach. *J. Synchrotron Radiat.* **2006**, *13*, 19–29. [CrossRef] [PubMed]
206. Benfatto, M.; Della Longa, S. MXAN: New improvements for potential and structural refinement. *JPCS* **2009**, *190*, 012031. [CrossRef]
207. Lima, F.A.; Bjornsson, R.; Weyhermuller, T.; Chandrasekran, P.; Glatzel, P.; Neese, F.; DeBeer, S. High-resolution molybdenum K-edge X-ray absorption spectroscopy analyzed with time-dependent density functional theory. *Phys. Chem. Chem. Phys.* **2013**, *15*, 20911–20920. [CrossRef] [PubMed]
208. Delgado-Jaime, M.U.; Zhang, K.; Vura-Weiss, J.; de Groot, F.M.F. CTM4DOC: Electronic structure analysis from X-ray spectroscopy. *J. Synchrotron Radiat.* **2016**, *23*, 1264–1271. [CrossRef] [PubMed]
209. Munoz, M.; Farges, F.; Argoul, P. Continuous Cauchy wavelet transform of XAFS spectra. *Phys. Scr.* **2005**, *T115*, 221.

210. Funke, H.; Scheinost, A.C.; Chukalina, M. Wavelet analysis of extended X-ray absorption fine structure data. *Phys. Rev. B* **2005**, *71*, 094110. [CrossRef]
211. Filez, M.; Redekop, E.A.; Poelman, H.; Galvita, V.V.; Ramachandran, R.K.; Dendooven, J.; Detavernier, C.; Marin, G.B. Unravelling the formation of Pt-Ga alloyed nanoparticles on calcined Ga-modified hydrotalcites by in situ XAS. *Chem. Mater.* **2014**, *26*, 5936. [CrossRef]
212. Filez, M.; Redekop, E.A.; Poelman, H.; Galvita, V.V.; Marin, G.B. Advanced elemental characterization during Pt—In catalyst formation by wavelet transformed X-ray absorption spectroscopy. *Anal. Chem.* **2015**, *87*, 3520–3526. [CrossRef] [PubMed]
213. Mesu, J.G.; Beale, A.M.; De Groot, F.M.F.; Weckhuysen, B.M. Synchrotron radiation effects on catalytic systems as probed with a combined in situ UV-Vis/XAFS spectroscopic setup. *J. Phys. Chem. B* **2006**, *110*, 17671–17677. [CrossRef] [PubMed]
214. Martis, V.; Nikitenko, S.; Sen, S.; Sankar, G.; van Beek, W.; Filinchuk, Y.; Snigireva, I.; Bras, W. Effects of X-rays on crystal nucleation in lithium disilicate. *Cryst. Growth Des.* **2011**, *11*, 2858–2865. [CrossRef]
215. Peng, J.; Porsgaard, S.; Borondics, F.; Kober, M.; Caballero, A.; Bluhm, H.; Besenbacher, F.; Salmeron, M. Room-temperature reaction of oxygen with gold: An in situ ambient-pressure X-ray photoelectron spectroscopy investigation. *J. Am. Chem. Soc.* **2010**, *132*, 2858–2859.